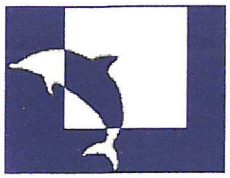

University of Southampton

Faculty of Engineering and Applied Science

Department of Electrical Engineering

DEPOSITION OF PARTICLES IN HUMAN NASAL REPLICATE CASTS

by

Sabine Häußermann

Submitted for the Degree of

Doctor of Philosophy

Southampton April 2000

UNIVERSITY OF SOUTHAMPTON

ABSTRACT

FACULTY OF ENGINEERING AND APPLIED SCIENCE
ELECTRICAL ENGINEERING

Doctor of Philosophy

DEPOSITION OF PARTICLES IN HUMAN NASAL REPLICATE CASTS

by Sabine Häußermann

Studies of aerosol deposition in the nasal airways play a significant role in developing our understanding of deposition and retention in the respiratory tract. The nose not only determines the amount of particles reaching the lungs, but also contributes to systemic uptake. Artificial nasal replicate casts were used for quite some time to determine the influence of particle size and flow rate on deposition, without validating the results by comparing them to the data gained with a human volunteer. To be able to make this comparison realistic human breathing patterns need to be simulated, the cast needs to be anatomically accurate and nasal deposition needs to be measured on a human volunteer.

To simulate human breathing patterns, a breathing simulator has been designed and constructed. It allows artificial breathing patterns as well as recorded human breathing patterns to be implemented. Additionally, two artificial nasal cavities were built utilising magnetic resonance imaging (MRI) of different human volunteers. One of the casts was made from a human volunteer taking part in nasal deposition and clearance experiments. In this study the ability to use both the cast of a human volunteer and his exact breathing pattern provided the ground for comparisons between in-vivo and in-vitro experiments. Furthermore the influence of different breathing patterns, flow rates and particle sizes has been studied. Thirdly, the exact location of particles deposited in the cast was obtained under the same experimental conditions as in-vivo. Also the cast was dismantled and deposition on each plate was measured independently to determine regional deposition.

The results show that constant flow (as used in most previous studies) causes significantly more deposition than realistic human breathing patterns. The comparison of the nasal cast and the human volunteer showed significant higher deposition in the cast for light exercise, which is apparently caused by the change of cross-sectional area of the volunteers airways with exercise. The main deposition site in the cast is the anterior end of the middle turbinate, where particles deposit by impaction. The region of and behind the nasal valve shows no higher deposition than other regions of the nose, contrary to what was suggested in previous studies.

ACKNOWLEDGEMENTS

Many thanks to Professor Adrian G. Bailey (University of Southampton, UK) for his supervision. His interest, advice and his encouragement were extremely helpful. I am grateful for the work of Mr Dennis White (University of Southampton, UK), who built the mechanical part of the breathing simulator. Many thanks also to Dr Trevor Williams (University of Southampton, UK) for his tireless efforts teaching me English. I am very grateful to Mr Chrisitan Maul (University of Southampton, UK) for teaching me Electronics and for his help and advise in building the control of the breathing simulator.

I am very grateful to the National Radiological Protection Board for funding this project. Sincere thanks to Dr Mike Bailey and Dr George Etherington (NRPB, UK) for their advise and their great interest in my work. Also to Dr Jenny Smith and Dr Mike Youngman (NRPB, UK) for the invaluable benefit of their time and experience. Many thanks to Mr John Campbell (NRPB, UK) who built the electric part of the breathing simulator.

It is greatly appreciated that Ray Guilmette from LRRI (Albuquerque, NM) let me use his laboratories, machinery and tools and taught me how to make nasal casts. I am also very grateful for the technical help of Mr Roland Rodger and the discussions with Gordon Zwartz, both from LRRI (Albuquerque, NM).

Further I want to thank my former colleagues from GSF (Munich, Germany) for their support especially Dr W. Stahlhofen who set the ball rolling and Mrs Christa Roth for valuable discussions.

I am very grateful to all my friends for their support and friendship. I also want to thank my parents, who enabled me to do this thesis with their financial and moral support.

CONTENTS

1 INTRODUCTION

Since the nose filters inhaled air it is an important route for the intake of airborne aerosols into the body. Traditionally, more effort has been devoted to the experimental determination and modelling of aerosol deposition in the lung rather than the nasal passages. However, the majority of humans at rest breathe primarily through the nose (Niinimaa et al 1980). Material deposited nasally is of importance since it finds its way into other parts of the body, via mucosal absorption and clearance into the stomach, as well as defining what passes to the lungs. Furthermore the material deposited in the nose can cause a number of medical conditions such as cancer (Hady et al 1983; Hildesheim & Levine 1993; Leopold 1994).

This thesis is concerned with aerosol particle deposition in a nasal cast. The work is a collaborative venture between the University of Southampton and the National Radiological Protection Board (NRPB). Scientists at NRPB are studying nasal deposition and clearance with human volunteer subjects. (Smith et al 1996, Etherington et al 1998)

Although aerosol deposition in humans can be measured using radio labelled particles, the exact pattern of particle deposition cannot be determined. Even using a gamma-camera which gives a three dimensional image does not show the exact location without uncertainties, since gamma rays from other sources will be detected (cross fire). It is also difficult to determine in-vivo the various influences (e.g. breathing pattern, changes in anatomy) on the deposition of particles. Researchers have attempted to overcome these problems by using artificial nasal cavities (cast). The nasal cast may be used to measure deposition regarding the influence of: particle size, level of particle charge, breathing pattern and flow rate.

Previous studies on nasal cast deposition have been limited by their methodology in several ways. Firstly, the particles were usually inhaled using a uniform pump that produces constant flow rather than cyclic flow patterns or even specific human breathing patterns. Secondly, nasal passages have been reproduced based on cadavers rather than living human beings. A cadavers anatomy is not only physically different from living humans, but also excludes the possibility of comparing the data gained with the cast with the data of the human volunteer the cast was made from. Thirdly, models were integrated and could not be dissembled for examination of regional deposition. Various studies used casts made according to the anatomy of living human volunteers, but non of them used realistic breathing patterns or compared the data with data of the volunteer the cast was made from.

To overcome those problems a breathing simulator (electromechanical lung) has been designed and constructed, to simulate human breathing patterns. It is computer controlled, and allows artificial breathing patterns as well as recorded human breathing patterns to be implemented. Additionally, artificial nasal cavities were built utilising magnetic resonance imaging (MRI) to simulate the nasal anatomy of different human volunteers. One of the casts was made from a human volunteer taking part in the NRPB experiments mentioned above. Since naso-pharyngeal flow patterns vary widely among different humans it has been difficult to make meaningful comparisons between cast data and data from a human being. In this study the ability to use both the cast of a human volunteer and his exact breathing pattern provided the ground for comparisons between in-vivo and in-vitro experiments. Furthermore the influence of different breathing patterns, flow rates and particle sizes could be studied. Thirdly, the exact location of particles deposited in the cast could be obtained under the same conditions as existed in the in-vivo experiment. Also the cast was dismantled and deposition on each plate was measured independently to determine regional deposition.

The thesis starts with some basic background information about nasal anatomy and physiology, rhinometry and airflow through the nose. A short overview of aerosol science is given, including particle deposition and surface interaction. The chapter also contains a literature review of nasal particle deposition. Chapter 3 describes the main objectives of this thesis. Chapter 4 is concerned with nasal casts and their construction, particularly with the cast used in this work. Chapter 5 describes the design, manufacture and validation of the breathing simulator, and chapter 6 is concerned with materials and methods. Chapter 7 contains the data of total deposition in the casts obtained using different breathing patterns, different anatomies and different particle sizes. Chapter 8 looks at the deposition distribution within the cast of various particle sizes and breathing patterns, and chapter 9 compares in-vivo versus in-vitro deposition. Finally, conclusions are drawn from the experiments in chapter 10 and future work is suggested in chapter 11.

2 THEORETICAL BACKGROUND AND LITERATURE REVIEW

The respiratory tract is exposed to particles and gases flowing in and out with each breath. Some of these inhaled materials are chemically and biologically active, with effects which might be either beneficial or harmful. Since the nose is an important route into the lungs it is of great interest to determine the deposition of those materials in the nasal cavity.

The deposition of particles is influenced by size and shape of particles as well as their physical and chemical properties. Also the velocity and changes in direction of the airflow around the particle greatly influence its deposition behaviour.

The anatomy and physiology of the nose determine its airflow direction and velocity. To find a correlation between anatomy and physiology and particle deposition in the nose, scientists have not only measured the velocity of the air entering the nose, but also resistance of the nose to airflow and cross-sectional area of the nasal cavity. The following section gives an overview over those topics, an overview of aerosol behaviour and a literature review of particle deposition in the nose.

2.1 NASAL ANATOMY AND PHYSIOLOGY

During inhalation, air enters the lungs via the nose or mouth; at rest 80 % of humans breathe through the nose (Niinimaa et al 1980). Oral or oro-nasal breathing takes place at higher ventilation rates (e.g. during exercise), when the nasal airways are constricted, or during speech (Proctor 1977).

The nose has a unique anatomy, which permits various important functions:

i) It filters hazardous airborne particulates.

ii) It warms and humidifies inhaled air.

iii) The olfactory region is located in the nasal cavity (sense of smell).

iv) The nasal cavity and attached sinuses act as resonating chambers during speech.

2.1.1 ANATOMY

The external portion of the nose is called the nares or the nasal vestibule. This is a double airway opening onto two nostrils, each of which measures 1.5 - 2 cm in length and 0.5 - 1 cm in width (ICRP 1994; Kesavanathan et al 1998).

The nose is divided transversely in two by the septum that extends from the nostrils to the naso-pharynx. The nasal vestibule consists of compliant cartilage lined with epithelium cells, like the outer skin, and has coarse hairs, which act as a fibrous filter (Swift & Kesavanathan 1996). The nasal valve, which has the smallest total cross-sectional area in the upper respiratory tract, is situated in close proximity to the junction of the cartilaginous vestibule and the rigid bony cavity of the nose (Bridger 1970; Haight & Cole 1983).

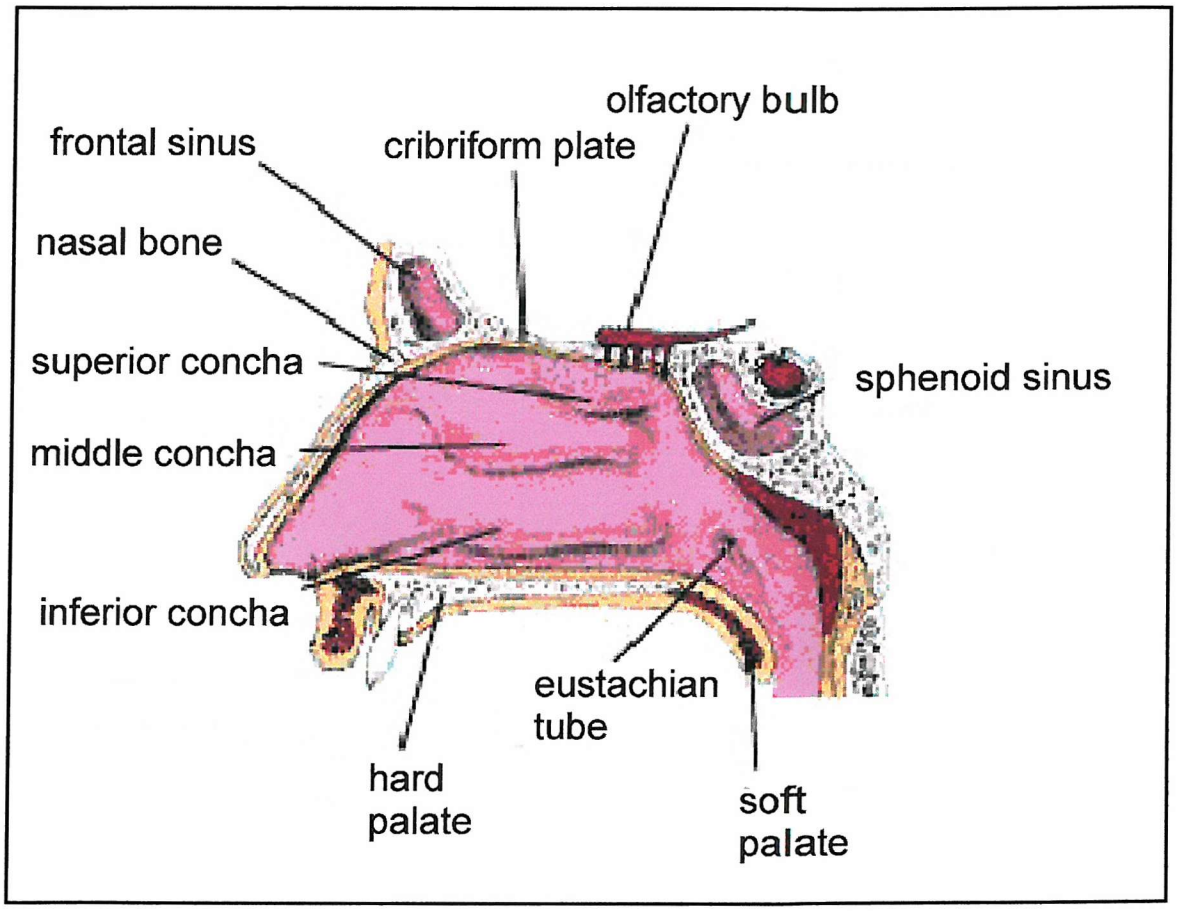

Figure 2.1: Sagittal cut of a nasal cavity (MSEncarta1997)

Following on from the nasal valve are internal passages which are also divided transversely by the nasal septum and which form a large cavity above the mouth. The cribriform bone

forms the roof of the cavity, whereas hard and soft palates form the floor. The nasal conchae bones, also called turbinates, form the lateral walls of the nasal cavity. The presence of the turbinates greatly increases the surface area of the nasal cavity, to about 140 - 160 cm^2, which enhances the cleaning, warming and moistening of inhaled air. The conchae bones and the septum are lined with erectile tissue, which regulates the nasal lumen. The internal area is mostly lined with ciliated mucosa, apart from the olfactory region, which is lined with olfactory epithelium. The olfactory region is the superior portion of the main cavity.

At the nasopharynx, about 8 - 12 cm from the nostrils, the septum disappears and the two airways merge into one. From here, there is a transition to squamous airways as far as the larynx.

The bones of the face contain the paranasal sinuses which are air spaces surrounding the nose on three sides. They are lined with respiratory epithelium and connected to the main nasal cavity by small orifices (Proctor & Swift 1971).

2.1.2 PHYSIOLOGY

CLEARANCE OF THE NOSE

Deposited substances in the airways are cleared by several mechanisms and pathways which lead mainly to the GI tract, the lymphatic system and the blood. Clearance of the airways is accomplished by particle transport and absorption. Particle transport removes the particles by secretions and ciliary action. Absorption refers to transport of material into the blood, which involves dissociation of the particles. It is the aim of the NRPB study to examine particle transport after particles are deposited by inhalation and therefore insoluble particles were used in the in-vivo study. For this reason this section is limited to particle transport in the nose and is not concerned with absorption.

The nose can be divided into two regions with regard to particle transport. These are the anterior region, which is cleared by nose-blowing or wiping, and the posterior region, which is cleared by mucociliary action.

The mucus, which lines the nasal cavity behind the vestibule, is transported by the ciliary beat. It moves from the posterior nasal region towards the pharynx and is then swallowed. Occasional sniffing assists this action (Lippman 1970). Proctor et al (Proctor 1977; Proctor & Andersen 1976) found that there is a band between the anterior inactive region and the main ciliated passage which has rapid mucociliary clearance forward, other authors assumed that mucociliary action is purely towards the pharynx.

ICRP66 (p 307-308) gives a concise review of mucus movement and draws the conclusion that the movement of the mucus layer is not uniform, and therefore not all regions are cleared with the same speed.

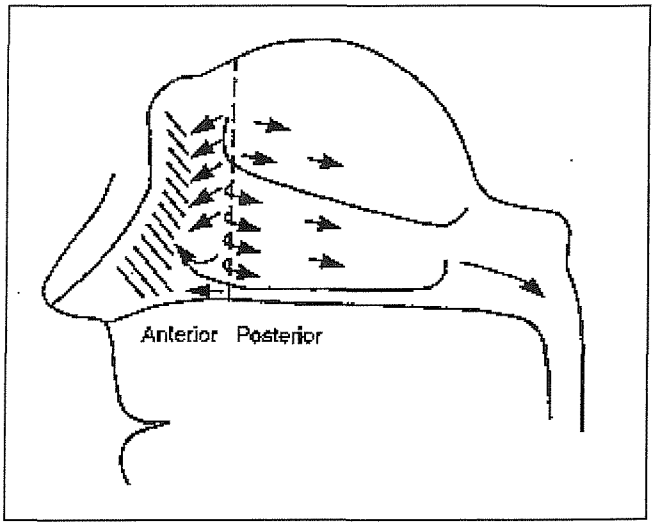

Figure 2.2: Clearance zones of the nose

The speed of mucociliar transport was measured from quite a few authors usually by putting some labelled material onto the mucus and measure the time it need to reach the pharynx. The speed of the cilia varies between the subjects, so different authors give different speeds: 0.5 - 26.6 mm/min (Proctor & Andersen 1976) and 4.0 - 45 mm/min (Bang et al 1967).

Lippman et al (Lippman 1970) measured nasal retention of inhaled particles (d_{ea} 1.3-7.3), and found particles were retained in the ciliated region up to 7 hours, even though most particles were cleared in the first 3 hours.

Fry and Black (Fry & Black 1973) also measured retention of inhaled particles and they found considerable inter and intra subject variability, also here long term clearance was retention.

Since the anterior part of the nose is mainly cleared by nose blowing and wiping the retention time not only depends on the amount of particles removed by nose blowing but also on the frequency the subject blows the nose. Hence it is very variable but Lippman and Fry and Black both showed that the particles are retained for at least 6 hours.

NASAL RESISTANCE

Several different components cause resistance in the respiratory tract. The airflow in the airways causes resistance, as do the expanding lung tissue and the moving chest tissue. The latter two resistances are called compliance. The nose has a rather high resistance to airflow which is about one half of the total resistance (airway resistance + compliance) and two-thirds of the airway resistance (Ferris et al 1964).

The nasal resistance has a static and a dynamic component. Static resistance results from the anatomy of the nose. The nasal valve is the passage with greatest resistance arising from its smallest cross-sectional area (Bridger 1970; Haight & Cole 1983). The turbinate region also contributes significantly to nasal resistance. Both the nasal valve and the turbinates are also responsible for part of the dynamic resistance.

The dynamic aspect of resistance has two time-varying components, which arise from morphological adjustments resulting from the movement of the alae and changes in erectile tissue. The alae are the movable part at the side of the outer nose and their movement changes the resistance of the vestibule breath by breath. This variation is only slight during ventilation at rest but increases as the breathing volume increases (Cole et al 1985). If the alae are widely dilated, the total nasal resistance is approximately halved (Cole 1988).

Changes in the mucosal tissue, which is erectile and starts at the nasal valve, lead to changes in resistance to airflow. In any individual, such resistance to airflow is unequal in either side of the nose and varies during the day. In most subjects, resistance varies over time, within a day, and independently in either side of the nose. This behaviour is called nasal cyclic (Eccles 1978). The word cyclic is somehow misleading, since it implies periodicity. Even though about 80 % of humans have these changes, for most of them the

changes do not occur periodically (Cole & Haight 1986). Nasal cyclic is affected, though not controlled, by ambient air conditions. Airflow distribution differs by 20 - 80%, from one side of the nasal cavity to the other, without causing discomfort in the subject. The cycle has been found to disappear during exercise, emotionally upset and in elderly people (Flanagan & Eccles 1997; Mirza et al 1997).

Changes in ambient air condition, alterations in posture, and condition of the volunteer (e.g. state of health or exercise) can also affect nasal resistance (Proctor 1977). Alterations in position and state of the volunteers are especially interesting for this project, since the cast is made according to MRI images taken from recumbent volunteers, but the aerosol administration is done for volunteers sitting and at light exercise. For example Cole and co-workers found that the resistance can increase dramatically if the volunteer is recumbent (Cole & Haight 1986). It can be also very different for different volunteers, Flanagan et al (Flanagan & Eccles 1997) measured 4 volunteers and each of them had a totally different cyclic behaviour. According to this study each volunteer is affected differently by exercise.

These aspects of dynamic resistance (ie erectile tissue and moving alae) are each controlled by independent autonomic and voluntary neural mechanisms (Cole et al 1985).

Schreck et al (Schreck et al 1993) assessed nasal resistance by measuring pressure loss across a cast. They distinguished between three regions in the cast: (i) the external region, starting from the nostrils and including the nasal valve; (ii) the interior region, including the complete turbinates, and (iii) the naso-pharynx. The external region gave the greatest resistance (~ 43 % pressure drop) whereas the naso-pharynx gave the lowest (~ 25 % pressure drop). Further enlargement of one turbinate, which decreased the cross section of the passage, caused the resistance to double. They conclude that the resistance of the interior nose can exceed that of the external nose in the case of congestion. The turbinates of the casts used in the present study appear to be significantly larger than in the cast used by Schreck et al and, therefore, the surrounding airways are smaller. The reason is that Schreck's cast was made post mortem which leaves the erectile tissue (mentioned in section 4.1) without blood and therefore the turbinates are much smaller. Thus, it is expected that the interior region will exhibit greater resistance, in the present study, than in the work of Schreck et al.

2.2 RHINOMETRY

The anatomy of the nose and its resistance are thought to be very important to the determination of particle deposition and flow behaviour. One way to determine the resistance of the nose is rhinomanometry, which measures the pressure loss over the nasal cavity in-vivo. Two different methods are employed: anterior and posterior rhinomanometry. Posterior rhinomanometry measures the total nasal passage pressure loss by measuring the pharyngeal pressure through a tube held in the closed mouth. Anterior rhinomanometry measures the pressure loss of one side of the nose to the nasopharynx by measuring pressure through a seal at one nostril. Both anterior and posterior measurements are influenced by the airflow through the nose, and therefore the human volunteers have to perform certain breathing patterns or the flow has to be measured. The resistance of the nasal cavity is then calculated from the pressure loss and the flow. Since anterior rhinomanometry only measures unilateral resistance, the total resistance has to be calculated according to Ohm's law: $1/R=1/R_1+1/R_2$ (Naito & Iwata 1997).

In recent years the method of acoustic rhinometry has been developed. Contrary to rhinomanometry it is a static method, independent of airflow. The advantage of this method is that it delivers more detailed data than rhinomanometry. The acoustic reflections of sound signals incident on the airway walls are measured and analysed by computer software. The results show the cross-sectional area of the airways as a function of distance from the entrance of the nostrils. For acoustic rhinometry the sound axis follows roughly the geometrical axis (Hilberg et al 1993). The same study shows that it is likely to overestimate the posterior part of the epipharynx. In in-vivo measurements the maxilliary sinuses are likely to contribute to the acoustically determined areas (Hilberg & Pedersen 1996). Nasal passage volumes can be calculated from contiguous cross-sectional values.

2.3 AIRFLOW THROUGH THE NOSE

Typical average airflow rates in human beings are approximately: 9 L/min at rest, 25 L/min during light exercise and up to 50 L/min during heavy exercise (ICRP 1994, p 23). These values are average inhalation flow rates.

At rest about 80 % of humans breathe through the nose (Niinimaa et al 1980). As a result of the high resistance to airflow through the nose, the amount of air available to the body is restricted. Therefore oro-nasal or oral breathing is adopted during exercise or if the nasal passages are congested. The critical flow rate where breathing switches from nasal to oro-nasal breathing in most subjects is 30 L/min according to Haight et al (Haight & Cole 1983) or 35 L/min according to Niinimaa et al (Niinimaa et al 1980). These values are inhalation peak flow rates. Niinimaa et al also state that it should be noted that the alae start to collapse at this velocity, which can restrict the flow of air significantly. Another study showed that the switching point from nasal breathing to oro-nasal breathing can be between 38 L/min and as high as 65 L/min (Malarbet et al 1994) depending on the subject. Malarbet suggests that the reason for the different results might be a different experimental setting in the other studies, which has more resistance to flow. It is also possible that Malabert et al had a higher number of volunteers and therefore had two amongst them who had a late switching point from nasal to oro-nasal breathing.

Immediately after the subject switches from nasal to oro-nasal breathing, ventilation was to 57 % through the nose decreasing to 40 % under conditions of maximal exercise (Niinimaa et al 1980).

To describe airflow through the nose, some comments on fluid dynamics are appropriate. For particle behaviour and deposition it is important to know if flow in the nose is laminar or turbulent. At laminar flow the pattern of streamlines is smooth, with no streamline crossing or looping back on itself. Velocity and direction of flow is always the same at a certain spot. At turbulent flow the streamlines are chaotic and velocity and direction change for the same spot with time. An indicator for this is the Reynolds number. Reynolds numbers smaller than 2500 indicate laminar flow and above 4000 turbulent. The numbers in between indicate unstable flow. Also the profile of the flow can be an indicator of laminar or turbulent flow. Stable laminar flow has a parabolic profile, whereas turbulent flow shows a profile looking like a plug, the parable is flattened at the top.

Particles that are close to the wall are more likely to deposit, therefore it is necessary to look at the airflow in the region near the wall. Flow around a solid or along a wall is affected by viscous friction, even though it is only a very thin layer near the wall, which is affected. This layer is called the boundary layer, the closer the airflow is to the wall the slower it becomes till it reaches zero at the wall. The higher the velocity of airflow the

thinner the boundary layer in a circular duct. It is not that straight forward in other geometries, but in general it can be said that particles are more likely to deposit in turbulent flow since they experience higher flow velocities closer to the wall.

The route taken by the air upon entering the nose can be described as follows: the air enters the nose flowing vertically up into the nostrils. Between the nostrils and the turbinates is the nasal valve, where the airflow has to follow a bend of 90°, at the same time the airways become quite narrow. After the valve the flow becomes extremely turbulent, since the nasal passage suddenly opens up from its narrowest part to its widest part. Here the nasal passages are divided in three by the turbinates. After the two airways merge into one the air has to follow a 90° bend to the throat.

Some authors report experimental studies of airflow in nasal casts. Hornung et al used a cast of one fossa (one side of the airways) made from a cadaver. Radioactive xenon was used to make the flow visible at constant flow rates of 2.5, 7.0 and 20 L/min. The results show that the flow towards the olfactory region seems to come from the lateral wall rather than from the septum. Also a region of turbulent flow in the external nares was found, which increases with increasing flow rate. Additionally with increasing flow rates the amount of activity going into the olfactory region was increasing (Hornung et al 1987).

Girardin et al (Girardin et al 1983) used a nasal cast made from a cadaver and constant flow of 10 L/min to measure the velocity fields in the nose. Laser Doppler anemometry was used to measure the flow velocity in their study. From their measurements they concluded that the airflow was streamlined by the turbinates with lower peak velocity, the velocity was greater near the septum, the nasal valve has directional influence on the inspiratory flow and the flow is usually greater in the lower half of the cast. The Reynolds numbers they calculated were between 750 and 2400, which indicates laminar flow but the measured velocity fields and profiles indicate the flow to be turbulent. It has to be noted that the flow they used experimentally was not as high as it would be in a human being at rest and the airways are probably too wide, since the cast was taken from a cadaver (because of the blood loss from the erectile tissue). Even though the airways were enlarged and airflow was too low they were able to detect turbulence, but do not describe the location where turbulence occurred.

Hahn et al (Hahn et al 1993) used a large scale model (x20 the size of a normal nose) of one side of the nose, anatomically correct, produced according to a CAT scan to obtain detailed results of the flow patterns in a nose. The velocity of flow was measured with a hot film anemometer probe inserted through different holes in the cast. The nasal flow used in this study was constant and 20 times higher than in real noses, to reach the same Reynolds number. The flow rates corresponded to 66 L/min, 33.6 L/min and 10.8 L/min in a real nose, which was thought to correspond to a forceful sniff, medium sniff and average breathing rate, respectively. Their results suggest that the flow distribution is similar for all flow rates. About 50% of the inspired air flows through the combined middle and inferior airways and 14% through the olfactory region. The local Reynolds number was from 250 in the olfactory region to 4500 in the inferior airway for a medium sniff flow rate (33.6 L/min). As found by Girardin et al before, they support the idea that turbulent flow develops in the nasal cavity at far lower Reynolds numbers (Re) than it would do normally. It usually develops around Re = 2000. Their results suggest that the airflow inside the nasal cavity model is moderately turbulent at most physiological flow rates. The comparison of flow with and without nasal hair showed that the nasal hair might be responsible for a slight increase in turbulence in the external nares, whereas it does not seem to affect regions further behind. It must be noted that the highest probability of turbulence occurs after the nasal valve, because the rapid increase in area is very likely to create vortices, and in the turbinate region because of the irregularity of the airways.

2.4 AEROSOL BEHAVIOUR

An aerosol consists of small airborne particles, which may be distinguished by size, shape and physical, chemical and biological properties. Particle size is important because it largely determines the behaviour of the particle in gas suspension. The shape and the physical properties (e.g. density) also have a great influence on the behaviour of airborne particles. The chemical (e.g. hygroscopic growth) and biological properties can have influence on deposition but will be neglected here, since the experiments for this work were carried out exclusively under controlled laboratory conditions and the particles used in the experiments were generated for our purpose and are not hygroscopic. The aerosol used in the in-vivo

study consisted of solid monodisperse polystyrene particles and the one used in the in-vitro study consisted of liquid monodisperse sebacate oil droplets. The following section describes the general behaviour of particles in gas (air), their deposition mechanisms and their interaction with the airway wall upon which they are deposited.

2.4.1 SIZE OF AEROSOL PARTICLES

Generally, particles bigger than 0.5 μm are better described with the tools of fluid dynamics, whereas the behaviour of ultrafine particles (< 0.5 μm) is more governed by Brownian motion of the surrounding gas. The size range used in this work is limited between 1 μm and 10 μm, so the emphasis here is on mechanisms influencing this size range. Mechanisms that govern ultrafine particles will only be touched upon in this thesis.

Existing equations for describing particle motion are only valid for spherical particles. However, the motion of a particle is influenced not only by its size but also by its shape and density. The only naturally occurring spherical particles are droplets of diameter less than about 1 mm and some pollens, therefore, it is necessary to introduce an equivalent diameter which takes shape and density into account and allows comparison between particles of different shapes and materials (Hinds 1982).

The behaviour of particles larger than 0.5 μm in gas suspension is dominated by aerodynamic forces, therefore their characteristic size parameter is the aerodynamic equivalent diameter d_{ae}. It is defined as the diameter of the unit density sphere, which has the same settling velocity as the particle being measured. Reference to the aerodynamic diameter is useful for describing the particle's settling and inertial behaviour in the respiratory tract (Baron & Willeke 1993a). It is defined as:

$$d_{ae} = d_p \sqrt{C_c \frac{\rho_p}{\rho_0}}$$ **Equation 2.1**

d_{ae}	=	aerodynamic diameter	[μm]	ρ_p	=	density of particle	[g/cm^3]
d_p	=	physical diameter	[μm]	ρ_0	=	unit density	[g/cm^3]
C_c	=	slip correction factor	[1]				

The unit density ρ_0 is 1 [g/cm^3]. If a particle is very small it might be influenced by collisions with molecules in the air. Therefore a slip correction factor C_c is introduced to account for this phenomena. For particles above 1 μm this correction factor can be neglected, because it is approximately 1 (Baron & Willeke 1993a).

The diameters used in this thesis are always aerodynamic equivalent diameters unless stated otherwise.

2.4.2 Mechanisms of Aerosol Deposition

Five different principal mechanisms determine particle deposition within the respiratory tract. Particles which are larger in diameter than 0.5 μm are primarily governed by aerodynamic forces. This includes the deposition process of gravitational settling, referred to as sedimentation and the process of inertial motion, referred to as inertial impaction.

Gravitational settling occurs if a particle deposits under the force of gravity. It depends on particle density and velocity of the airflow; the latter determines the residence time. It is mostly important for particles larger than 1 μm. It is considered to be of minor interest for particle deposition in the nose, due to the small residence time (Lippman 1970).

Inertial impaction occurs if a particle cannot adjust quickly enough to an abrupt change in airflow direction, because of its inertia, and collides with the nearby airway wall. This mechanism depends on the aerodynamic diameter and the airflow velocity and is most important for particles of diameter $d_{ae} > 1$ μm. It is believed that impaction is the most important factor for nasal deposition, as the flow changes direction several times as described in section 2.3. For this reason it is discussed later on in more detail.

For fibres and very large particles **Interception** contributes to deposition considerably. It occurs if a particle follows the airflow and happens to come within one radius of the particle to the wall and is so captured because of its finite size. This mechanism does not depend on flow velocity.

Diffusion leads to deposition if the particles are small enough to undergo Brownian motion, which is true only for sub-micron particles.

Electrostatic charge can be extremely important but is difficult to classify. In general particles which are electrostatically charged can have an enhanced deposition. In the absence of external electrical fields, aerosols can have a low natural level of charge. In experiments, measures can be taken to ensure that the particles have a defined level of charge or are neutralised. Although the natural levels of charge are normally insufficient to influence the deposition behaviour, it is possible to charge particles to a level so that it is significant to increase deposition in the human airways (Hashish & Bailey 1991) ((Bailey 1997).

One mechanism to cause deposition is space charge, which arises if dense charged aerosols are inhaled. A second for this study more important mechanism is due to image forces, the charged particle induces image charge on a grounded surface. This becomes important if the particle is near to a surface (Bailey et al 1998) and therefore it could be very important for nasal deposition where the airways become relatively narrow.

An important factor for the mobility of a particle is the charge-to-mass ratio, which usually decreases with increasing drop size. Therefore other mechanisms, like impaction and sedimentation, will be dominant if the particle size is large. This implies that particles must be small in order to be influenced in their deposition behaviour by charge, i.e. the charge-to-mass ratio must be above a certain level (Bailey 1988). This is even more so the case since in these experiments no artificial external field is present. Therefore mostly particles which are close to the wall will deposit by image charge. Particle density might not be high enough for space charge to be significant.

There is a limit to the amount of charge that can be sustained by a droplet above which it becomes unstable and disrupts. This limit is known as the Rayleigh limit, which is given by:

$$q_R = 8\pi(\varepsilon_0 T d^3)^{1/2} \qquad \textbf{Equation 2.2}$$

q_R	=	Rayleigh limit	[C]	d	=	diameter of particle	$[10^{-6}m]$
ε_0	=	permittivity	$[\frac{C}{Vm}]$	T	=	surface tension of the liquid	$[\frac{N}{m}]$

(Bailey 1988)

As an example sebacate oil which is used in this work, may be described. The permittivity of sebacate oil is 2.2 C/Vm and the surface tension is $27*10^{-3}$ N/m. Therefore the Rayleigh limit for 3 μm sebacate droplets is about 27 C. This is not very likely to be reached in the experiments described later.

2.4.3 INERTIAL IMPACTION

To describe inertial impaction a few statements about the movement of particles in gas flow are appropriate.

A very useful parameter to describe the state of the airflow is the Reynolds number Re. It indicates the ratio of the inertial force of the gas to the friction force of the gas moving over a surface:

$$\mathrm{Re} = \frac{\rho_{gas} V d}{\eta} \qquad \textbf{Equation 2.3}$$

d	= dimension of the object	[cm]	ρ_{gas}	= density of gas	[g/cm^3]
V	= relative velocity of gas	[cm/s]	η	= viscosity of gas	[g/cm s]

Note that there is a distinction between the flow Reynolds Number Re_f and the particle Reynolds Number Re_p. The former defines flow in a tube or channel of a cross-sectional diameter d, the latter one describes gas flow around a particle of the diameter d.

Since the difference between the particle velocity and the velocity of the surrounding gas is usually small and the particle size is also small, the particle Reynolds Number has usually a very small numerical value (<< 1) (Baron & Willeke 1993b).

At small Reynolds Numbers (approximately < 2000) the flow is laminar, at higher Reynolds Numbers (approximately > 4000) the flow is turbulent. In the intermediate range it is critical, the flow is sensitive to the history of the gas motion. This is only true for unobstructed ducts. Obstructions or alterations in direction can cause turbulent flow at Reynolds numbers much less than those mentioned above (Baron & Willeke 1993b).

Several forces determine the motion of a particle in the surrounding gas. The drag force is opposed to external forces such as gravitational and electric force and balances against

them. The particle drag force relates the resistive pressure of the gas to the velocity pressure and is determined by relative motion between particle and surrounding gas.

The drag force is defined as:

$$F_D = 3\pi\eta v_P d_P \qquad \textbf{Equation 2.4}$$

d_P	= particle diameter	[μm]	η	= viscosity of gas	[g/cm s]
v_P	= velocity of particle	[m/s]			

This equation is also known as Stokes' law. It is assumed that the particle is spherical and is only applicable for $Re_p < 1$. As described above Re_p is usually much smaller, therefore Stokes' law is applicable in most cases. For particles, which are small enough to be influenced by the Brownian gas motion, a slip correction factor has to be introduced into the drag force. Since particles of such a size are not considered in this thesis, it will be neglected here.

Inertial impaction can be described by the distance in which the particle will come to a rest, the stop distance S. The stop distance is a product of the initial particle velocity v and the relaxation time τ. It is useful to determine how far a particle moves across the air streamlines when flow makes a right angle bend.

$$S = v * \tau \qquad \textbf{Equation 2.5}$$

The relaxation time is the time the particle needs to adjust to a new condition of forces.

$$\tau = \frac{\rho_P d_P^2 C_C}{18\eta} \qquad \textbf{Equation 2.6}$$

d_P	= particle diameter	[μm]	η	= viscosity of gas	[g/cm s]
C_C	= slip correction factor	[1]	ρ_P	= density of particle	[g/cm^3]

For particles larger than 1 μm C_C is approximately 1. This approximation is better the larger the particle.

An important indicating factor for inertial deposition is the Stokes Number, Stk. It is the ratio of the particle's stop distance, S, to the characteristic dimension of the obstacle, d_C.

$$Stk = \frac{S}{d_C}$$ **Equation 2.7**

Using the equations above the Stokes Number is:

$$Stk = \frac{v\rho_P d_P^2 C_C}{18\eta d_C}$$ **Equation 2.8**

The Stokes Number is the ratio of the particle's inertia to the size of the obstacle. The nearer Stk is to zero the better the particles follow the streamlines of the gas flow. When the Stokes Number Stk approaches 1, inertia becomes an important factor.

If one can neglect buoyancy, in the case of rather compact particles, one can simplify the equation and Stk becomes dependent on the d_{ae}. Therefore the Equation can reduced to:

$$Stk = \frac{v d_{ae}^2}{18\eta d_C}$$ **Equation 2.9**

As mentioned earlier, electrostatic charge can enhance the deposition efficiency drastically. Wang et al investigated the deposition by inertia and electrostatic forces (Wang et al 1986). The results show that deposition is more effectively increased by increasing charge rather than the velocity of a particle. Deposition efficiency increases linearly with charge, for low Stokes Numbers (Stk <0.5), whereas the increase is less rapid for higher Stokes Numbers.

Since the airflow experiences two 90° changes in direction within the nose (nasal valve, throat) as described in section 2.3, one could try to describe the deposition at these places

in the same manner as the inertial deposition in bends. A bend is usually characterised by its bend to pipe radius $\Delta = R/a$, where R is the radius of the bend and a is the radius of the pipe. The sharper the bend the stronger the effects of secondary flow fields.

Crane at all (Crane & Evans 1977) gave a simple correlation for the impaction efficiency E of particles in a bend for laminar flow, as a function of Stokes Number and bend angle Φ, which is independent of the bend radius:

$$E = Stk\Phi/2 \qquad \textbf{Equation 2.10}$$

The effect of turbulence on impaction in a bent pipe was established by McFarland et al (McFarland et al 1997). They show that turbulence increases the deposition of particles in a bend considerably. Furthermore once the flow is turbulent, the influence of the Reynolds number can be neglected, whereas the Stokes Number and the bend angle have dramatic influences on deposition. These findings would suggest that the particle properties and the bend angle rather than the flow rate determine deposition in a bend.

2.4.4 ADHESION OF PARTICLES AND BOUNCE

After a particle meets a surface it either remains on the surface (deposits) or bounces back into the air. The reason for discussing particle bounce at this point is that solid particles are used in the in-vivo study, which do not cause problems there because of the soft tissue in the human nose, but bounce in the artificial nasal cavity. Therefore liquid oil droplets of the same aerodynamic diameter were used for the deposition study in the nasal cast.

Once the particle has been deposited, re-suspension is relatively unlikely since the adhesion forces for submicron particles are very strong, and exceed other forces by orders of magnitude (Hinds 1982). Re-suspension of particles sometimes occurs by other particles if the particle density is relatively high, as it is in an impactor (Hinds et al 1985; John & Sethi 1993). Adhesion is linearly dependent on diameter and increases with decreasing diameter. Thus large particles become detached more readily than small ones. Individual particles

smaller than 10 μm are not likely to be removed easily, once deposited (Baron & Willeke 1993a).

Impact adhesion can be described in terms of an energy balance. Xu et al (Xu et al 1993) state that deposition and rebound depend on radius, mass and velocity of the particle which approaches the surface and the impact angle. The impact energy is:

$$E_{ki} = mv_i^2 / 2 \qquad \textbf{Equation 2.11}$$

To take account of the impact angle the velocity is resolved into a normal component, v_{in}, and a tangential component, v_{it}.

Upon impact with the surface the total kinetic energy of the particle is the sum of the initial kinetic energy and the adhesive energy gained upon approach to the surface. When the particle velocity is reduced to zero, part of this energy is dissipated by various mechanisms (e.g. plastic deformation, elastic deformation). The stored elastic energy is recovered and converted into kinetic energy again. If the recovered kinetic energy is less that the energy required to separate the particle from the surface then the particle remains adhered to the surface. On the other hand, if the recovered kinetic energy is greater than the separation energy, then the particle will rebound away from the surface: it bounces. Whether particles bounce not only depends on the type of particle (physical property, shape, size), but also on the type of surface. Grease or oil on the surface will generally increase the likelihood of adhesion, but after a layer of particles has been deposited, the incoming particles may bounce from the top surface of those previously deposited. Paw U et al (Paw U 1983) studied particle bounce from different surfaces for several different particles. They concluded that the type of particle is more important than the type of surface in governing the rebound phenomenon.

E_{eo} represents the energy stored in elastic deformation, when deformed over a radius R_e. When the elastic stress limit of the particle or the impact surface is exceeded an amount of energy E_p is lost in plastic deformation.

Finally the particle leaves the impact surface with a certain rebound velocity and kinetic energy, if it can overcome the sum of energies caused by plastic deformation and adhesion. In general the angle of rebound is different from the incident angle (John 1995).

The ability of liquid droplets to deform elastically, and thus to store energy, depends on the surface tension, but is generally very low. Since adhesion for particles smaller than 10 μm is very high, the energy from the elastic deformation is much smaller than the adhesion energy and the particle remains on the surface. Therefore almost all the energy will be lost in plastic deformation. Consequently one can safely assume that the rebound of liquid particles is not significant.

An experiment conducted by Wang et al (Wang & John 1987) confirms this assumption. They compared the deposition of liquid particles on a stainless steel ring versus that of solid particles on the same ring, but soaked with vacuum oil. The results for both, the solid and the liquid particles fell on the same curve.

For the experiments described in this thesis it is assumed that the deposition of liquid particles on a solid surface does not differ significantly from the deposition of solid particles on a wet surface.

2.5 Particle Deposition in the Nose

The deposition of particles in the nose relies on the mechanisms that are described in the section above. Respiratory deposition occurs in a system of changing geometry and at a flow which changes with time and cycles in direction. This added complexity means that predictions of nasal deposition cannot be made from basic theory and one must rely to a great extent on empirical data and empirically derived equations. In this section the mechanisms of deposition in the nose and previous experiments on deposition in the nose are referred to.

2.5.1 INHALABILITY

There is an aspiration efficiency that depends on the size of particles and the velocity of the surrounding air and predicts the percentage of particles that can enter the respiratory tract. It is called inhalability of particles and decreases with increasing particle size. It depends on the size of the aerosol, the velocity of the surrounding air, the inhalation flow rate and whether nose or mouth breathing is used. In general the inhalable particle size is larger if the surrounding air is moving, but it depends on the velocity and the direction of the surrounding air stream. The experiments in this thesis are only performed in a controlled laboratory environment, where the surrounding air is still, and nose breathing only is used, therefore the studies mentioned below are only studies of nasal inhalability conducted in still air.

Breysse et al (Breysse & Swift 1990) showed with a human volunteer experiment, that nasal inhalability in still air is less than 100 % for particles larger than 18 μm and ends at a particle size of about 40 μm. The inter-subject variability in total deposition seems to decrease with increasing particle size. The experiments carried out by Hsu and Swift (Hsu & Swift 1999) on manikins showed inhalability greater than zero of much larger particles. They measured inhalability of around 20 % for particles of 40 μm in diameter and the inhalability reduced to zero at around 110 μm. It is also notable that the difference between breathing at rest and moderate exercise is not significant here.

The discrepancy could be due to the use of human volunteers by Breysse et al and manikins by Hsu and Swift manikins. Also Breysse et al measured inhalability only up to a particle size of 30.5 μm and interpolated from there to 0 % inhalation efficiency at 40%. However this still does not account for the large difference and further experiments should be conducted with human volunteers

2.5.2 MECHANISMS OF PARTICLE DEPOSITION WITHIN THE NOSE

Not only aerosol behaviour, but also flow pattern and airway morphology influence the total amount of particles depositing and moreover their distribution within the nose.

AEROSOL BEHAVIOUR IN THE NOSE

Of major importance for nasal deposition is inertial impaction for larger particles ($d_{ae} > 1\mu m$), due to changes in airflow direction at the nasal valve and at the bend to the throat. While the total area of the airway increases on moving from the nasal valve to the turbinate region, the individual channels become narrower. The increase in total area causes the flow to slow down, and the decrease in width brings more of the particles to within a small distance of the wall. For both these reasons diffusive deposition (principally of ultrafine particles) is more effective in the turbinate region; this constitutes a second major mechanism for nasal deposition. As described in section 2.3 flow is assumed to be turbulent throughout the nose, which should enhance deposition by impaction. Interception could occur at the coarse hair in the nostrils and in the narrow nasal valve, but its contribution is larger with increasing particle size or for fibres. The residence time of particles in the nose is too short for sedimentation to be a dominant factor (Swift 1981). If the electrical charge and the aerosol concentration are high enough it might enhance deposition in the nose, although Fry (Fry 1970) found that particles which are electrically charged during their production with the spinning top aerosol generator do not have greater deposition than particles which are neutralised with a ^{85}Kr source. The author suggests that the influence of impaction is higher than that of electrostatic charge for particles larger than 1 μm. However, the charge on the particles in this study was at a level which occurs naturally during the production of the particles. It is far lower than that of deliberately charged particles. It remains to be investigated whether high charge levels induced by corona discharge can enhance deposition.

INFLUENCE OF AEROSOL CHEMISTRY

Water-soluble particles deposit in a more complicated way due to hygroscopic particle growth within the warm and humid environment of the respiratory tract. For this reason, deposition could be different for hygroscopic rather than for non-hygroscopic particles of the same initial size. Ferron (Ferron 1977) describes the deposition behaviour of such particles in general, and finds that particles smaller than 1 μm reach a plateau of maximum growth relatively soon, whereas larger particles grow more slowly. He implies that particles larger than 2.2 μm undergo half of their relative size increase after passing the naso-pharyngeal region. Therefore, only the smaller hygroscopic particles are likely to change their deposition behaviour within in the nose.

Influence of Airflow

The airflow pattern has a great influence on particle deposition. Increasing air velocity (which reduces residence time) increases deposition by impaction, whereas that due to the sedimentation and diffusion mechanisms decreases. The air velocity varies during both the inhalation and exhalation parts of the breathing cycle (i.e. a constant value cannot be assumed which complicates algorithms used to model deposition).

Influence of Anatomy

Rasmussen et al (Rasmussen et al 1990) suggest that the airway dimensions alone cannot be used to predict deposition. They did not find a correlation between the anterior minimum area and deposition, nor one between the shape of the nostrils and deposition.

Contrary to Rasmussen et al, Kesavanathan et al (Kesavanathan & Swift 1998) suggest that the shape of the nostrils and the minimum area of the nose do influence the deposition efficiency DE. A formula was developed which takes the ellipticity of the nostrils E, the minimum nasal cross-sectional area A_{min}, the volumetric flow rate, Q, and the aerodynamic diameter, d_{ae}, of the particles into account: $DE = d_{ae}^{1.78}(Q/100)^{1.12} A_{\min}^{-1.33} E^{1.26}$. The authors suggest that as the length/width ratio of the nostrils increases the deposition in the anterior part increases.

Cheng et al (Cheng et al 1996) found that nasal deposition of ultrafine particles increases for subjects whose airways have smaller cross-sectional area and larger airway surface.

Location of Deposition

A high percentage of larger particles tend to deposit in the anterior part of the nose (Fry & Black 1973). Two main reasons can be given for this: firstly, the coarse hairs in the vestibule act as a fibrous filter (Swift & Kesavanathan 1996) and, secondly, at the nasal valve the air must pass the narrowest passage in the nose and at the same time take a 90° bend, which filters larger particles by impaction.

Ultrafine particles tend to deposit in the region of the conchae, which subdivide the cavity on each side into a series of groove-like passageways and turbinate the airflow. An appreciable fraction of ultrafine particles tends to deposit at the nasal hair (Swift & Kesavanathan 1996).

Reviews of Nasal Deposition

Several studies have been concerned with the total aerosol deposition in the human nose in-vivo. Mercer et al (Mercer 1975), Lippman (Lippman 1977), Yu et al (Yu et al 1982), Schlesinger (Schlesinger 1985), Stahlhofen et al (Stahlhofen et al 1989), and ICRP Publication 66 (ICRP 1994) reviewed some of them. These studies provide comprehensive data, which enable the determination of deposition in an average subject as a function of particle size over a given range. The results suggest that total deposition is at its minimum for $0.5 < d_{ae} < 1$ μm. The deposition of particles smaller than 0.5 μm increases with decreasing particle size, whereas the deposition of particles larger than 1 μm increases with increasing particle size. However, it should be noted that there is a high inter-subject variability.

Model of Nasal Deposition

Due to the complex anatomy and the complex flow pattern in the nose, not many models of nasal deposition exist. Scott et al (Scott et al 1978) developed a numerical model of particle deposition in the human nose. They partitioned the nose into five compartments and simplified their geometry. Further they calculated deposition in these compartments caused by direct inertial impaction and found that the amount predicted is not as high as the amount measured experimentally. Only when taking inertial impaction caused by secondary flows after the nasal valve into account, did the calculated deposition agree with that measured empirically. Furthermore they state that the vortices behind the nasal valve are more efficient in depositing particles then direct impaction in other sites of the nasal passage. They also found that small changes in geometry cause large changes in deposition.

Correlation of Resistance or Airflow on Deposition

Some authors have tried to correlate deposition patterns with the three important factors of particle diameter, airflow and anatomy:

Hounam et al (Hounam et al 1969; Hounam et al 1971) have shown that individual deposition patterns, which vary between subjects, correlate better with nasal resistance than with flow rate. They found that increasing resistance increases the deposition. However Becquemin et al (Becquemin et al 1991) have shown that deposition correlates better with inspiratory airflow than with resistance.

Rasmussen et al (Rasmussen et al 1990) found that, despite large inter-subject variability, the total deposition in the nose increases if the size of airway area increases and therefore the resistance decreases. They used a particle size of 2.6 μm and speculated that decongested airways increase the flow rate within the turbinate region and therefore deposit by impaction in the turbinate region (the anterior part where particles of this size usually mainly deposit does not have erectile tissue and cannot be decongested). This is also contrary to Hounam et al.

Another study from Kesavaneathan et al (Kesavanathan et al 1998) attempted to make the connection between deposition and resistance. They found only a significant dependency during unilateral breathing, whereas during breathing through both nostrils the dependency is not significant.

All four studies used about the same range of particles and the same range of airflow. The difference, which might cause the different results, is: Hounam et al and Kesavanathan et al used flow through the nose and out of the mouth with glottis closed, whereas Becquemin et al and Rasmussen et al inhaled into the lung then expired through the mouth. The closed glottis could alter the flow condition in the nose and therefore the deposition.

Yu et al (Yu et al 1982) conducted a statistical analysis of the deposition in the nose and used the results of previous experiments of several authors for this. They found a dependency on flowrate rather than pressure drop, but had high scattering in their data and therefore suggested a high biological variability.

SUMMARY

The diverse of the results show that it is very difficult to draw conclusions as to which are the dominant factors influencing the nasal deposition. Not only the inter-subject variability but also the intra-subject variability contribute to this. In most of the studies above, there was a high degree of scatter in the data and the conclusions were derived from statistical calculations. These conclusions therefore contradict each other very often. To clarify this it could be helpful to determine where exactly particles are depositing, and the changes in deposition that occur if only one parameter is changed. Thus replicate casts are used in this work since they can be dissembled. Also the conditions inside the cast are constant with regard to humidity, anatomy, airflow and it is possible to have reproducible results. If changes are made they can be made in a controlled way.

2.5.3 LITERATURE REVIEW OF PARTICLE DEPOSITION IN NASAL CASTS

Fewer studies of nasal deposition have been performed in-vitro than in-vivo, and most of them have used ultrafine particles. Two different methods of obtaining casts are normally used: one technique is to take a cast of the airway passage of a human cadaver and the other one is form the nasal passage according to images of the airways. Their advantages and disadvantages are described in section 4.1.

STUDIES USING COARSE PARTICLES

Itoh et al (Itoh et al 1985) and Kim et al (Kim et al 1985) both used the same post-mortem cast, moulded in transparent plastic from one half of a human nasal tract.

Itoh et al used particle sizes from 0.4 to 4 μm and a constant flow rate of 13 L/min (half of the normal flow rate), and investigated the effect on deposition of different carrier gases (He, SF_6 and air). It appears that deposition increases with increasing gas density, but the differences diminish as particle size increases. They also found that the largest aerosol deposited selectively at the anterior part of the middle turbinate. The smaller size (1.3 μm) also deposited at the anterior part of the middle turbinate as well as shortly behind the nasal valve. The submicron particles had a more diffuse deposition pattern, though for them the deposition was also highest in the first half of the nose. The reason they give for these deposition patterns is: The largest particles are not so greatly influenced by the vortices occurring after the nasal valve and therefore travel directly ahead and impact at the beginning of the middle turbinate. In contrast the 1.3 μm particles are affected by these vortices and deposit after the nasal valve as well as impacting on the middle turbinate. The smallest size particles are not greatly influenced by impaction, but deposit by diffusion and are therefore more scattered.

Kim et al used monodisperse oleic acid particles, of diameter 3 μm and 5 μm, labelled with fluorescent dye, to determine deposition patterns at constant flow rates of 15 L/min (at rest) and 30 L/min (exercise). Their results also suggest that the majority of particles deposit in the anterior part of the nose; for 15 L/min the majority even deposits before reaching the first turbinates. For the higher flow rate the distribution of deposition in the front and in the turbinate region seems to be more equal.

Swift et al (Swift 1991) used two casts based on MRI scans of the nasal passage, which were hand carved. One cast was from an adult and one from a child (1.5 years) and they

used a range of particle size from 1 to 10 μm. The flow rate was constant and in the range of 7 to 50 L/min. Some parts of the adult cast were exchangeable to simulate decongested and congested airways. Additionally the cross-sectional area of the airways was measured by acoustic rhinometry.

The results show individual deposition curves for each flow rate which increase with increasing particle size. As expected the deposition increases with increasing flow rate. The same data plotted using the inertial parameter d_a^2Q, where d_a is the aerodynamic diameter and Q is the volumetric flow rate show the data on one single, smooth, S-shaped curve. The authors therefore conclude that deposition is flow dependent and using the inertial parameter is a valid method. This implies that impaction is the dominant factor for deposition in the nose. When simulating a congested, a normal and a decongested nose, the deposition was highest for the congested state, less for the decongested state and smallest for the normal nose. The results which compare the adult and the child cast suggest that the total nasal aerosol deposition for an adult and a child is similar for the same state of breathing.

In another study Zwartz and Guilmette (Zwartz & Guilmette 1999) used 5.5 μm particles and a cast based on MRI scans and then milled in plates using a computer controlled milling machine (cast 2 is a duplicate of it). Particles were drawn through at a constant flow rate at 20 L/min. The total deposition in the cast is 36 %. Localising the particles with a system to detect fluorescence, described in the same paper, shows that almost all the deposition is before the nasal valve. The maximum is at the first half of the nostrils, but very little deposition in the turbinate region and basically nothing afterwards.

Studies Using Ultrafine Particles

Strong et al (Strong & Swift 1987) used a cast, which was also used by Itoh et al above. They measured the deposition of particles (5 to 150 nm) in the cast and established that the deposition of ultrafine particles increases with decreasing particle size.

Cheng et al and Yamada et al (Cheng et al 1988; Yamada et al 1988) used the same equipment and considered a particle size range of 0.005 - 0.2 μm. They compared the flow resistance of the cast (which was made from a post-mortem negative cast) with several values from the literature and found good dynamic similarity (the pressure drop, in terms of

flow rate, was similar in the two cases). Cast deposition measurements were made for constant inspiratory flow rates between 4 and 50 L/min.

Cheng et al established an equation for the deposition in the nose: $\eta = 1 - \exp(-40.3 * Q^{-1/8} * D^{1/2})$, where η is the deposition efficiency, Q is the volumetric flow [L/min] and D is the diffusion coefficient [cm^2/s].

Yamada et al also measured expiratory deposition at a flow rate of 1 L/min. The deposition of particles smaller than 0.2 μm was found to increase with decreasing particle size.

Gradon et al (Gradon & Yu 1989) studied the deposition behaviour of ultrafine aerosols in a surrogate model of the human nose. This was made from epoxy resin and silica and based on images from computer tomography. Particle deposition kinetics were simulated using a layer of benzoic acid and boric acid, which coated the inner surface of the cast, and a glycerol-water solution was used to simulate air flow though it. The dissolution of the acid into the glycerol-water solution was measured and used to calculate the deposition efficiency. The conclusion here was that the deposition efficiency depends only weakly on the flow rate, and that diffusional deposition becomes significant for particles smaller then 0.01 μm. Furthermore the flow in the nasal passage is predominantly turbulent.

Swift et al (Swift et al 1992) used a post-mortem cast (also used by Cheng et al, 1988 and Yamada et al, 1988) and three others which were made using MRI scans. One was made for a normal child aged 18 months whereas the other two were for normal, non-smoking, middle-aged adults. The two adult casts were smaller than the post-mortem cast. Ultrafine aerosol deposition of particles, with mean size from 0.006 - 0.2 μm, was measured in all four casts in three different laboratories. The results appear to depend on particle size and flow rate rather than the size of the cast and were summarised in the equation:

$\eta = 1\text{-}\exp(-bQ^{-1/8}D^{1/2})$, where η is the fraction of particles deposited, Q is the volumetric flow [L/min], D is the diffusion coefficient [cm^2/s] and b is an empirical value 12.65 ± 0.17.

Martonen et al (Martonen & Zhang 1992) commented on various experiments described above. They compared the results of Cheng et al 1988 and Yamada et al 1988 with those of Gradon et al 1989 and pointed out that the deposition rate differed by a factor of ten for the same particle size and flow rate. Furthermore, cast deposition data were compared with those from human volunteers and some discrepancies were found. They commented on the findings as follows: "Human replica casts and anatomically correct surrogate models are

difficult to obtain and related deposition data, therefore, very important. So an issue to be addressed is: to what can the disparities be attributed?" They suggested possible reasons for this but did not perform experimental checks.

Cheng et al (Cheng et al 1993) used four replicate models, two based on MRI scans and two from cadavers, where one of each had nasal hair to determine the deposition of particles between 0.006 and 0.2 μm. The results show lower deposition than that predicted by the equation of Cheng et al (1988) but confirm the equation of Swift et al (1992) written above. Furthermore the deposition was found to increase with decreasing flow rate and decreasing particle size. Nasal hair increased the deposition only slightly. Also in this case the highest deposition occured in the vestibule, before the valve, with a second peak at the beginning of the turbinate region and a third at the nasopharyngeal region.

Cheng et al (Cheng et al 1995) compared casts, which were constructed from MRI scans, of children (1.5, 2.5 and 4 years). Deposition was measured with particles from 0.2 to 4.6 μm and flow rates of 3, 7, and 16 L/min. The results show that the equation previously established by Swift et al (1992) and Cheng et al (1993) also applies here, but with coefficient b expressed as a function of age, b(t).

Cheng et al (Cheng & Swift 1995) studied the deposition in a post mortem cast (also used in Cheng et al, 1988, and Swift et al 1992) and used a particle size range from 0.0036 to 0.15 μm. The flow was constant and ranged from 4 to 30 L/min. The results suggested that there is no significant difference in total deposition between uninterrupted flow and simulated breath holding.

Cheng et al 1998, (Cheng et al 1998), compared the deposition of a post mortem nasal casts with that in human volunteers for ultrafine particles. They used constant airflow of 4 L/min and 20 L/min for both studies. The deposition efficiency matched reasonably well for particles smaller than 0.01 μm and was slightly higher in the human volunteers for particles between 0.01 and 0.1 μm. The human volunteers were different subjects than the one the cast was made from.

SUMMARY

Both in-vivo and in-vitro studies show that for coarse particles deposition increases with increasing particle size, whereas the opposite is the case for ultrafine particles. Fine

particles appear to deposit mostly in the anterior region; only if the flow rate increases does particle deposition in the middle passage increase.

Much effort has been dedicated to find a formula which describes the total deposition in a nasal cast as a function of flow rate and particle size. Swift's finding of the decongested nose having a higher deposition than the normal nose also implies a dependency on flow rate, or Stoke's Number rather than pressure drop. The higher deposition could be caused by vortices of which there may occur more at this state. The question which was not addressed was how representative the results gained with a cast are. Only Cheng at al compared the pressure-drop flow dependency in the cast with values of human volunteers from the literature and found an agreement. They also compared deposition of ultrafine particles in a cast and in human volunteers, but did not have the same volunteer for the in-vivo study as for the cast. The problem here is again the inter-subject variability. Also most of the cast studies were made using constant flow to draw the particles through the cast, but the influence of breathing pattern on deposition has not been established. This thesis is concerned with this problem, amongst others, as described in the next section.

3 OBJECTIVES

The overall aim of the study is to investigate the regional deposition of aerosols in nasal airways. Prior to this study, some important aspects of the subject had received relatively little attention:

- The comparability of nasal casts and human volunteers
- The influence of various breathing patterns on deposition
- The exact location of deposited material in the cast under different particle size and flow rate conditions
- The influence of electrostatic charge on particle deposition in the nasal airway

These aspects form the subject of the study.

EQUIPMENT DESIGNED AND BUILT FOR THE STUDY

To determine the exact location of particle deposition and the various influences on it, the use of an artificial nasal cavity is preferable to a human volunteer. Two nasal models (casts) have been built, based on magnetic resonance imaging (MRI) scans of human volunteers. One of these volunteers is taking part in an *in vivo* study being carried out at NRPB to determine the total deposition of inhaled particles in the nasal airways and their clearance kinetics. The second cast is a duplicate of a cast which is used at the LRRI in Albuquerque NM, therefore results will be comparable. Additionally, two sets of nostrils representative of different ethnic groups have been built in order to establish the influence of nostril shape.

A computer controlled breathing simulator has been designed and built in order to deliver particles to the nasal cast. It allows previously recorded human breathing patterns to be implemented as well as artificial ones. The system has been tested and the results show that it produces the desired breathing pattern very accurately. It has proved to be a reliable tool for reproducing a wide variety of breathing patterns.

EXPERIMENTAL WORK

Naso-pharyngeal breathing patterns vary widely among different human subjects as does their nasal anatomy. Experiments have therefore been carried out to measure total deposition in the cast, using the same breathing patterns (recorded from the human

volunteer at rest and light exercise) and particle size range (1.5, 3 and 6 μm) as in the *in vivo* study.

Further experiments were carried out to measure total deposition in the cast:

- with different breathing patterns from different human volunteers, as well as different artificial breathing patterns (sine wave, rectangular wave, constant flow), to establish their influence on deposition.
- using the two casts with different nostril sets, with the same breathing patterns (constant flow and human breathing) and the same particle size (6 μm), to establish the influence of anatomy.
- with different particle sizes, using the same breathing patterns (constant flow and human breathing) in the same cast, to establish the influence of particle size. These experiments also allowed comparisons to be made with previous studies, since earlier studies have generally used constant flow rather than realistic breathing patterns.

Experiments with radio-labelled particles have been carried out in order to establish the distribution of deposited particles within the cast, using the same breathing patterns (human breathing at rest and light exercise) and particle sizes (1, 3 and 6 μm) as in the *in vivo* studies. As well as providing information on the distribution of deposited material, this work should contribute to our understanding of the clearance mechanisms in the nose. After depositing particles in the cast, it was disassembled and the total activity on individual plates measured. The distribution of activity on selected plates were measured by placing them in contact with X-ray film.

Further work was carried out to investigate the influence of electrostatic charge on particle deposition for at least one particle size. A device was built to charge the particles and measure the charge. Unfortunately the cast made from Perspex repels the charged particles after a few minutes and the experiments could therefore not be carried out. These experiments are postponed, since the surface of the cast has to be made conducting.

4 NASAL CASTS AND THEIR CONSTRUCTION

4.1 NASAL CASTS

Nasal casts were developed to simulate the anatomy of the nasal airways. This avoids endangering human subjects and also makes measurements independent of human subjects. However no artificial copy of a nose will exactly resemble the original, however good the copy is, it cannot replicate such important properties as mucus, hairs and cilia. It is a matter of choosing the method that comes closest to reality.

There are various methods of obtaining nasal casts. One technique is to produce a solid cast, post mortem, by filling the nasal cavity of a cadaver with any suitable casting material. After the material has cured, the surrounding bones and tissue are removed. Subsequently, a hollow nasal cast may be moulded from the solid cast. An advantage of this method is that the anatomy of the nose is duplicated quite accurately. Most of the smallest structures can be reproduced, but the casting material does not always fill the fine structures. However, most of the interior lining is formed from erectile tissue, which collapses post mortem and so enlarges the air passages. The consequence is that the post-mortem nasal cast is a better match to a decongested nasal cavity (Guilmette et al 1989), than to a normal nasal cavity.

It is also possible to make a solid cast based on in-vivo images produced by MRI scans (Magnetic Resonance Imaging), using stereo lithography. With this method the cast is cured out of liquid plastic by a laser beam. The laser cures layer by layer according to the MRI scans. This method has the disadvantage of having an edge between each layer which cannot be smoothed, since the inside of the cast is inaccessible.

Another method based on MRI scanning was used here. Using MRI scans may not be very accurate, with regard to very small structures, since their resolution is only about 1 mm. In some areas, the images are unclear and must be interpreted. Such uncertainty is not regarded as significant. The main advantage is that the sizes of the airways are much more representative of the in-vivo state. As mentioned above the cast behaves differently from the human nose, but with the potential to compare deposition in the human volunteer with that in the corresponding cast, it might be possible to improve the cast.

Nasal casts were made from coronal MRI scans of two white male subjects without any history of nasal diseases. In-vivo deposition data for one of the subjects (subject 1) is available for comparison with cast deposition. The cast named subject 2 is the duplicate of a cast used at Lovelace Respiratory Research Institute (LRRI), Albuquerque, NM and made from a subject who also took part in many experiments and whose deposition and breathing are also available. For each subject, the nasal cavity was imaged at intervals of 3 mm, from the tip of the nose to the back of the throat. The geometries were digitised and then milled into about 70 transparent acrylic plates (2 per scan). The assembled plates resemble the nasal cavity. The benefit of using contiguous plates is that the cast can be dismantled and the edges arising between the plates can be smoothed by hand.

Additionally, two sets of nostrils were made which were based on a male Asian and a male Afro-American volunteer. The reason for this is that the nostril shape can influence nasal deposition (Kesavanathan et al 1998). The sets of nostrils stop before the appearance of the first turbinate, when the nasal valve has been passed, since the nasal valve appears to play a major role in nasal deposition (Haight & Cole 1983). Both nostril-sets can be used to replace the nostrils in either of the main casts.

4.2 Construction of the Nasal Cast

The method used for the construction the nasal casts from MRI scans was established in the Lovelace Respiratory Research Institute in Albuquerque NM, USA. Dr. Ray Guilmette of this institute kindly offered the facilities (Guilmette & Gagliano 1995). Therefore the casts used in this work were made by the author in Albuquerque.

Following steps were involved to produce the casts

- Take coronal MRI scans from a human volunteer
- Digitise the images so the software for the milling machine can read it
- Import into milling machine software and define the tool-paths for the end-mill
- Use of CNC milling-machine to mill out plates and refine them by hand if necessary
- Assemble plates to cast

The coronal images obtained from MRI scans were stored as *.tif files, i.e. they are stored in pixels, line by line. These had to be converted into a vector format compatible with the "Smart Cam" software which is used to control the milling machine and so produce the acrylic cast plates. This could not be done automatically because bones and air appear exactly the same on MRI scans and, as mentioned above, some airways are too small to be seen clearly. Airways, which were not distinguishable from the background, had to be defined in terms of the neighbouring images. Identification of the airway was usually straight forward. Only in very few cases was it impossible to identify the geometry and, in these cases, it was necessary to refer to anatomical books (e.g. the connection to the olfactory bulb, which must exist but could hardly be identified).

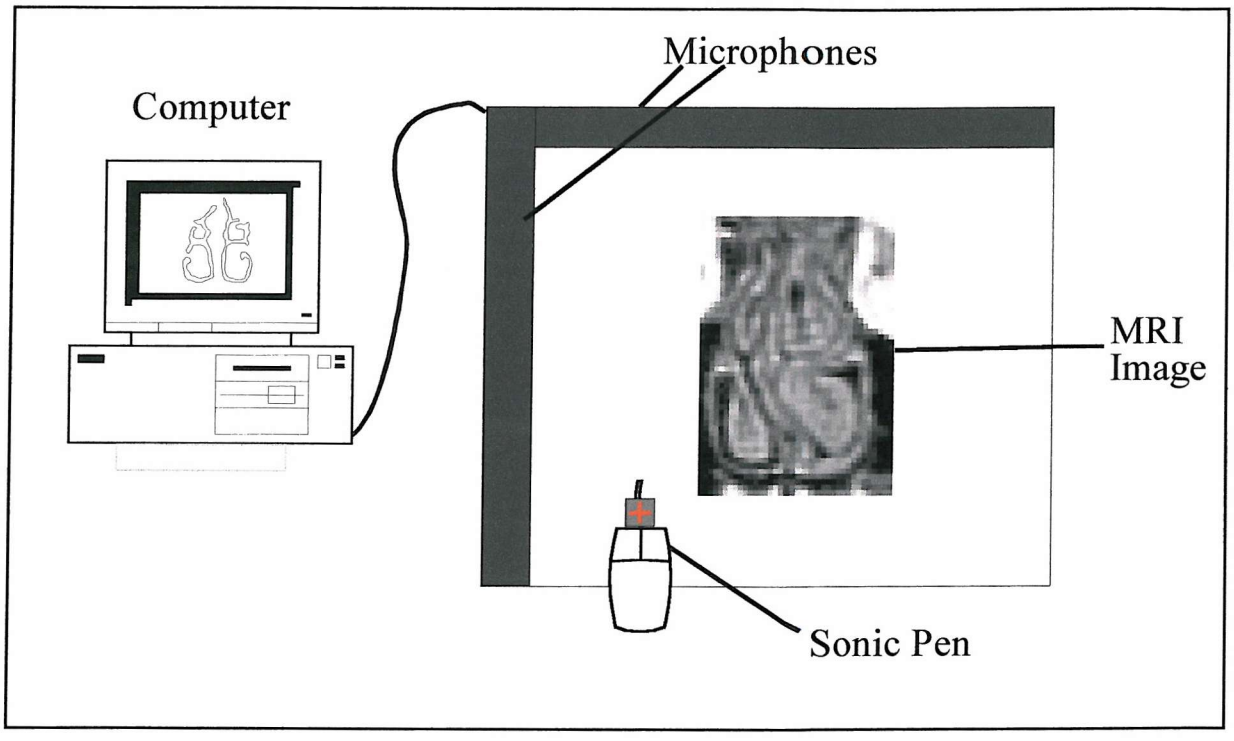

Figure 4.1: Set-up for digitising the geometries

For digitisation, the geometries were printed onto paper and redrawn using a sonic pen, as shown in Figure 4.1. The co-ordinates of the sonic pen were recorded using two microphones and so it was possible to store the vectors from point-to-point.

As described above two casts from different subjects, who are called subject 1 and 2. Also two different sets of nostrils were made, who are called subject 3 and 4. All four casts were derived from men without former respiratory diseases, subject 1 and 2 ethnic Caucasian, subject 3 ethnic Afro-American and subject 4 ethnic Asian.

Figure 4.2 shows all the perimeters of subject 1 as they were digitised starting from the throat (image1) to the tip of the nose (image 34). Figure 4.3 shows the perimeters of subject 2, from the throat to the tip of the nose, image 1-37. As mentioned above, the sets of nostrils stop before the first turbinate appears, therefore, the connection plates to cast 1 and 2 are made before the first turbinate. Additionally connections were made between cast 1 and nostrils of cast 2 and vice versa.

Also connections for casts and the two nostril sets were made. They start after geometry 25 for cast 1, and for cast 2 after geometry 27. Therefore, connection plates were made between geometry 25 of subject 1 and the first geometry of subject 3 or 4, called in both cases geometry 28, and geometry 27 of subject 2 with the first geometry of subject 3 or 4 (geometry 28). The subjects for the nostril sets were not only chosen for their ethnic affiliation but also because the same side of the nose was restricted as in subject 1 and 2.

Figure 4.4 and Figure 4.5 show the perimeters of the nostril sets 3 and 4 respectively.

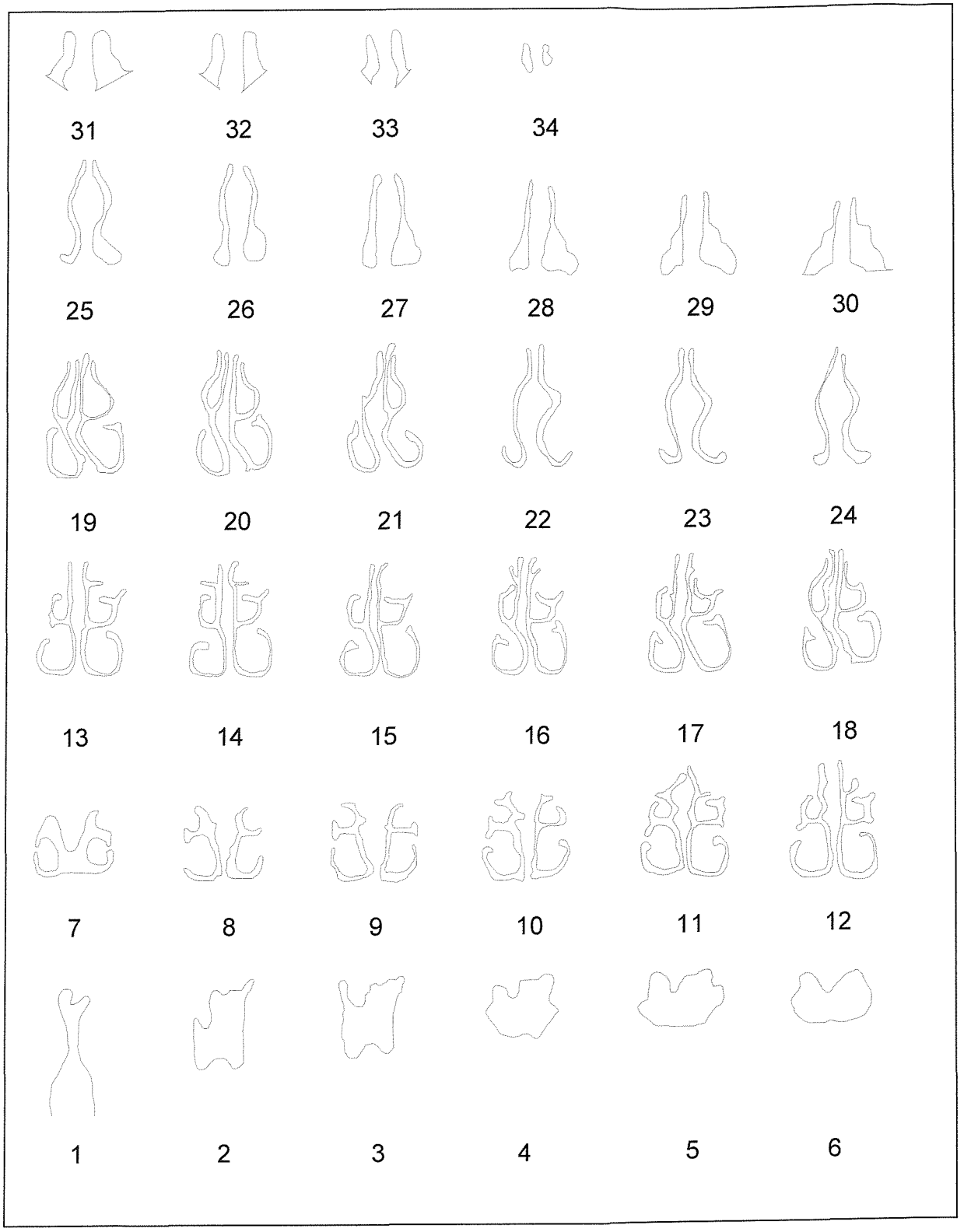

Figure 4.2: Perimeters of subject 1

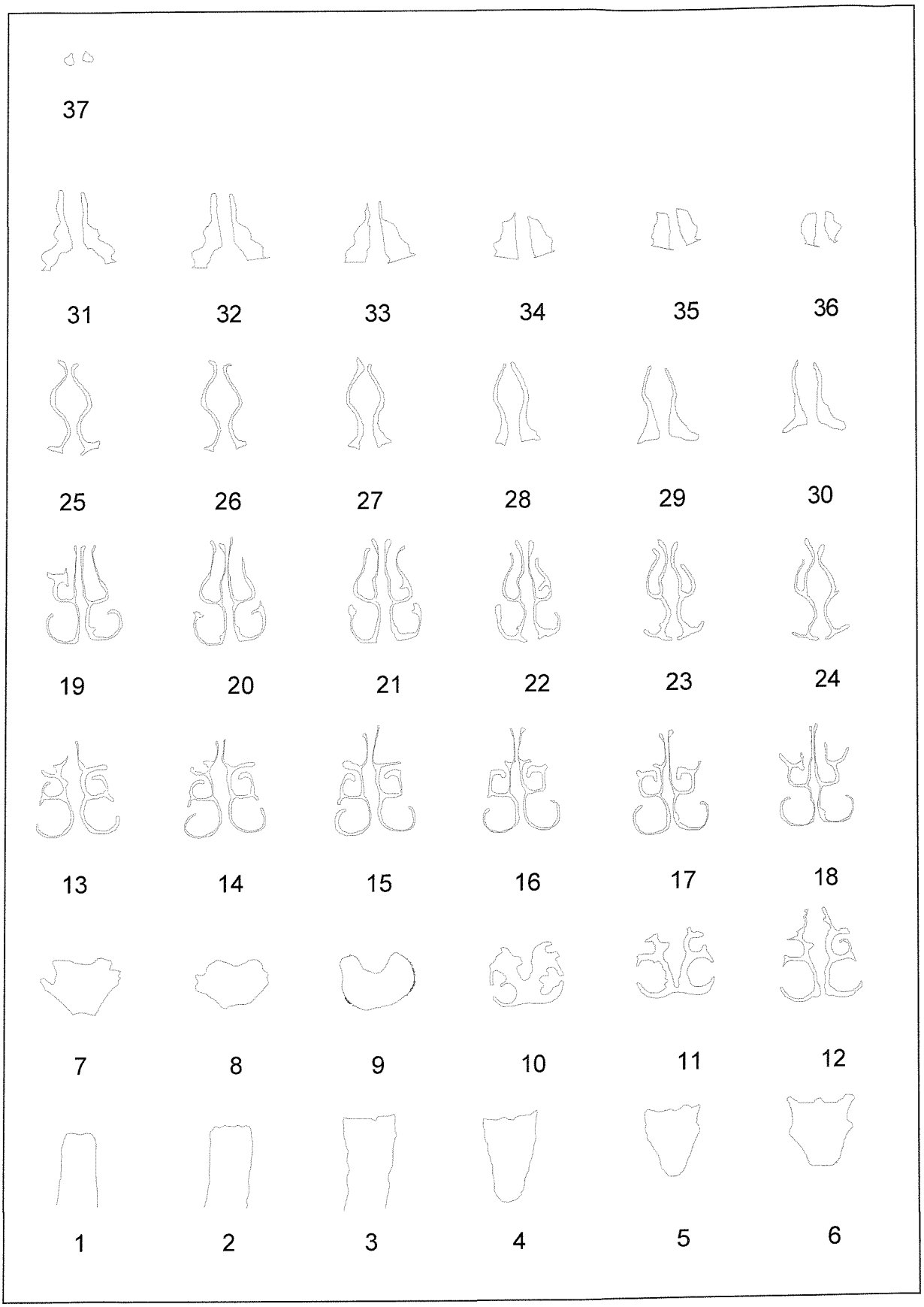

Figure 4.3: Perimeters of subject 2

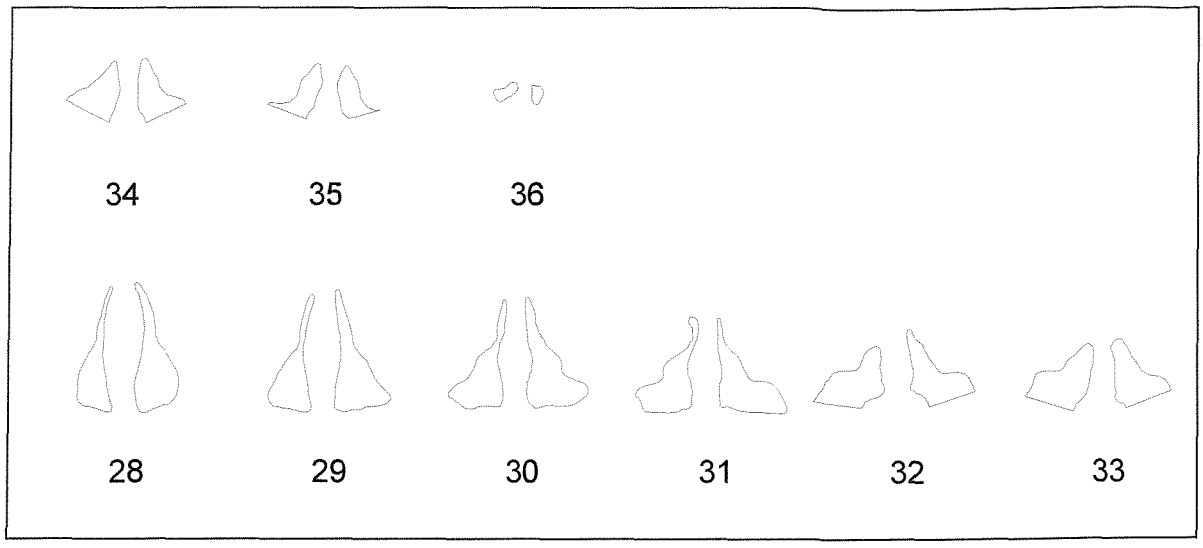

Figure 4.4: Perimeters of nostril 3

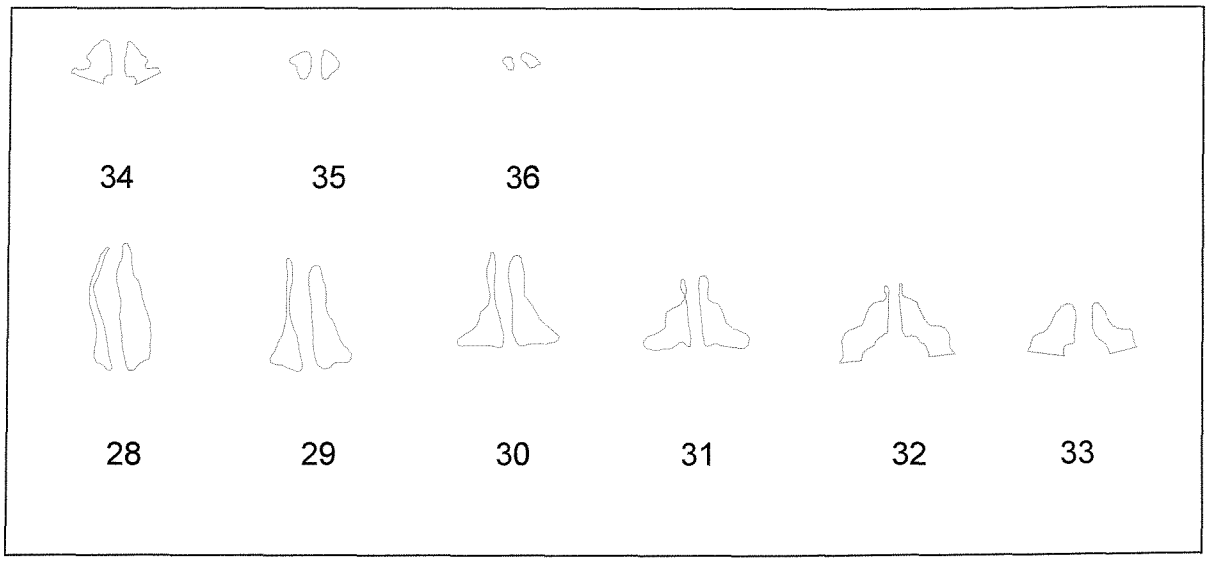

Figure 4.5: Perimeters of subject 4

With the exception of the first and last plates, the perimeters (defined as *.dxf files) are imported to the "Smart-Cam" software two at a time. Two adjacent perimeters are assigned different z-co-ordinates, separated by a distance of 3 mm, and then connected by a numerically defined tool-path, as shown in Figure 4.6 (repeating the process until all the tool-paths are defined).

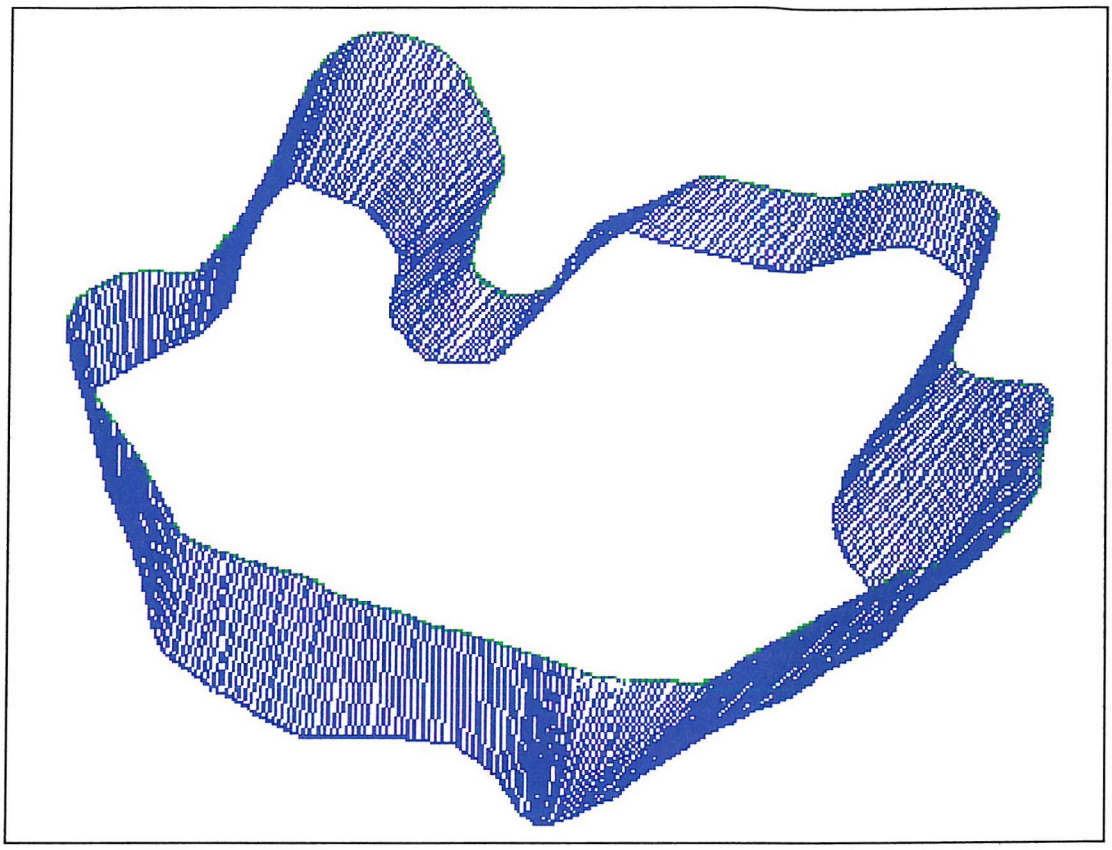

Figure 4.6: Perimeters 3 and 4 (subject 2) connected by a tool-path

As the first and the last perimeters end abruptly a smoother ending had to be devised. These geometries were merged smaller and smaller and each of the smaller geometries set a bit deeper. This method led to a curve, 2.6 mm deep for each geometry 1 and 1.2 mm deep for each of the last geometries.

The endmill could not cut deeper than 1.5 mm, but the MRI scans were 3 mm apart. Therefore two plates, each 1.5 mm thick, had to be milled, instead of one 3mm thick. For that reason, an intermediate, substitute perimeter was created by cutting the tool-path horizontally in half and storing the halves in two separate files, as for example, geometry 3-4 top and 3-4 bottom (abbreviated and carved at the plates 3-4 TOP and 3-4 BOT).

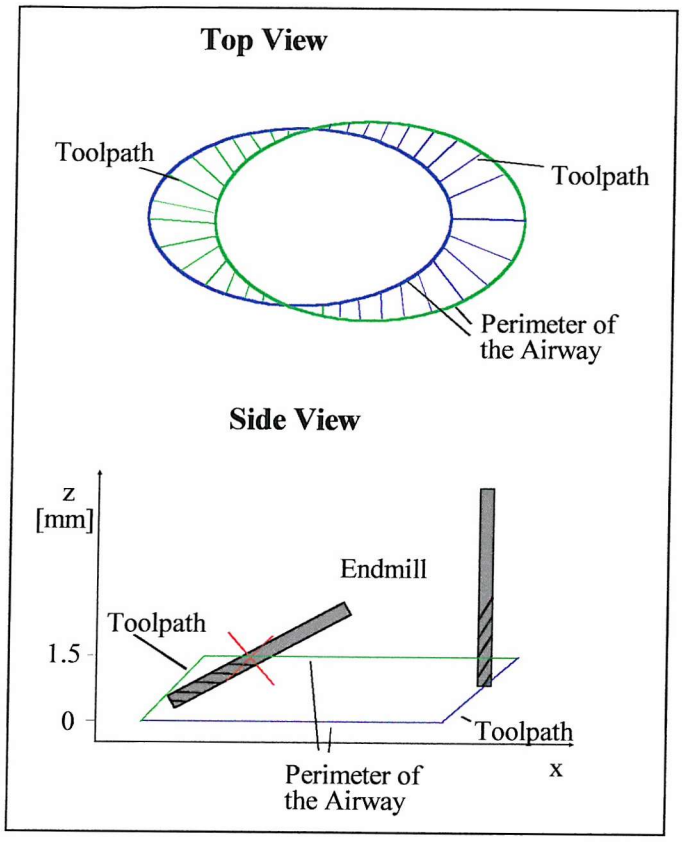

Figure 4.7 shows two simplified geometries with the green perimeter above the blue one. The milling machine can only move in the x,- y-and z- co-ordinate directions. The cutting head cannot be angled and so the plates must be milled from two sides, which can easily be distinguished from the top view.

If the green tool-path is outside, it must be milled from the front, whereas, if the blue one is on the outside, it must be milled from the back.

Figure 4.7: Schematic perimeters in top and side view.

Figure 4.8 shows two real perimeters, again with the green on top of the blue. Two actual tool-paths are shown in Figure 4.9. The blue tool-path must be milled from the front, and the green from the back.

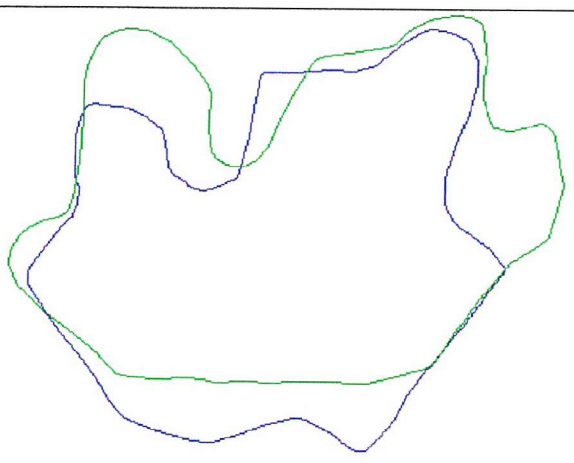

Figure 4.8: Perimeters in top view

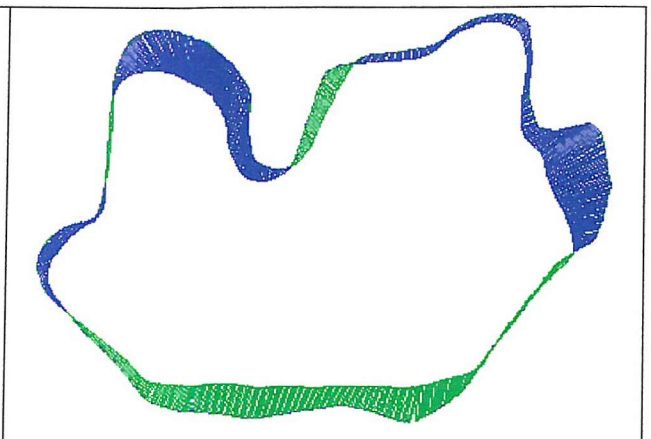

Figure 4.9: Tool-paths in top view

For positioning after flipping, two holes with known co-ordinates were inserted in the plates while milling the front side. Each plate was also identified, on the front side, by engraving the plate number and the subject's number.

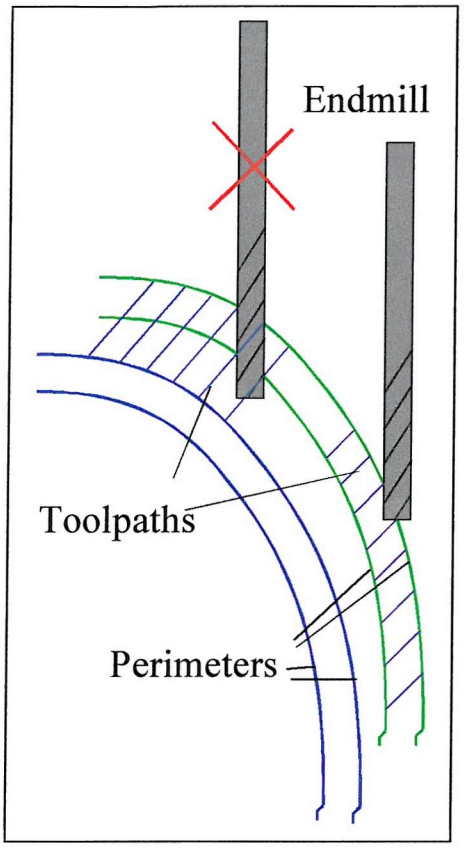

Though the end-mill is very fine (0.2 mm diameter), there were practical limitations regarding its ability to cut the narrower airway profiles.

This is because the cutter could not be angled (though angular cuts could be made, by simultaneously moving the end-mill in more than one co-ordinate direction, as for the larger airways). In the turbinate region, the airways are sometimes very narrow and full-depth end-milling would remove too much material, resulting in the airways being much wider than required.

However, the tool-path could be shortened which prevented the end-mill from cutting in too deeply and removing excessive material.

Figure 4.10: Schematic narrow airway

The schematic diagram of Figure 4.10 shows that the tool-path could only extend to the adjacent airway perimeter (viewed from above) for restricted geometries such as this. Any excess material had to be removed by hand with the end-mill cutter mounted in a dental drill. A second type of hand finishing, used on all the plates, was the blending of consecutive profiles, two at a time, by edge-smoothing (again using the end-mill cutter in the dentist's drill). This procedure, which was performed under a microscope (about x20), was necessary since plate thickness varied between about 1.47 and 1.52 mm which led to imperfect matching. The square acrylic plates all have an alignment hole in each corner. Four brass studs pass through these corner holes and hold the plates together as an aligned assembly. After assembling the cast, the nostrils were shaped according to photos of the nostrils in vivo.

5 DESIGN AND DEVELOPMENT OF THE BREATHING SIMULATOR

In order to deliver particles to the nasal cast, it was necessary to develop a device which "breathed" air and aerosol through the cast. This device was required to be able to simulate human breathing patterns at flow rates that are typical for humans. For the purpose of these experiments a breathing rate up to 50 L/min was sufficient. This is the flow rate humans achieve during light exercise. The reason for this limitation was that nasal airflow only was to be simulated and airflow in the nose is restricted as described in section 2.1.2. The human breathing pattern used for simulation was recorded from in-vivo experiments in which particles were administered to human volunteers who were at rest or performing light exercise. The simulator was also required to enable the generation of artificial breathing patterns e.g. sinusoidal waves. An example of a human airflow pattern is shown below.

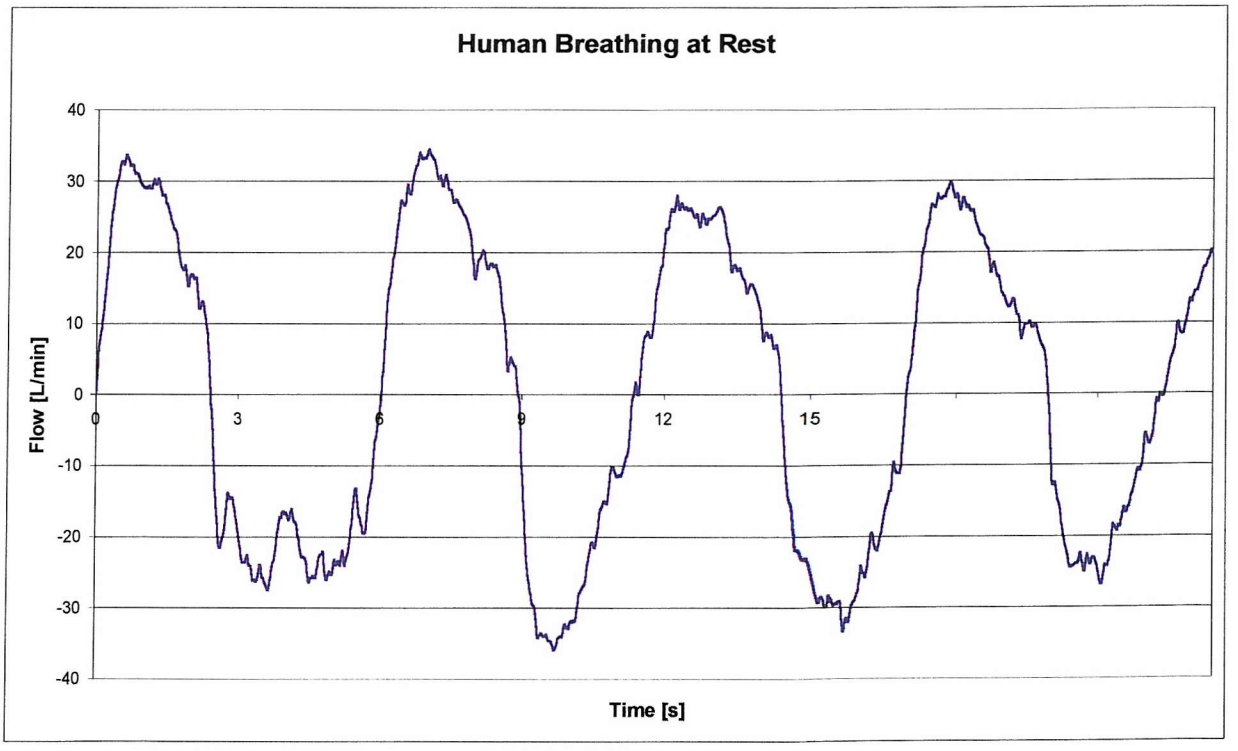

Figure 5.1: Airflow pattern of a human volunteer

In order to simulate such breathing an electromechanical device is needed. Several devices have been built to simulate human breathing, although most of them can only drive

predefined patterns such as sinusoidal waveforms. A few of the devices are more sophisticated and are able to drive user-defined patterns.

One device with the tradename "Electronic Lung" (MacArthur & Fleck 1997) was developed by Technology Partnership and is described by Brindley et al (Brindley et al 1994). It is specially designed to draw aerosol from several sources (for instance dry powder inhalers) through size measuring devices such as cascade impactors. High-speed airflow profiles (for example 4L in 0.2 sec) are required with varying rates and accelerations to overcome the resistance of the dry powder inhaler and the impactor. This device delivers required profiles closely (Burnell et al 1998), but the emphasis appears to be on high speed rather than precision.

Therefore another device was designed and built here to fulfil the requirements of those experiments which are described in Objectives on page 38. The different considerations for the design are described in the sections below. Afterwards the individual parts of the device, its control and its validation are outlined.

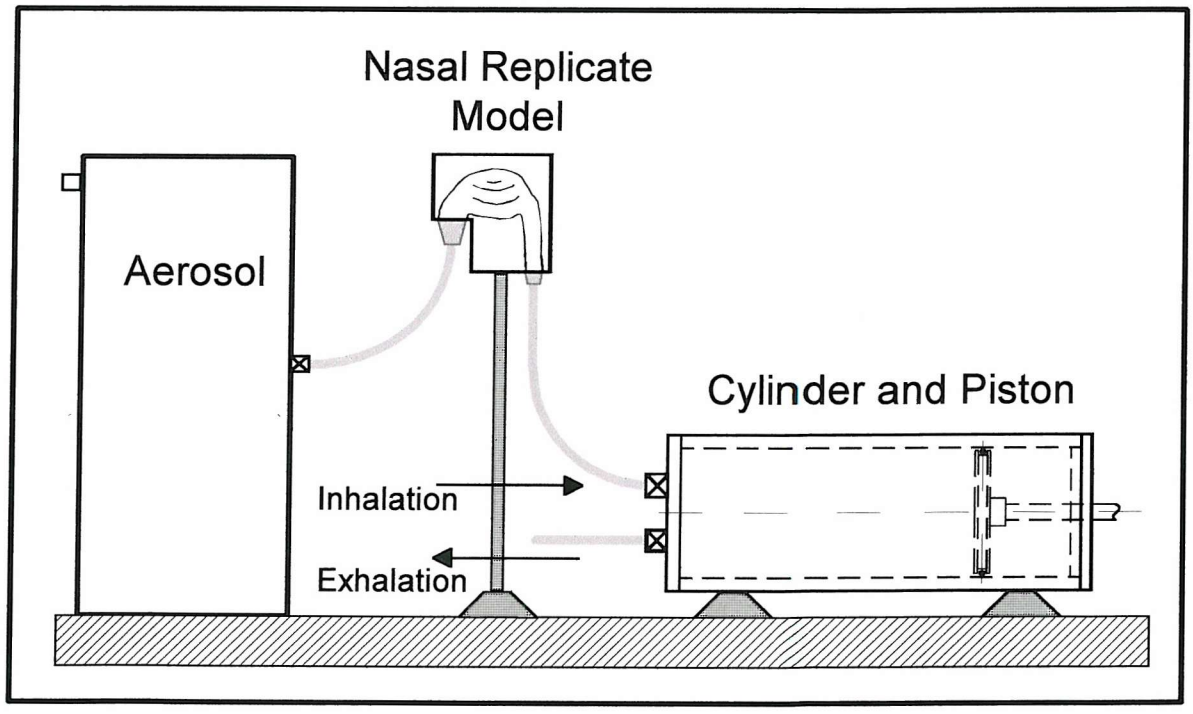

Figure 5.2: Schematic drawing of experimental set-up

5.1 CONCEPTUAL DESIGN OF CONTROL AND POWER TRANSMISSION

To control the drive pattern mechanical methods (e.g. cam-control) are possible, but they are not flexible enough, since flow and volume change constantly in human breathing, and each breathing cycle is different from the one before. Therefore the motor which drives the system has to be computer controlled to be flexible enough. The rotation of the motor has to be transmitted into a translational motion of the piston. The power transmission could be a drive belt, a threaded rod, or a crankshaft. The drive belt was not considered because it is difficult to avoid slippage of the belt, which makes it difficult to have precise movement. The threaded rod (called a linear actuator) and the crankshaft are discussed below.

5.1.1 CRANKSHAFT

The transmission principle of the motor power to the piston via a crankshaft is shown in Figure 5.3.

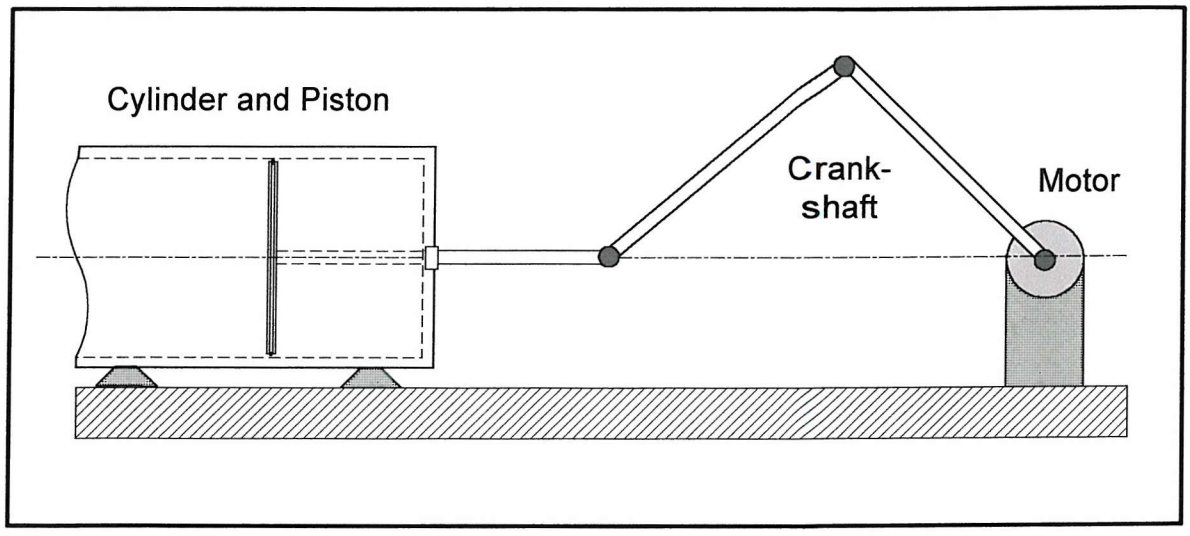

Figure 5.3: Power transmission by a crankshaft

Using the crankshaft design, the piston could be displaced fast, without driving the motor fast. It would be straightforward to drive a sinusoid artificial breathing pattern, just letting the crankshaft rotate. However the bearing for the reciprocating rod must be strong, because the centrifugal forces in this system are not static and the motor must be able to

withstand the fluctuation. The crankshaft would be superior to a linear actuator for driving pattern with always the same volume, because then the motor could always rotate in the same direction. But since the volume is always varying in human breathing, the motor has to change direction It was therefore easier to take a linear power transmission, because the forces are more static and linear actuators are very common and easy to obtain.

5.1.2 LINEAR ACTUATOR

The chosen solution is sketched in Figure 5.4 showing a configuration in which the motor shaft is connected to a linear actuator. The linear actuator consists of a threaded rod which passes through a trapped nut, known as a lead screw. Since the trapped nut cannot rotate, this arrangement allows drive to be transmitted to the piston. Piston speed is determined by both the pitch of the thread and the rotational speed of the motor. Piston direction is given by to the rotational direction of the motor.

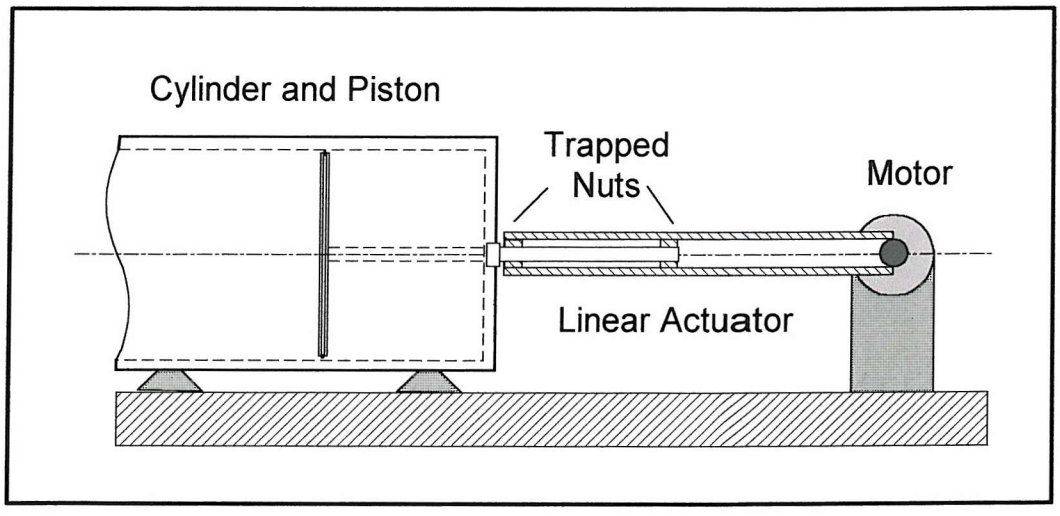

Figure 5.4: Power transmission using linear actuator

The advantages of this system are that the driven volume is only limited by the cylinder specifications and length of the linear drive, the transmission is linear and the forces are more static than in the other system. The disadvantages of this system are that the demand on the motor is high, with fast acceleration and deceleration rates at high torque. The motor must be able to drive high velocities at high torque for this design.

5.2 COMPONENTS OF THE BREATHING SIMULATOR - OPTIONS AND SPECIFICATIONS

The cylinder has inlet and outlet valves to enable the performance of inhalation and exhalation to be measured separately if required. Piston displacement is achieved by a synchronous motor via a linear actuator utilising a lead screw. The drive signal for the motor is generated by a personal computer and has to be processed by a hardware controller. A diagram of the breathing simulator is shown in the figure below.

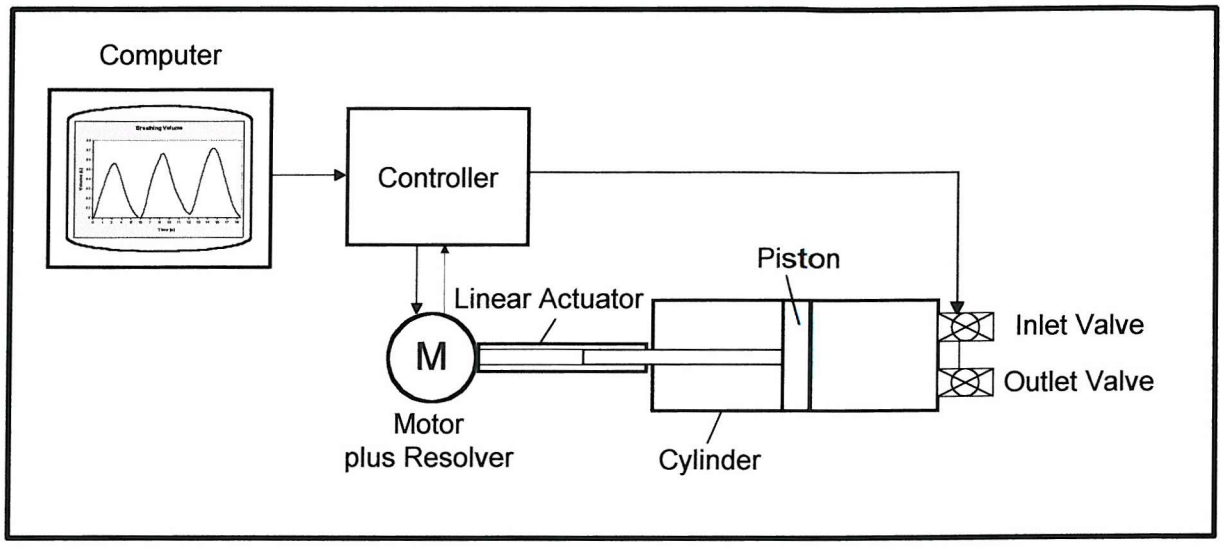

Figure 5.5: Conceptual Draft of the Breathing Simulator

The specifications of the individual parts of the breathing simulator are described in the following sections.

5.2.1 CYLINDER AND PISTON

The specifications of the cylinder are determined by the required volume and the travel distance of the piston. The cylinder material should not promote electrostatic charging as this could lead to aerosol deposition in the cylinder, especially in the case of charged aerosols. It should be inert and transparency would be an advantage since the position of the piston and any deposition of aerosol could then be observed easily. The latter was not considered feasible since precision glass cylinders tend to be very expensive and fragile.

Stainless steel is an acceptable and less expensive alternative material but unfortunately not transparent.

The total volume of the pump is 3 L. The choice had to be made between a short travelling distance of the piston, with slower motor movement and, therefore, a large diameter of the piston, or high accuracy, with a long travelling distance for the piston, faster motor movement, and a small diameter of the cylinder. A good compromise reached was to use a cylinder diameter of 120 mm. The displacement of the piston was then about 50 mm for a normal tidal volume (600 mL) and for the maximal volume (3000 mL) about 265 mm.

The piston was also made from stainless steel. An appropriate sealing had to be chosen. Many seals cause less frictional loss than O-rings, but it is believed that the friction of an O-ring is needed to dampen the inertial forces, which the system experiences while changing direction.

5.2.2 Selection of the Motor

Motors are specified by speed and torque they can produce. The speed is determined by the lead of the linear actuator and the diameter of the cylinder. The torque of the motor is determined by losses due to: the friction of airflow in the system, the friction of the linear actuator and the friction of the O-ring determine the torque of the motor. Therefore these losses where determined below.

Losses in the System and Calculation of Required Motor Power

Pressure Loss in the Tubing

The nasal casts and the connecting tubing form the cast to the pump have a certain resistance to airflow. Also a filter had to be used to prevent radioactive material to reach the ambient air.

A few statements on fluid mechanics are appropriate. Due to relative movement between layers shear forces are present in a fluid. These forces depend on the viscosity of the fluid and its velocity. If the viscosity is independent of the velocity gradient in straight and parallel flow, the fluid is called a Newtonian fluid. If a gas undergoes a negligible change of volume under pressure, its behaviour is similar to that of liquid and it may be regarded as

incompressible. A gas which is incompressible can then be regarded as a Newtonian fluid. The equations used later on are equations for Newtonian fluids.

Steady flow is a condition where velocity, pressure and density at any point do not change with time. For the breathing pattern used here, the velocity changes over time and the flow is therefore not steady. The calculation of unsteady flow is much more complex than for steady flow and easier to perform empirically. Consequently, in this calculation the flow is assumed to be steady, and a maximum and a minimum velocity is used.

Additionally the flow is non-uniform, because the diameters of the different compartments in the system are not equal. Nevertheless it is possible to perform calculations for the single compartments one by one and so treat the flow in these compartments as uniform. The compartments are the filter, the cast, the cylinder and the tubing as shown below in Figure 5.6.

The shear forces in the fluid cause a pressure loss in the system. In laminar flow this loss is much less than in turbulent flow. Therefore, laminar and turbulent flow are very different in their effects. An indication of flow type is the Reynolds Number (Re), which is dependent on flow velocity, viscosity and density of the fluid and pipe diameter. $Re < 2000$ indicates laminar flow and $Re > 4000$ indicates turbulent flow. For the intermediate range the state of flow depends on its history, so to be on the safe side turbulence was assumed above Reynolds number of 2000.

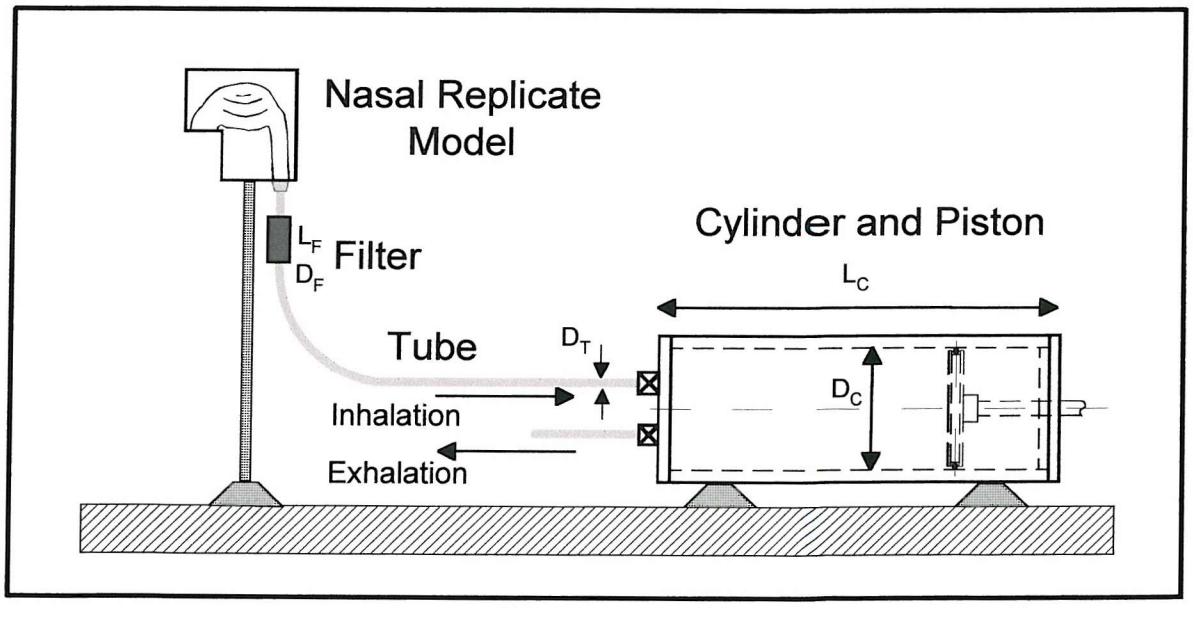

Figure 5.6: Schematic drawing of the compartments of airflow

CALCULATION OF THE LOSSES

The pressure loss depends on the dimensions of the vessels and the velocity of airflow through them. The dimensions used in the calculations are:

	Length [cm]	Diameter [cm]
Tubing	100	1.7
Filter	5	0.5
Cylinder	30	12

To determine the velocity of airflow two human breathing manoeuvres were used. Breathing at rest, which is assumed to be normal breathing behaviour and forced expiration volume in 1 second, which is the most extreme breathing manoeuvre and should therefore give the highest losses. The breathing volume of a human at rest is about 600 mL inhaled in 2.5 sec. The maximum volume that can be exhaled in 1 second is about 3000 mL. This volume is called FEV_1.

The equation below is used to determine the velocity of airflow in the cylinder:

$$v = \frac{V}{A * t}$$ **Equation 5.1**

v = velocity [m/s] V = breathing volume [mL]

A = cross section of the tube [m^2] t = breathing time [s]

(Miller 1971; Miller 1978)

The velocities in the other tubes can be calculated according to the equation:

$$v_1 = \frac{v_2 * A_1}{A_2}$$ **Equation 5.2**

where:

v_1 and v_2 are velocities in two tubes of different diameter

A_1 and A_2 are the corresponding cross-sectional areas

(Miller 1971; Miller 1978)

The velocities are as follows:

	Breathing at rest	FEV_1
Velocity in cylinder	$2.1*10^{-2}$ [m/s]	$26.5*10^{-2}$ [m/s]
Velocity in tube	1.05 [m/s]	13.2 [m/s]
Velocity in filter	12.12 [m/s]	152.9 [m/s]

The Reynolds Number (Re) indicates whether the flow is laminar or turbulent in the compartments.

$$Re = \frac{\rho * v * d}{2 * \eta}$$ **Equation 5.3**

v = flow velocity [m/s] d = tube diameter [m]

ρ = fluid density [kg/m^3] η = absolute fluid viscosity for air [kg/ms]

for air ρ = 1.139 kg/m^3 η = 18.93 x 10^{-6} kg/ms

The loss of pressure in a pipe during laminar flow is

$$\Delta p = \frac{\rho * v^2 * l}{2 * Re * d}$$ **Equation 5.4**

Equation 5.3 inserted in Equation 5.4:

$$\Delta p = \frac{v * l * \eta}{d^2}$$ **Equation 5.5**

Δp = pressure loss [kg/ms^2] d = tube diameter [m]

l = tube length [m] Re = Reynold's number [1]

v = flow velocity [m/s]

ρ = fluid density [kg/m^3] η = absolute fluid viscosity for [kg/ms]

for air ρ = 1.139 kg/m^3 air η = 18.93 x 10^{-6} kg/ms

(Miller 1971; Miller 1978)

The loss of pressure in a pipe during turbulent flow is

$$\Delta p = \tfrac{1}{2} v^2 \frac{\lambda * l}{d}$$ **Equation 5.6**

where λ = friction of the pipe surface

$\lambda = 0{,}3164/(Re)^{1/4}$ for $2320 < Re < 10^5$

(Beitz & Kuettner 1995)

The formula for the pressure loss in the nose can be found in ICRP 66, where the pressure loss in the nose is described as $0.15 \frac{kN}{m^2 * L}$ (ICRP 1994)

	breathing at rest	FEV_1
pressure loss in tubing	$6.87 * 10^{-2}$ N/m²	0.86 N/m²
pressure loss in filter	0.92 N/m²	11.58 N/m²
pressure loss in cylinder	$5.09 * 10^{-6}$ N/m²	$1.85 * 10^{-4}$ N/m²
pressure loss in nose (ICRP66)	90 N/m²	450 N/m²

The losses in the different sections can be taken to calculate the force F, which is required to overcome the calculated pressure losses

$$F = \Delta p * A \qquad \textbf{Equation 5.7}$$

If one sums the single forces, the total force to overcome the friction due to airflow at rest is 90 N and for the forced expiration manoeuvre it is 462 N.

Friction of the O-Ring

The friction caused by a reciprocating O-ring can be determined according to Martini (Martini 1984), who developed a graphical method. The diagrams are called nomogram and dynamic frictional forces can be determined. Static friction is higher than dynamic friction as explained later.

Dynamic Friction:

Martini developed a nomogram method, where: " The amount of dynamic friction caused by an elastomeric O-ring seal used in a reciprocating application can be approximated using nomograms. These were devised from theoretical modelling and empirical data." "The first Figure gives the O-ring friction caused by the differential pressure across the O-ring sealing surface, while the second Figure gives the O-ring friction caused by the squeeze incurred by

the O-ring seal. The total dynamic friction is the sum of the dynamic friction from both nomograms." (page 116)

The O-ring used in this application has an outer diameter of D_O = 120 mm (4.7 in) and a cross-sectional diameter of W = 7 mm (0.275 in).

The differential pressure Δp is the pressure of the gas, which is to be sealed, and was calculated in the section above. The pressure across the piston is therefore $\Delta p = 463.5$ N/m^2 (0.07 psi).

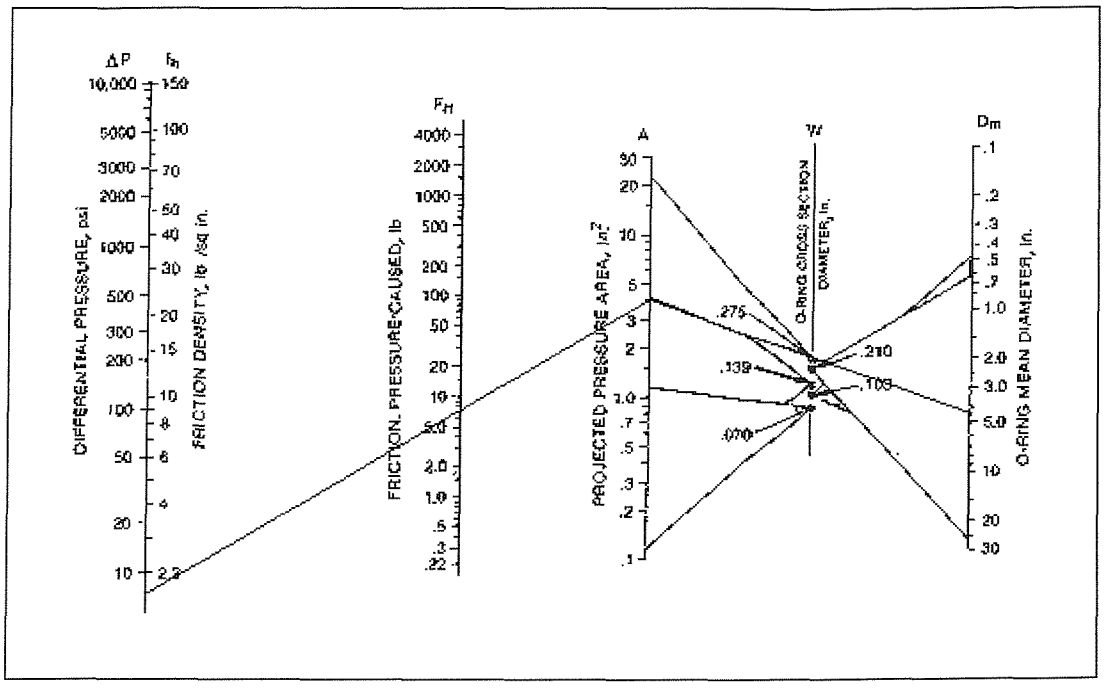

Figure 5.7: O-ring friction due to differential pressure

Using Figure 5.7 for nominal dynamic friction it is

D_m = 120 mm - 7 mm = 113 mm (4.425 in)

W = 7 mm (0.275 in)

$\Delta p = 463.5$ N/m^2 (0.07 psi)

one finds that the projected area is 4 in^2, Δp is off the diagram, but extrapolating one finds the force which is friction F_H = 8 lbf, F_H = 35.6 N.

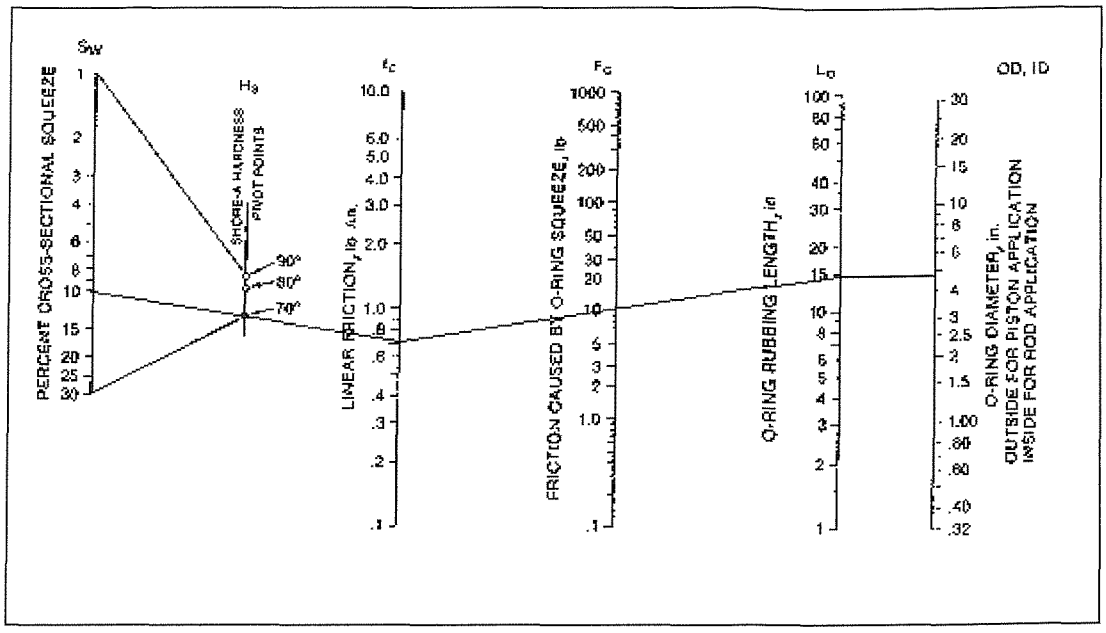

Figure 5.8: O-ring friction due to cross-sectional squeeze

Using Figure 5.8

D_O = 120 mm = 4.7 in

squeeze S_W = 10 %

Shore hardness H_S = 70

If one draws a horizontal line one finds L_0 = 15 in. Coming from the other side f_C is 0.7 lb/in, therefore F_C is then 10 lbf, F_C = 44.5 N.

The nominal dynamic friction is F = 44.5 + 35.6 = 80.1 N

STATIC FRICTION

The static friction is the force that is needed to start the motion. It is normally about 1.5 times the force required to maintain motion. This force can increase with the time the piston stands still, because the rubber has time to flow into the surface irregularities. Within the first 200 hours it increases to 3 times the dynamic force.

The nominal static friction is 3x80.1 = 240 N

THE REQUIRED TORQUE TO MOVE THE LINEAR ACTUATOR

The motor has to move the piston via the lead screw and by doing this to overcome the various frictional forces. But not only friction has to be taken into account, also the force to turn the lead screw. The torque necessary to turn the lead screw is calculated according to following equation:

$$T = \frac{F_R * p}{2 * \pi} \qquad \textbf{Equation 5.8}$$

where T = Torque [Nm] p = pitch of the thread $0.05*10^{-3}$m

F_R = total frictional forces, calculated above

(Beitz & Kuettner 1995)

REQUIRED TORQUE OF THE MOTOR

The losses caused by airflow, piston movement and linear actuator were summarised to determine the torque of the motor. The torque for breathing at rest is T= 13 Ncm and for the forced exhalation manoeuvre is T = 42 Ncm.

SELECTION OF THE MOTOR

Two kinds of motors are normally used for controlled applications, stepper motors and synchronous motors. Stepper motors are usually used for speed or position control. They are ideal for point to point position, and do not need a closed loop (feed back) for the position control. They need little maintenance and are relatively cheap. Stepper motors can operate either with high-friction loads or at high speeds, but not both. The solution of a linear actuator driving the piston, which was introduced before, needs a motor which can withstand high loads, and must accelerate and decelerate very quickly.

Therefore, a brushless synchronous motor was chosen for this application. It has low inner inertia, which is crucial for high acceleration, and is able to operate with high loads. For this kind of motor a closed loop control must be implemented, as described later in section 5.2.5.

The rotor is formed as a permanent magnet, and is rotated by means of a three-phase stator winding. It has a resolver mounted on one side, to enable speed and position control.

The 3-phase sinusoidal rotating field is steered true to the angle by the resolver or by its exploitation respectively, so that in every rotor position, an optimum current supply of the stator follows: The rotational speed of the synchronised motor is proportional to the rotation frequency of the stators. The principle of the speed control with cascade current regulator finds application here. The resolver also provides an incremental output. Two main digital pulse trains are generated, one at the phase angle of 90° to the other in order for the direction of rotation to be indicated. Mattke Antriebstechnik supplied the motor with the resolver mounted on it.

5.2.3 Linear Actuator

As mentioned above, the movement of the motor was transmitted to the piston via a lead screw. It was necessary to chose a lead screw which can withstand the forces in the system and the lead must be sufficient to keep the movement of the motor slow.

The linear actuator CATR33Hx300x4G2, manufactured by SKF was chosen. It has a maximum displacement of 300 mm and a lead (displacement at one rotation) of 1.27 mm. The maximum dynamic load is 1000 N and the maximum static load is 4000 N. Compared with the forces calculated in section 5.2.2 the maximum load for the linear actuator is more than sufficient.

5.2.4 Valves

The experimental set-up requires an inlet and an outlet valve on the cylinder to investigate deposition during either inhalation or exhalation or a whole breathing cycle. The inlet valve must be open and the outlet valve closed during inhalation and the settings reversed during exhalation. One possibility was to use non-return valves, which open and close mechanically with the flow of air. These would have been easy to implement, but the valve design causes too much resistance to airflow, and a certain air-pressure has to be reached before it opens. This would have caused a delay in opening. Additionally there is a tendency for aerosol particles to deposit in such valves by impaction.

For that reason valves were used which open and close under computer control. It was required that these valves have a low resistance to the airflow and a straight path for the airflow through the valve.

The pneumatic actuated ball valves (type PKB 70, supplied by W Adolph) fulfil these criteria. Valves with an inner diameter of 1" were chosen.

5.2.5 CONTROL OF THE DEVICE

Many applications for motor control are for constant motor speed and if the load is also constant an open loop system is usually sufficient. In this application neither the load nor the speed of the motor are constant and, therefore, a closed loop control has to be implemented. Here closed loop system uses the actual position of the motor and compares it with the desired signal at any time. The difference between those is called the error signal, which is used as the signal to drive the motor.

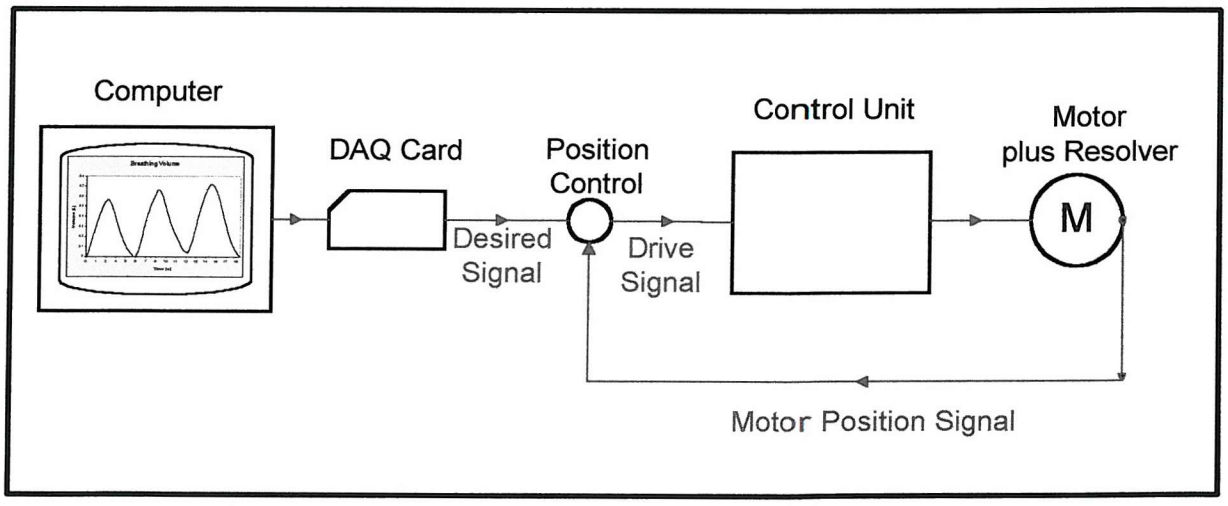

Figure 5.9: Block diagram of the motor control

The principle of the motor control system is as shown in Figure 5.9. The desired signal to be followed by the motor is sent from a PC via the D/A converter of a data acquisition card (DAQ) (National Instruments). It would be possible and cheaper to use the serial port of a PC for the output of the signal. However, the use of a DAQ card has the advantage of the card having a timer on it. This timer is independent of Windows operating system and can

be used to set the output rate. It is able to supply real time output, which is not possible over the serial port.

Attached to the motor is a resolver, which gives a signal proportional to the position of the rotor shaft of the motor. The digital signal of the resolver (1024 counts per revolution) is fed back to the position control unit. The signal is counted there, converted to an analogue signal and then compared with the desired signal from the computer. The difference between the desired signal and the actual signal is the drive signal for the motor. Additionally the position control gives the signal for opening and closing the valves on the cylinder, depending on the direction of motor rotation.

The control unit takes the signal from the position control and transforms it into a speed signal for the motor. For most applications it would be sufficient to have the control unit without the position control. But for the reciprocating piston position control is vital if drift is to be avoided and therefore it was incorporated.

Purpose-written software reads in the ASCII file in which the breathing pattern is stored and writes it to the analogue output of the DAQ card in real time.

CONTROL UNIT

The control unit, which is supplied with the motor by Mattke Antriebstechnik, provides the necessary current for the motor and has a four-quadrant regulator. A four-quadrant regulator has the ability to accelerate and brake in both directions of rotation. For braking it uses an internal ballast circuit, which can convert a maximal sustained-action brake output of 150 W into heat.

It has a speed regulation circuit that consists of a speed regulator and a motor-tacho-simulation-combination. The user set the motor speed by applying a voltage between –5 and +5 Volts.

POSITION CONTROL

Because the load is not static, due to the changing velocity (which causes changing frictional forces of air and sealing as described in section 0) the speed regulator alone does not prevent drift. The fluctuation of load can lead to slip of the rotor and therefore to

position errors of the piston when operated over a longer time. To avoid this drift of the piston, position control is implemented.

The digital signal of the resolver (1024 counts per revolution) attached to the motor is fed to the position control unit. When the piston travels from one end of the cylinder to another the resolver gives a total of 241889 (between 2^{17} and 2^{18}) pulses. For this reason the counter has to have a minimum of 18 bits to count the pulses over the whole distance. Of these the 12 upper counting bits are connected to a D/A converter. Connecting only the upper 12 bits loses some accuracy, but still 6 pulses per revolution of the motor are counted. Counting 6 pulses per 1.27 mm of travel gives 0.2 mm accuracy in position measurement. The output of the D/A converter is a signal of 0-10V, which is proportional to the position of the piston. The set value from the computer and the real value from the D/A converter are then compared in a proportional controller (p-controller) and the difference is output to the control unit. This is the position which the piston drives to.

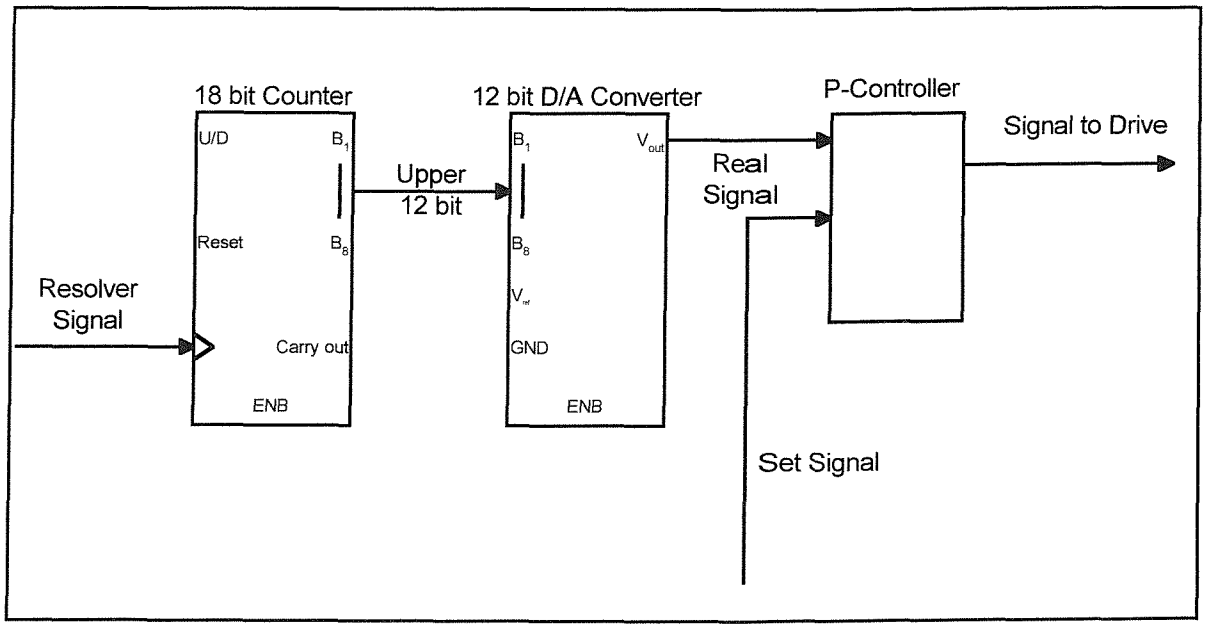

Figure 5.10: Block Diagram of Position Control

CONTROL OF THE VALVES

As described in section 5.2.4 one valve must be open for inhalation while the other one is closed and vice versa. Therefore opening and closing of the valves is initiated by a signal from the position control box. The output signal of the position controller is fed into a

comparator, which gives a digital output: 0 for exhalation and 1 for inhalation. The comparator is used to detect the direction and the valves switched accordingly. The comparator used has a hysteresis, which prevents the signal switching below a certain value. This hysteresis avoids the valves switching with noise. However, when the motor stands still the noise becomes too high. Therefore to avoid opening or closing of the valves while the motor stands still, the software described below disables switching of the valves and only enables it when the piston drives.

THE SOFTWARE TO CONTROL THE BREATHING SIMULATOR

Software was written for the output of the breathing pattern, its user interface is shown in Figure 5.11. The programming environment used was LabWindows/CVI from National Instruments. LabWindows/CVI is a programming environment for developing instrument control, automated test, and data acquisition applications based on ANSI C. Additionally it has many more functions and libraries to utilise a Data Acquisition (DAQ) card.

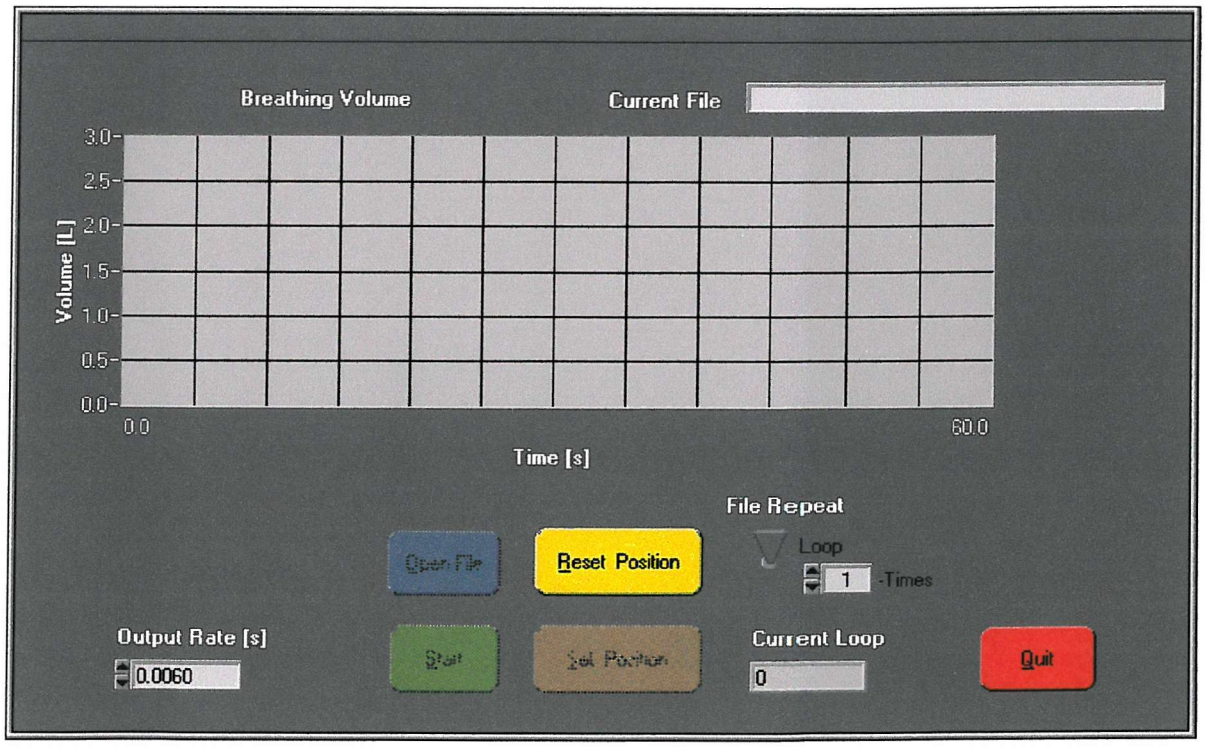

Figure 5.11: User Interface of Software

The single items on the User Interface are either for indication or call various routines, as described below.

Graph

The graph shows the desired breathing volume, to be driven by the piston.

Reset

This button has to be pressed first; it asks the user to reset the counters to zero in the position control, and enables the use of the start button.

Open

This opens an ASCII file containing the breathing pattern. It can either be a recorded pattern or an artificial one. The file contains one column of numbers which resemble the breathing volume.

Start/Stop

Pressing the start button enables the valves to open and close and then starts the output of the breathing pattern via the analogue output of the data acquisition card. Once the breathing operation has started, the start button changes colour and becomes the stop button.

The output is performed in double buffering mode, the advantages and operation of which are described as follows. For applications involving larger amounts of data output at high rates double buffering is required. LabWindows/CVI uses double buffering techniques for continuous, uninterrupted output of large amounts of data. For double buffered output operations the DAQ device retrieves data from the circular buffer for output. When the end of the buffer is reached, the device begins retrieving data from the beginning of the buffer again. The process constant ad infinitum until it is interrupted by a hardware error cleared by a function call.

Unlike single buffered operations, double buffered operations reuse the same buffer and are therefore able to input or output an infinite number of data points without requiring an infinite amount of memory. However, for double buffering to be useful, there must be a means to access the data for updating, storage, and processing.

To archive this the circular buffer is logically divided into two halves. By dividing the buffer into two halves, the DAQ card can co-ordinate user access to the data buffer. The co-ordination scheme is simple. The double-buffered output operation begins when the output device begins outputting data from the first half of the circular buffer. After the device begins retrieving data from the second half of the circular buffer, NI-DAQ can copy the prepared data from the transfer buffer to the first half of the circular buffer. The application can then update the data in the

transfer buffer. After the output device has finished accsessing the second half of the circular buffer, the device returns to the first half buffer and begins outputting its updated data. NI-DAQ can now copy the transfer buffer to the second half of the circular buffer. The data in the transfer buffer is again available for update by the users application. The process can be repeated endlessly to produce a continuous stream of output data from the application.

The application keeps on running either for the amount of chosen breathing pattern repeats or until the stop button is pressed.

Output Rate

Displays the output rate of the breathing pattern in seconds per output point and can be altered by the user. It must be the same rate as that used for recording the patterns or for generating the artificial patterns.

File Repeat

This enables the user to choose between an infinite or a finite number of file repetitions. A routine in the code counts the number of times breathing pattern has been repeated and ends the output after the defined number of loops is reached.

Current Loop

This displays the number of the current loop

Quit

Pressing Quit closes the software.

BREATHING PATTERN

The requirement for nasal deposition studies was to reproduce human breathing patterns as closely as possible. Typical nasal breathing patterns to be simulated were in the range of 20 L/min (peak flow at rest) to 50 L/min (peak flow at light exercise) (ICRP 1994).

The signals used to drive the simulator were either recorded human breathing patterns or artificial signals used for calibrating or other purposes. The flows of the human breathing patterns were measured with a pneumotachograph, a device which measures the pressure loss across a resistance to airflow and so determines the airflow. A computer recorded the signal of the pneumotachograph at a sample rate of 167 Hz. This signal was written in a file as ASCII code. This file was then integrated to give the volume/time profile and saved in a different file, which was then used to drive the motor.

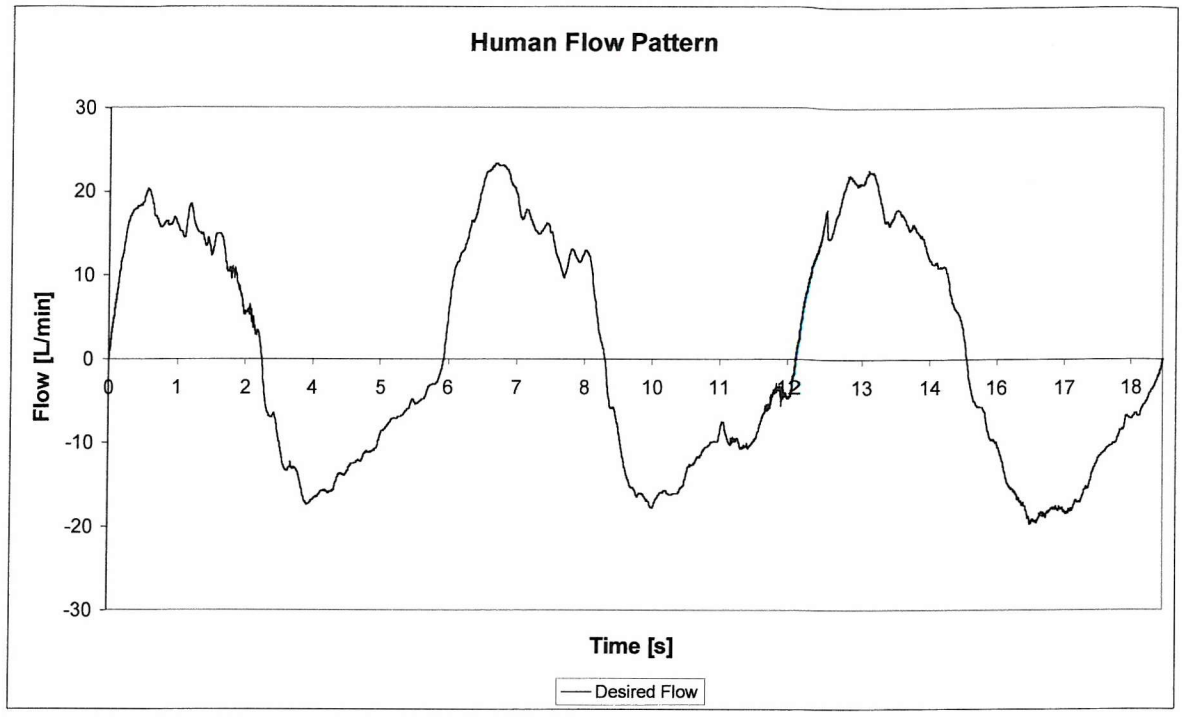

Figure 5.12: Human Flow

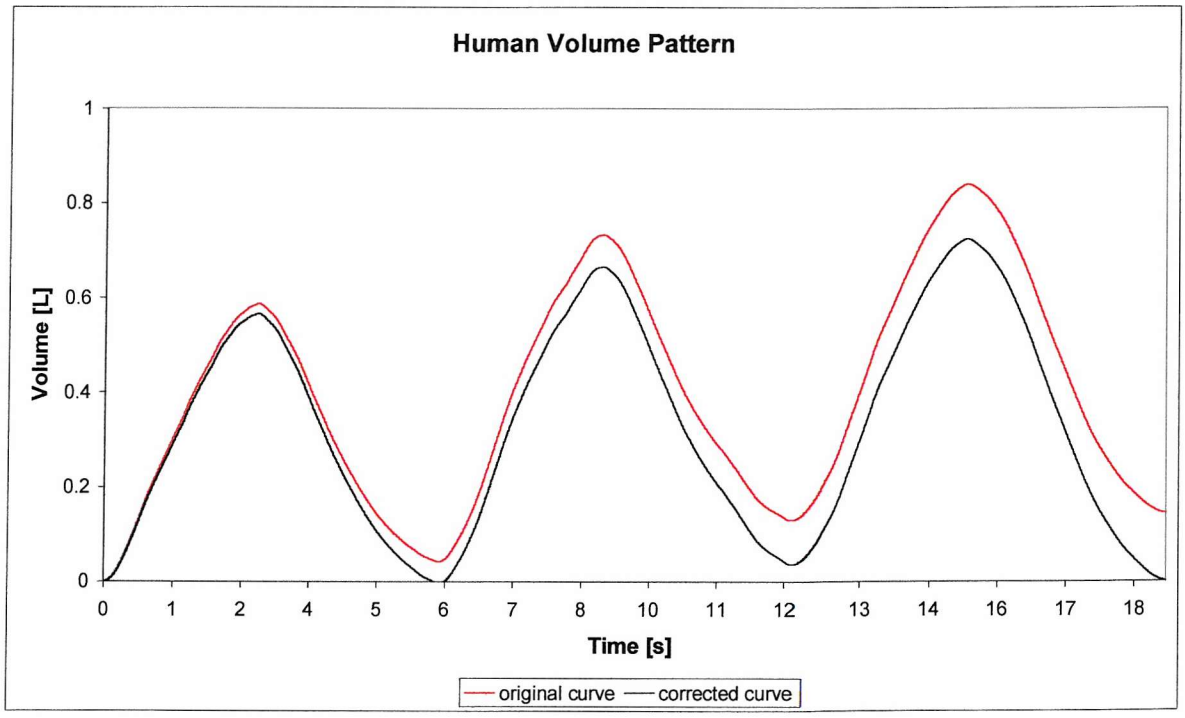

Figure 5.13: Integrated Volume

An example of a human breathing pattern is shown in Figure 5.12. A small offset or drift often occurs in measurements with the pneumotachograph and can accumulate during integration to give a significant error. Thus the volume/time curve very often drifts as shown in Figure 5.13 and the slope of the drift needed to be set to zero.
The artificial breathing patterns were generated in Microsoft Excel as flow numbers and then integrated. Particularly useful artificial breathing patterns are sine waves or rectangular waves.

5.2.6 THE BREATHING SIMULATOR ASSEMBLED

The parts are assembled as shown in Figure 5.14. The picture shows the cylinder in which the piston reciprocates and on which the inhalation and exhalation valves are mounted. The rotation of the motor is transformed into a translation by the linear actuator, which is connected to the piston. The motor is driven by the computer and controlled with the position control and the control unit.

To validate the breathing simulator the flow it produced was measured and compared with the desired flow as described below.

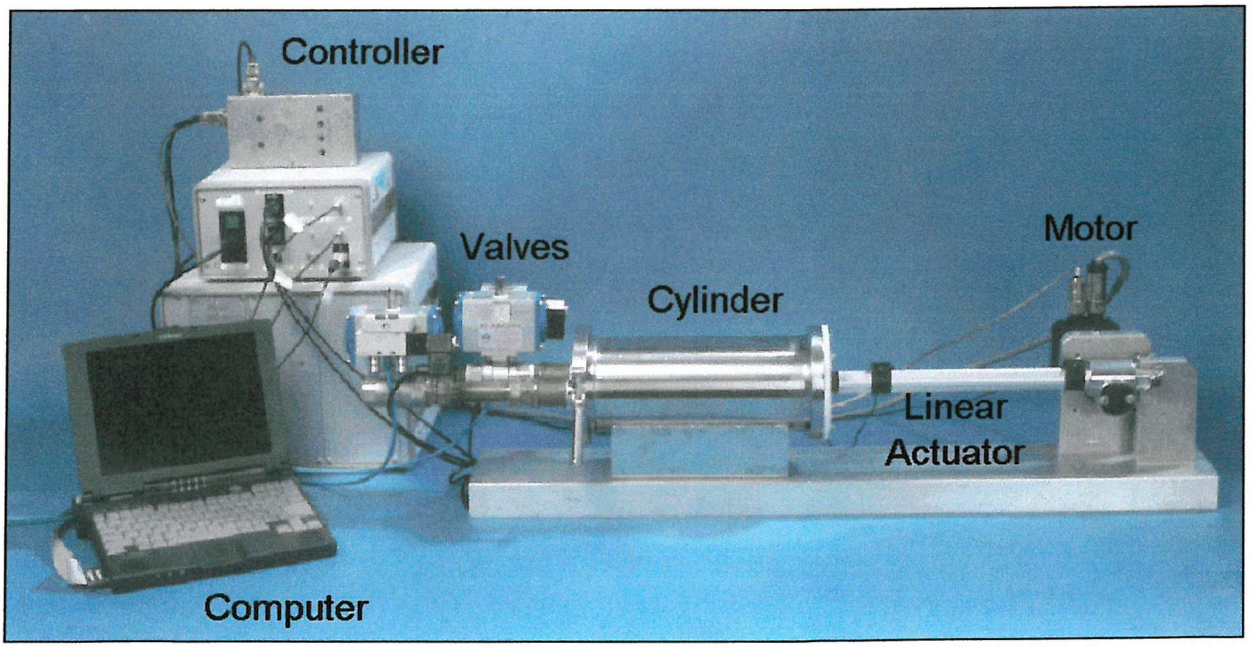

Figure 5.14 Photograph of the breathing simulator

5.2.7 VALIDATION OF THE BREATHING SIMULATOR

The flow pattern produced by the breathing simulator is measured using a pneumotachograph. A pneumotachograph is a device which measures the pressure loss across a resistance to airflow and so determines the airflow. A computer records the signal of the pneumotachograph at a sample rate of 167 Hz. The pneumotachograph must be calibrated and several authors have pointed out that the calibration must take place under the same conditions as the actual measurement (Kreit & Sciurba 1996; Miller & Pincock 1986). Changes in the tube connection, for example, lead to changes in the flow characteristic and therefore to errors.

For the validation the desired signal, which is fed to the controller, and the actual signal, which is produced by the breathing simulator, are compared.

To analyse a system its performance needs to be tested under various conditions. Control systems are dynamic in their performance, therefore they are usually specified in terms of transient response and steady-state response. Transient response is the response of the system as a function of time. Steady-state error is the error after the transient response has decayed. To test these it is appropriate to use artificial test signals, which are easy to compare and show the delay of the proportional response and eventual overshooting and/or oscillation of the system. Overshooting and oscillation can give rise to unacceptable errors and instability. To test the response of the system an extreme case is used: a step function. The desired step function and its response are shown in Figure 5.15.

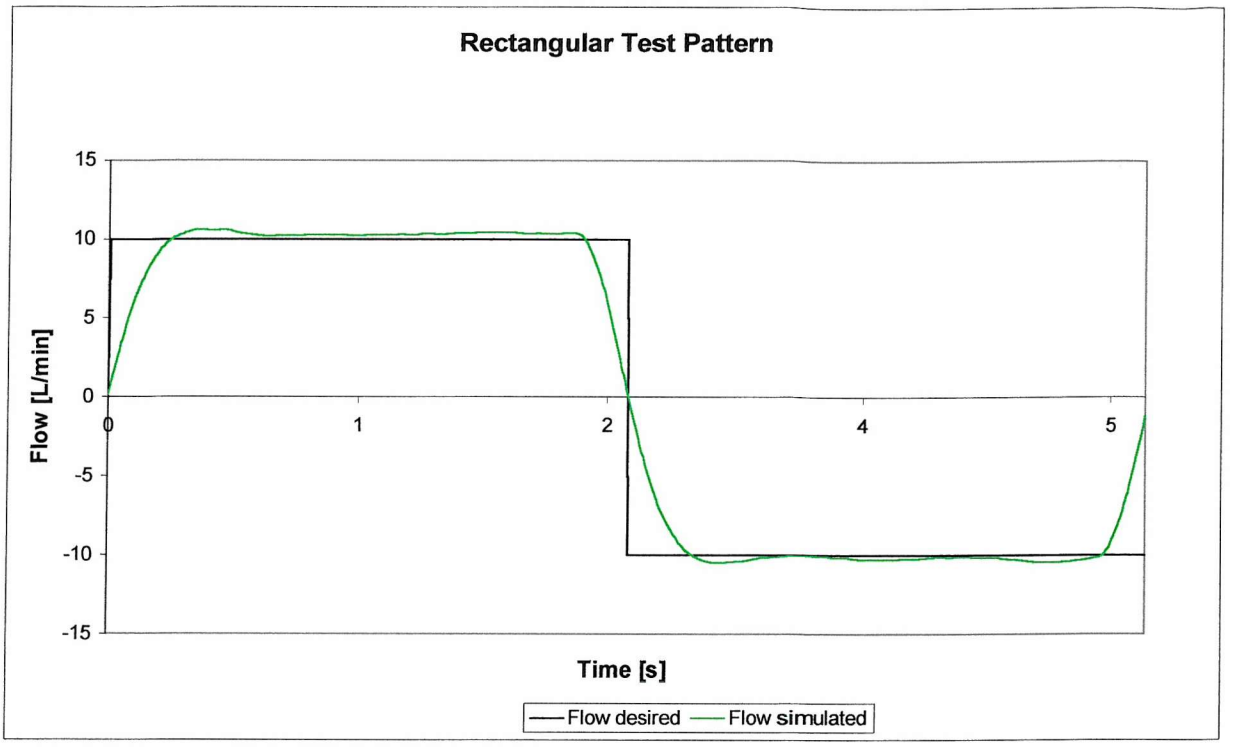

Figure 5.15: Simulated rectangular flow pattern

The specification of transient performance requires that the system should reach the required position as quickly as possible with minimum overshoot. The time the system needs for that is called settling time. The settling time, the overshoot and the steady state error can describe the performance of a step response very well.

This application needs a minimum of overshoot and oscillation, because stability is very important here. The output rate to the motor is 167 Hz, which could make the system unstable. The swiftness of the system is also important, but less so than stability, because normal human breathing is not very rapid. The step response shows a small overshoot (<5 %), which is followed by a small steady state error. The integral of the step function and its response are shown in Figure 5.16

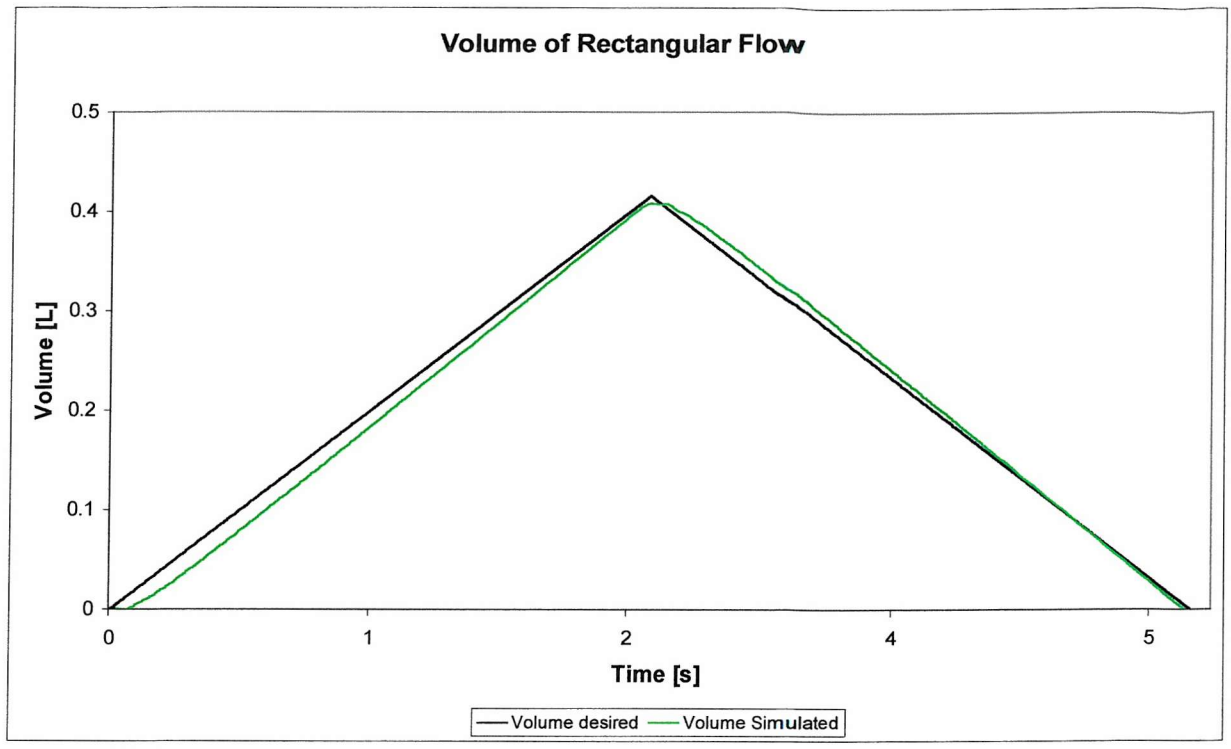

Figure 5.16: Integrated volume of rectangular flow pattern

A further test was to determine how closely the system follows a breathing pattern with different breathing rates. A pattern with rising breathing rates was used therefore, as shown in Figure 5.17. The graph shows that the breathing pattern follows the set signal very well, a difference is visible only above a rate of 40 L/min. For the breathing patterns at rest and light exercise (up to 40 L/min) the system is sufficiently fast.

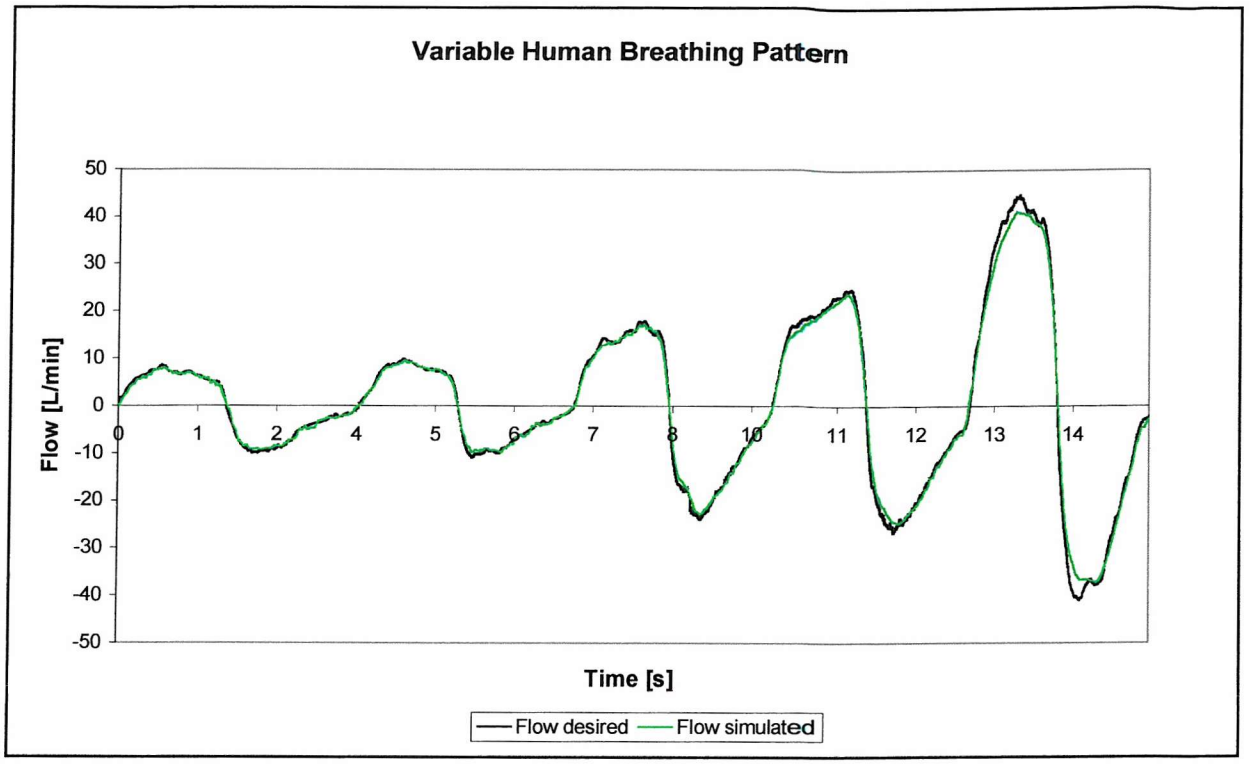

Figure 5.17: Variable human breathing pattern compared with its response

The integrated signal of the flow is shown in Figure 5.18. The simulated signal also followed the desired volume closely.

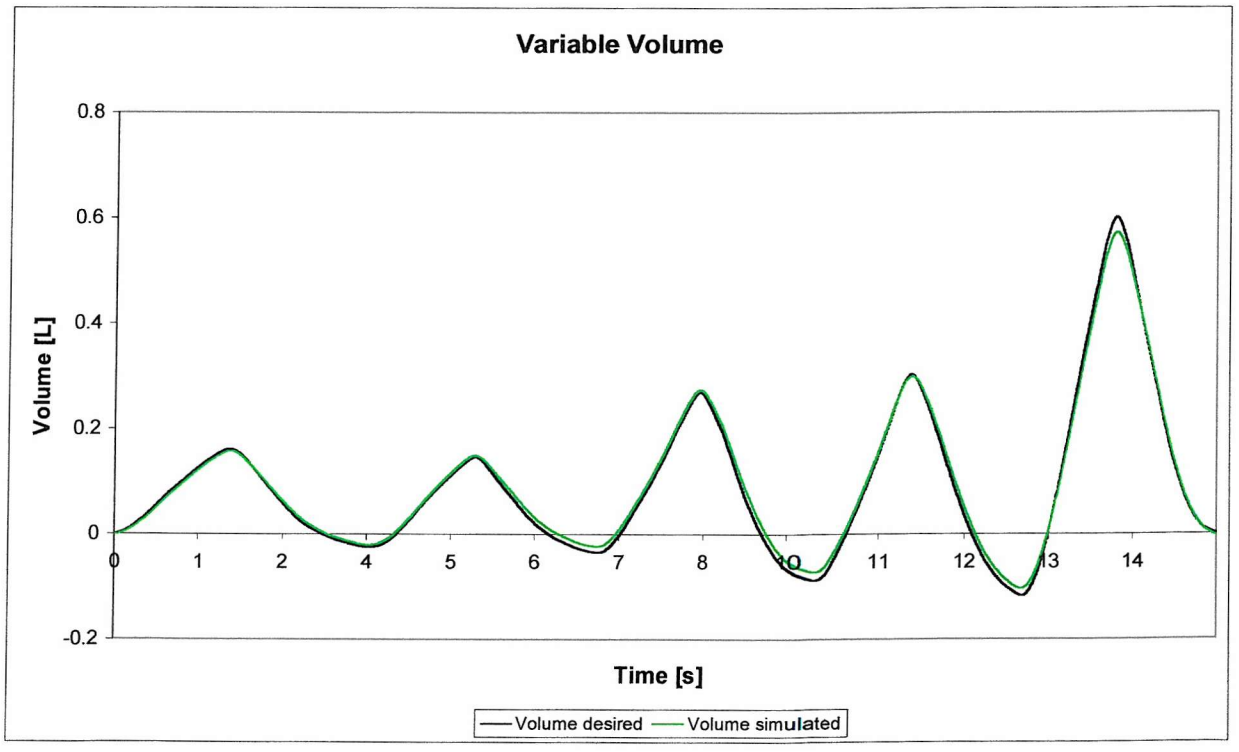

Figure 5.18: Integrated signal of the flow gives the volume

6 EXPERIMENTAL STUDY OF DEPOSITION IN NASAL CASTS -MATERIALS AND METHOD

The purpose of these experiments was to establish deposition in artificial nasal casts under various conditions such as different air flow rates, breathing patterns and particle sizes. Monodisperse particles of different aerodynamic diameters (1.7, 3, 6 and 10 μm) were drawn through casts using different flow rates and breathing patterns. The breathing patterns were: constant flow rate, sinusoidal waveform, rectangular waveform, and recorded breathing patterns of different human volunteers. Except for constant flow the breathing patterns were all produced with the breathing simulator. All these measurements were performed during inhalation only.

The production of the casts and breathing simulator are described in chapters 4 and 5 respectively. The generation of the aerosol, the breathing patterns used, the characteristics of the casts and the measurement of particle deposition are described in this chapter.

6.1 AEROSOL GENERATION

Monodisperse sebacate droplets were used for the deposition studies in the nasal casts. They were produced with a Vibrating Orifice Aerosol Generator (VOAG) Model 3450 from TSI Inc. The VOAG creates a cylindrical liquid jet through an orifice and breaks the jet into droplets of a uniform diameter by applying vibration at the orifice of a defined frequency. The stability, monodispersity, and diameter of the aerosol depend on the diameter of the orifice, the density and surface tension of the liquid, the velocity of the jet, and the frequency of the vibration. The particles are dispersed immediately after they are formed and the aerosol is diluted. Monodisperse aerosol can be produced in a wide size range by using the method of solvent evaporation. The non-volatile solute is dissolved in a volatile solvent, and so the diameter of the particles can be changed by varying the concentration and size of the non-volatile solute in the aerosol solution. The smallest diameter is determined by the concentration of the non-volatile impurities in the solvent.

The diameter of the initial droplet, d_d, and the aerosol particle after the solvent has evaporated, d_p, can be determined by following equations:

Diameter of initial droplet: $d_d = 10^4 (Q_l / 10\pi f)^{1/3}$ **Equation 6.1**

d_d	=	diameter of initial droplet	[μm]	f	=	frequency	[Hz]
Q_l	=	liquid feed rate	[cm^3/min]				

Diameter of particle: $d_p = C^{1/3} d_d$ **Equation 6.2**

d_p	=	Particle Size	[μm]
C	=	Volumetric concentration of solute in solution	[1]

Unfortunately the output aerosol concentrations are low, about 30-400 cm^{-3}, depending upon the primary droplet size. In addition the liquid suspension can clog the orifice, which can entail a long cleaning processes. It is even more difficult if radioactive aerosol is used, since the cleaning can only be performed after decay.

An advantage of the VOAG is that it produces aerosol of a narrow size distribution usually over a long time. The solvent evaporation method allows the radioactive label to be simply dissolved in the solution. In this application sebacate oil as well as the ^{99m}Tc saline is dissolved in ethanol. After the ethanol evaporates the ^{99m}Tc stays with the oil droplets and the particles are labelled (Kreyling 1999).

All particles are naturally electrostatically charged, moreover when particles are generated with the VOAG they become even more charged due to the triboelectric effect. Triboelectric charging is the effect when two materials, which have dissimilar conductivity move relatively to each other. The one with the higher conductivity will be negatively charged. It is desirable in most applications to discharge particles. In this study an ionising Krypton source (^{85}Kr) is used. ^{85}Kr is a $\beta - \gamma$ emitter, which ionises the air and produces positive and negative ions. Aerosol passing the source will be neutralised, not to a level where no charge is present anymore, but to a very low level of charge. This level is called

the Boltzman equilibrium and the amount of positively and negatively charged particles is the same (Liu & Pui 1974).

6.2 SPECIFICATIONS OF THE CASTS

Casts 1 and 2 were made from MRI scans of two Caucasian male healthy volunteers as described in chapter 4. An important factor for deposition is thought to be the cross-sectional area of the nose. The cross-sectional area is measured in-vivo using acoustic rhinometry as described in section 2.2.

To enable a comparison of the measurements taken from the human volunteer, acoustic rhinometry measurements have been done on the casts as well. The results are put into the following two diagrams. Figure 6.1 shows the cross-sectional areas of cast 1 perpendicular to airflow as a function of distance from the tip of the nose. It shows the cross-section of both airways together as well as each airway separate.

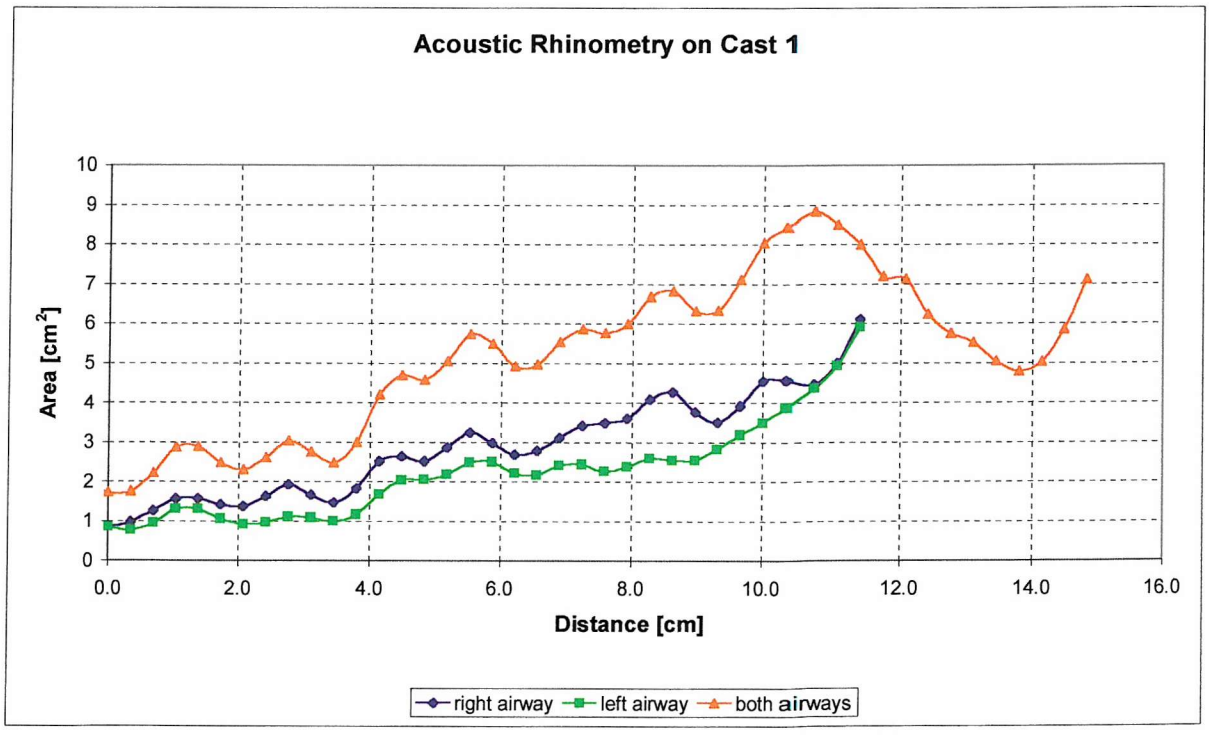

Figure 6.1: Cross-sectional area of cast 1 as a function of distance from the nostrils measured with acoustic rhinometry

Figure 6.2 also shows acoustic rhinometry performed on cast 2. The airways from 10 cm behind the tip of the nose onwards are too large, especially the left one. It is therefore considered an artefact, but the result as shown in Figure 6.2 was reproducible. It is not known what causes this artefact.

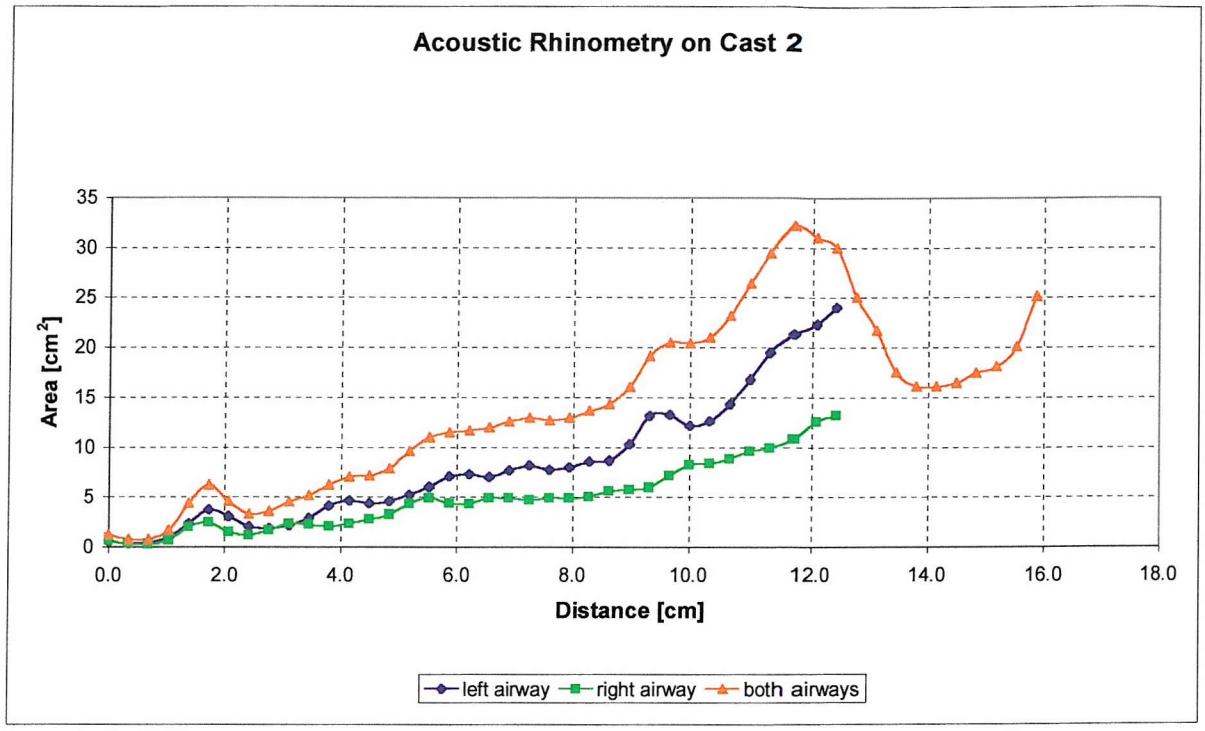

Figure 6.2: Cross-sectional area of cast 2 as a function of distance from the nostrils measured with acoustic rhinometry

Figure 6.3 shows the coronal cross-sectional area of cast 1 from the digitital MRI images that were used to produce the cast. The cross-sectional area starts at the left hand side at the nostrils, and ends at the throat.

Figure 6.4 shows the coronal cross-sectional areas of cast 2 starting at the nostrils.

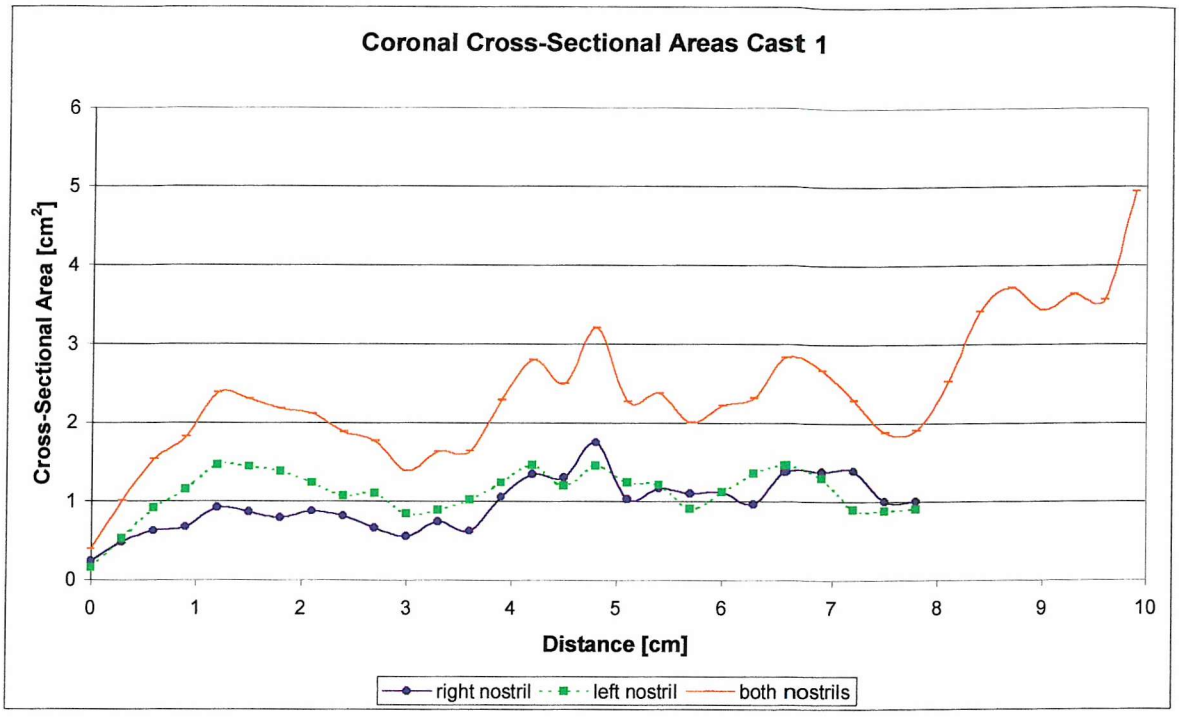

Figure 6.3: Cross-sectional Area of Airways Starting at the Nostrils of Cast 1

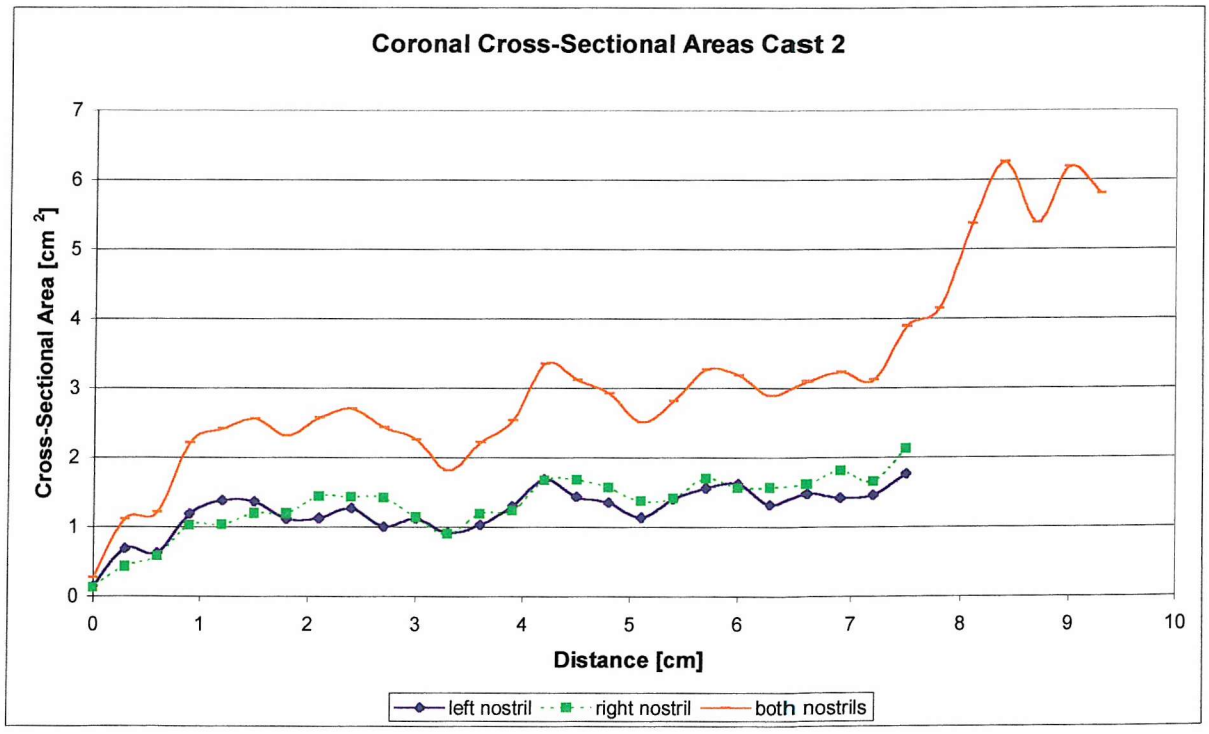

Figure 6.4: Cross-sectional Area of Airways Starting at the Nostrils of Cast 2

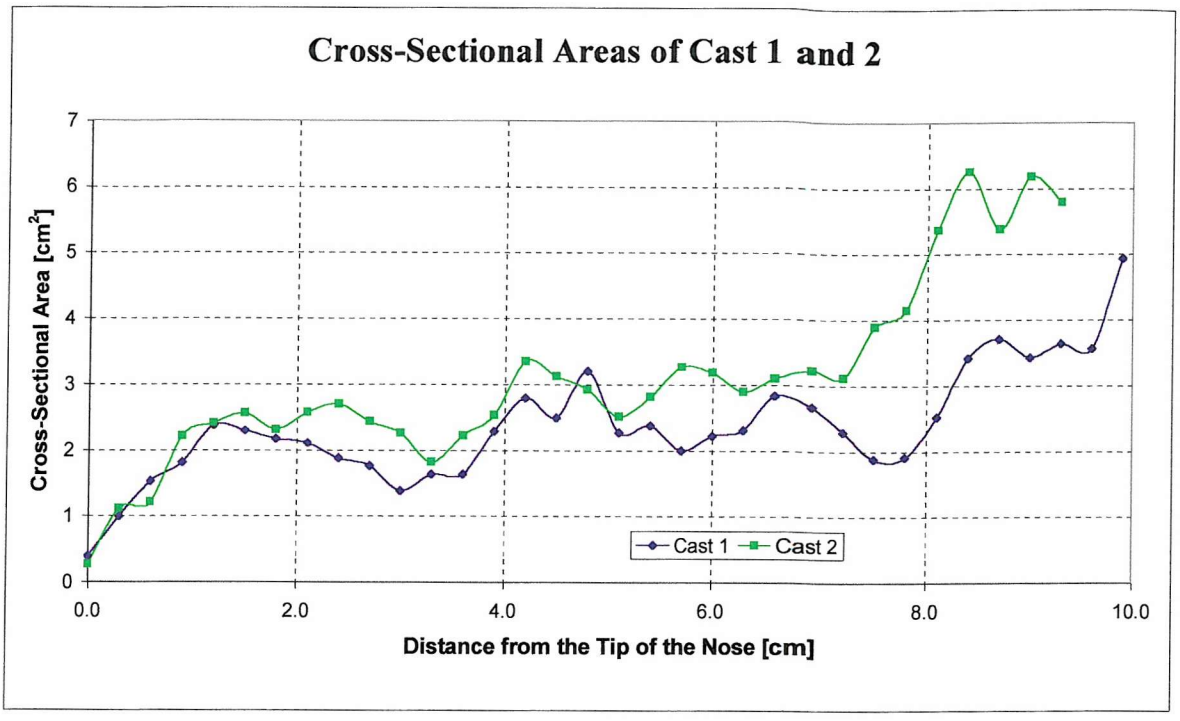

Figure 6.5: Cross Sectional Areas of Cast1 and 2 in Comparison

Figure 6.5 shows the two casts in comparison. It shows that the minimum cross-sectional area of cast 1 is slightly smaller and a few millimetres further up front than the one of cast 2. In general cast 1 has smaller cross-sectional area than cast 2, especially towards the throat.

Next to the cross sectional area the shape of the nostrils is thought to be an important factor for deposition (Kesavanathan et al 1998). Kesavanathan et al introduced a shape factor, which is the length to width ratio called ellipticity E. A large E suggests an elliptical opening of the nostril, while the closer E gets to 1 the closer the opening is to a circular shape. This factor is 2.3 for cast 1 and 2.5 for cast 2. Nostrils 3 and 4 were made from MRI scans of an Afro-American volunteer and an Asian Volunteer, respectively. Both nostril sets were made to end before the nasal valve to ensure that measured effects are only effects of the nostril shape, not of the smallest cross sectional area. Their nostril shape factor was 1.1 and 1.5 for nostril set 3 and 4, respectively.

6.3 BREATHING PATTERNS

Several different breathing patterns were used for the deposition measurements. The flow rates, the tidal volumes and the duration of the breathing cycles can be found in Table 6.1. The diagrams, which show all the breathing patterns can be found in the Annex A .

Breathing pattern	Flow Rates [L/min] maximum	Flow Rates [L/min] average	tidal Volumes [L] maximum	Duration of one breathing cylce [sec]
Constant Flow	10			
	15			
	20			
	25			
	30			
	35			
Sine Wave	10	6.4	0.33	6.3
	20	12.7	0.67	6.3
	30	19.1	1	6.3
	40	25.5	1.3	6.3
	50	31.9	1.6	6.3
Recangular Wave	10	10	0.4	5
	20	20	0.8	5
	30	30	1.2	5
Human Breathing A at Rest	30	22.6	0.9	6
Human Breathing A at Light Exercise	60	40	1.2	3
Human Breathing A	10	9.7	0.5	6.2
	20	13.9	0.7	6.8
	30	26.2	1.5	6.5
	40	31.6	1.5	4.4
	50	42.1	1.5	4.4
Human Breathing B	10	7.9	0.35	5
	20	15.6	1.1	8
	30	22.2	1.5	8.5
	40	31.8	2	7.6
	50	38.4	2.5	7.2
Human Breathing C	10	5.3	0.17	4
	20	13	0.6	6
	30	20.7	1	5
	40	30.1	1.4	5.5
	50	41	1.7	4.5

Table 6.1: Characteristics of the different breathing patterns

The flow pattern that was used as a standard was constant flow, generated by a vacuum pump. The breathing simulator produced all the other breathing patterns. The artificial ones were created as an ASCII file on the computer, whereas the human breathing patterns were recorded. Human breathing A was recorded from the volunteer from whom cast 1 was made. Human breathing A is relatively rapid compared to human breathing B and C, which were generally slower than human breathing A for the same breathing manoeuvres.

6.4 ADMINISTRATION OF AEROSOL TO THE CAST

The aerosol was administered during inhalation only. To draw the particles through the cast, either a vacuum pump was used for constant flow or the breathing simulator for the various breathing patterns. The aerosol was drawn online from the aerosol generator (VOAG) through the cast. To be able to neglect losses it was ensured that the tubing was the same in each experiment. Not only the tubing was physically the same, but also its position.

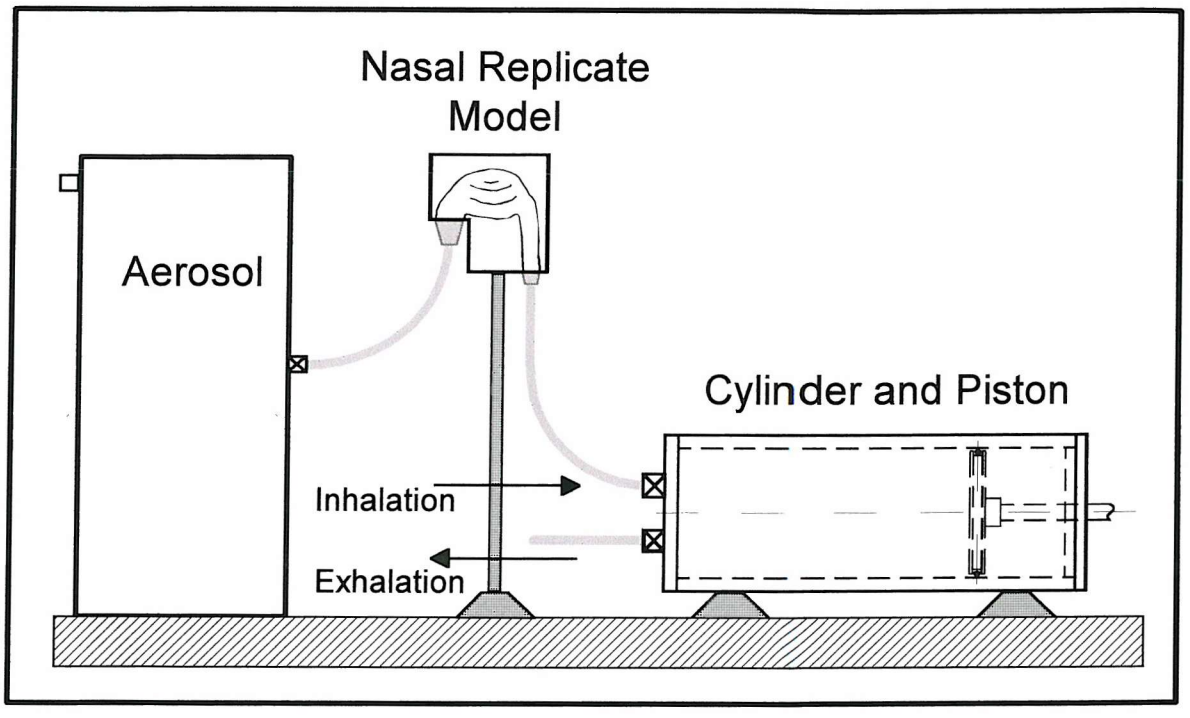

Figure 6.6: Schematic drawing of experimental set-up

To fix the tubing to the nostrils hand-carved adapters were manufactured. Each pair of nostrils had an adapter especially made up for its shape. These adapters cover both nostrils, so that the chance of air entering either nostril was the same. A Teflon gasket was put between the cast and adapter for sealing. The gaskets were also cut for the shape of each adapter. One adapter was also made for the outlet or throat of the cast. It leads in a piece of tubing and is the same for both casts. The same Teflon gasket material was used here for sealing.

6.5 Measurement of Total Deposition

The measurement of total deposition was performed with an aerodynamic particle sizer APS (TSI). The APS measures particle size and number concentration. In the measurement region of the APS the particle passes two laser beams, and scatters their light. This is measured and the time the particle needs to travel the distance between the two beams is uniquely related to it's aerodynamic diameter. Those measurements are used to calculate the aerodynamic diameter of the particle using calibration curves incorporated into the analysis software. The software takes particle density and shape as well as viscosity of the medium into consideration (APS Inc 1987).

The concentration is first measured without the cast at a certain breathing pattern and flow rate and then shortly behind the cast. The reproducibility of these measurements was good, variations being under ± 3%.

The total deposition (TD) of the cast was calculated according to this equation:

$$TD = (1 - \frac{outlet}{inlet}) * 100\% \qquad \textbf{Equation 6.3}$$

It was not tested if the APS measures the right concentration of particles. But since the result is relative, the absolute numbers do not matter.

6.6 Measurement of Deposition Pattern in the Nasal Cast

For the measurements of deposition patterns in the nasal cast, the particles were radioactively labelled with ^{99m}Tc, as described in section 6.1. Care was taken that the size stayed the same before and after labelling.

Particles were drawn through the cast using either human breathing A at rest or human breathing A at light exercise. The aerosol administration was performed for one hour. A filter directly behind the cast filtered the outlet aerosol.

After the administration the total activity of the cast, the exhalation filter, the adapters and the gaskets were measured. Also the area around the nostrils was wiped to ensure that no activity which is on the outside the cast was measured.

After these measurements, the cast was dissembled and the activity of each plate was measured with NaI detectors, which count the activity in Becquerel. ^{99m}Tc has a half-life of 6 hours, therefore one had to account for the decay of the isotope, which was done according to the equation below. A_0 is the activity in Becquerel (Bq) at the time of the administration, T_{el} is the elapsed time since administration in hours, $T_{1/2}$ is the half-life in hours and A is the measured activity in Bq.

$$A_0 = \left(\frac{0.693 * T_{el}}{T_{1/2}}\right)^{-1} * A \qquad \textbf{Equation 6.4}$$

Further plates, which had enough activity on them (>1000 Bq) were put on an X-ray film to determine the place of deposition. Unfortunately there was not enough time to develop a method to determine the amount of activity around the airway. But by taking the total amount on each plate and the place of the hot spots into account, it was possible to draw plausible conclusions.

7 TOTAL DEPOSITION IN THE NASAL CASTS

This section presents the results of the total deposition measurements in the casts. Both casts were used for these measurements and also the different nostril sets. The particle sizes were 1.7, 3, 6, and 10 μm. The particle concentration in the airflow was measured before and after the cast and total deposition calculated from these values. Total deposition is then

$$TD = (1 - \text{output/input})*100\ \%$$

Human breathing pattern A is the one that corresponds with cast 1. Cast 2 has unfortunately no corresponding breathing pattern. Since constant flow rate is widely used in the literature for cast studies it is used as a standard here. Also 6 μm is the standard particle size. The reason for this is that the experiments were performed inhalation only and for this size exhalation in-vivo should not contribute to deposition, since not many particles are thought to be exhaled from the lung.

Several different methods of presenting the data are possible:

- The total deposition with respect to changing particle size and flow rates
- the total deposition with respect to changing flow rates and different breathing pattern and fixed particle size
- the total deposition with respect to the impaction factor
- the total deposition with respect to different casts

7.1 TOTAL DEPOSITION VERSUS PARTICLE SIZE AND FLOW RATE

The following two diagrams show the total deposition in cast 1 versus particle size for different flow rates. Figure 7.1 and Figure 7.2 show deposition versus particle size using constant flow and human breathing A, respectively. The flow rates indicated in Figure 7.2 for human breathing A are the maximum flow rates.

The total deposition is a distinct curve for each flow rate. For human breathing A the curves are a more pronounced S-shape than for constant flow. Also with human breathing A there is a gap between 20 L/min and 30 L/min, which is largest for 6 μm droplets.

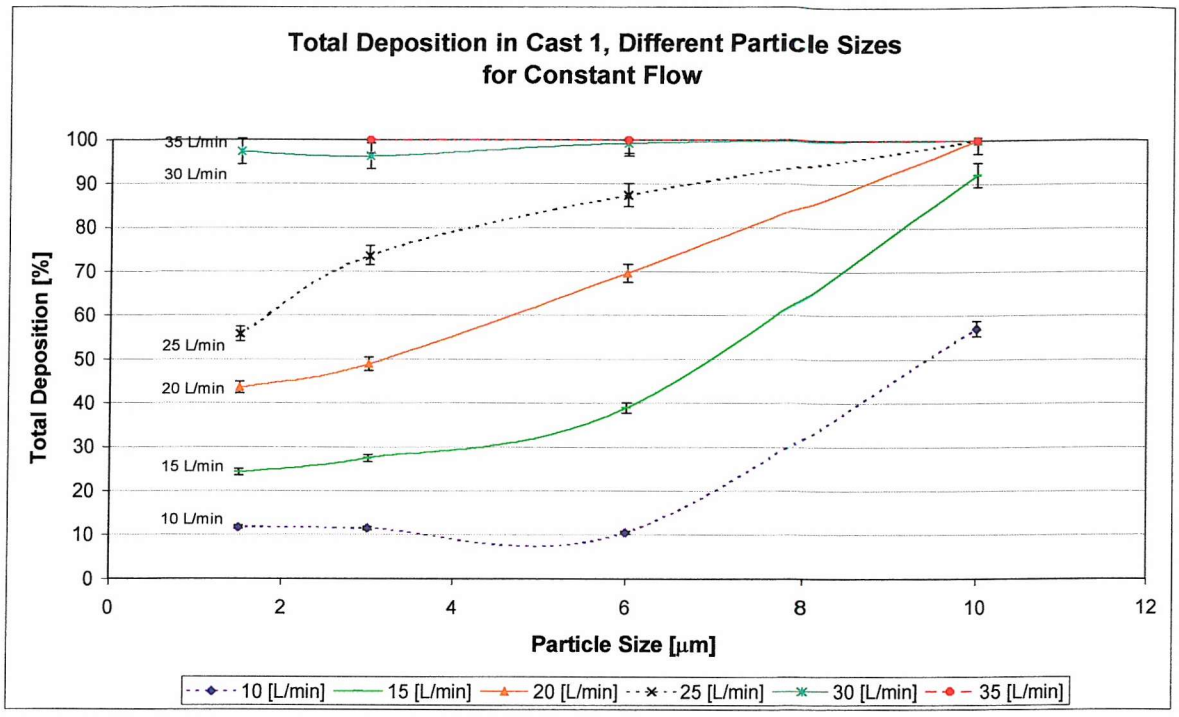

Figure 7.1: Total Deposition Versus Particles Size, Measured in Cast 1 for Constant Flow Rate

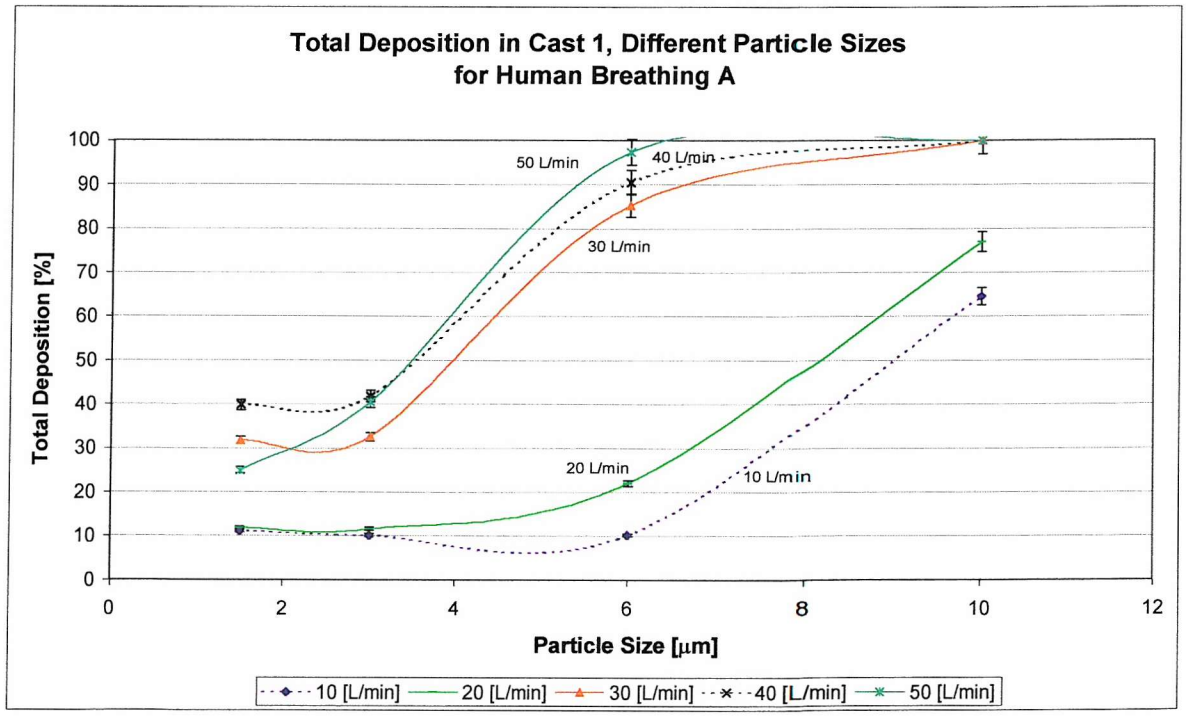

Figure 7.2: Total Deposition Versus Particle Size, Measured in Cast 1 for Human Breathing A

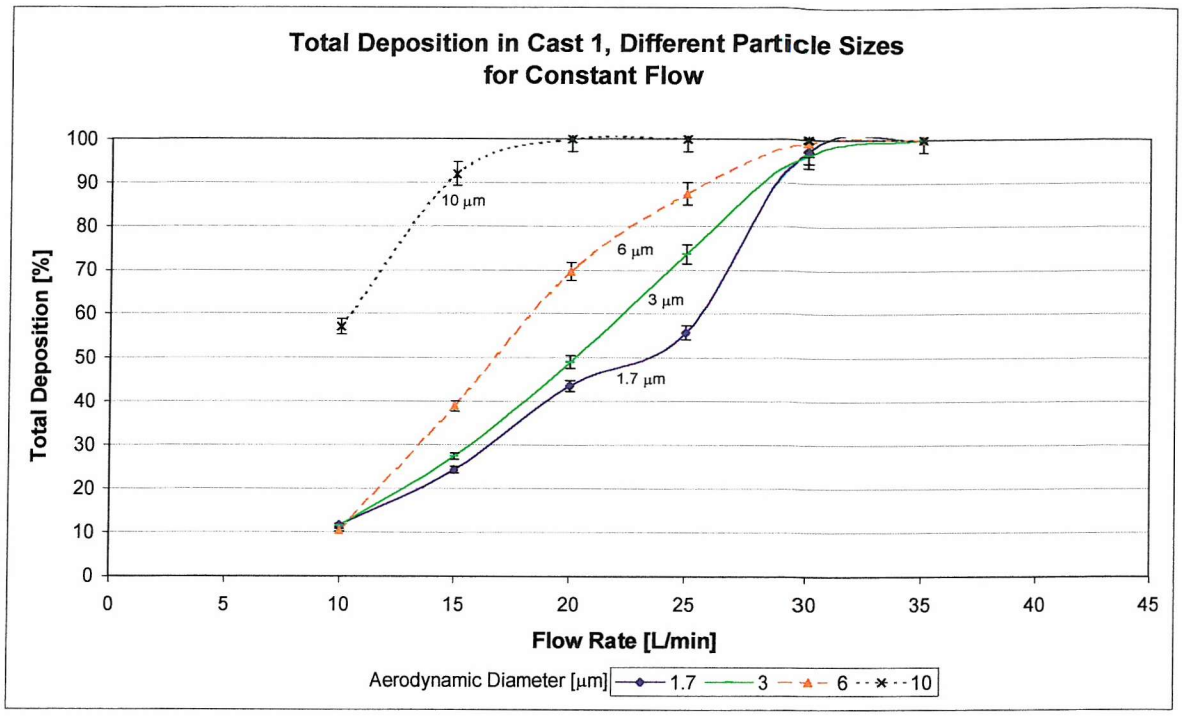

Figure 7.3: Total Deposition versus Flow Rate, Measured in Cast 1 for Different Particle Sizes and Constant Flow

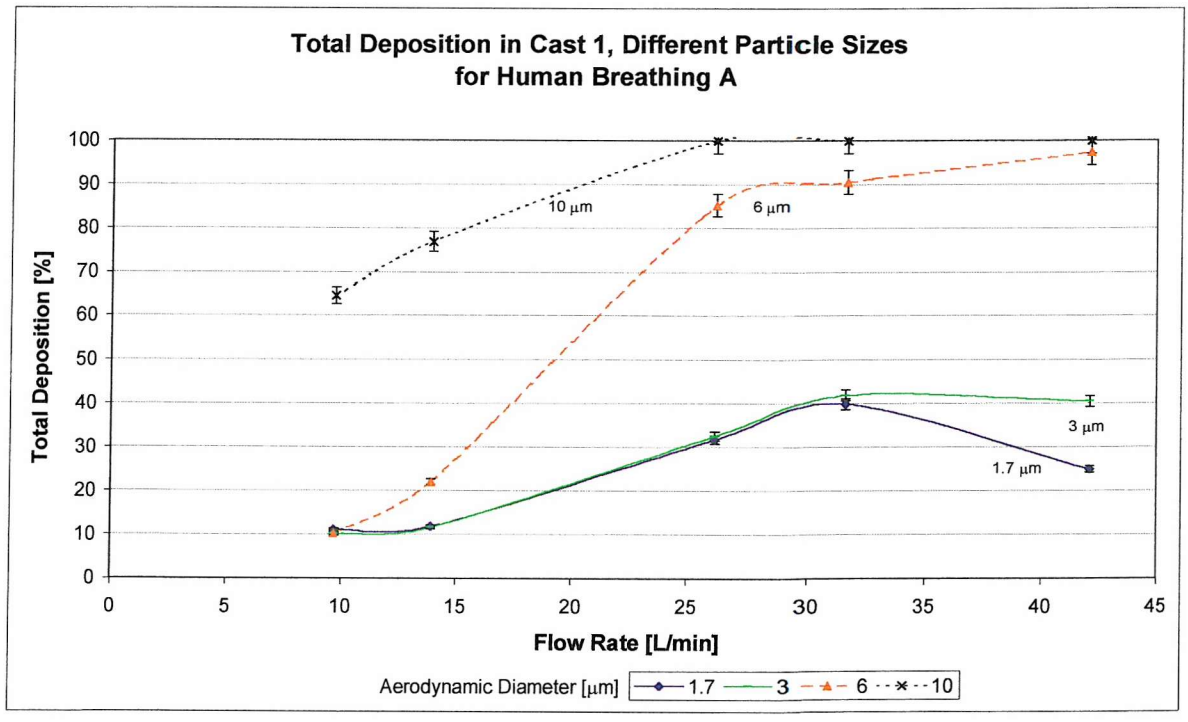

Figure 7.4: Total Deposition Versus Flow Rate, Measured in Cast 1 for Different Particle Sizes and Human Breathing A

Figure 7.3 and Figure 7.4 show total deposition versus the flow rate for constant flow and human breathing A, respectively. For 1.7 and 3 μm human breathing A causes only half of the deposition at the highest flow rates than constant flow.

7.2 TOTAL DEPOSITION VERSUS BREATHING PATTERNS

The following diagrams show the total deposition varying with breathing patterns using cast 1. As mentioned before particles of 6 μm diameter were used as a standard and, therefore, all the possible breathing patterns were used for this size. For the other particles sizes only constant flow and human breathing A were used. To be able to compare the constant flow rate with the cyclic patterns, the average flow rates were taken for the cyclic patterns.

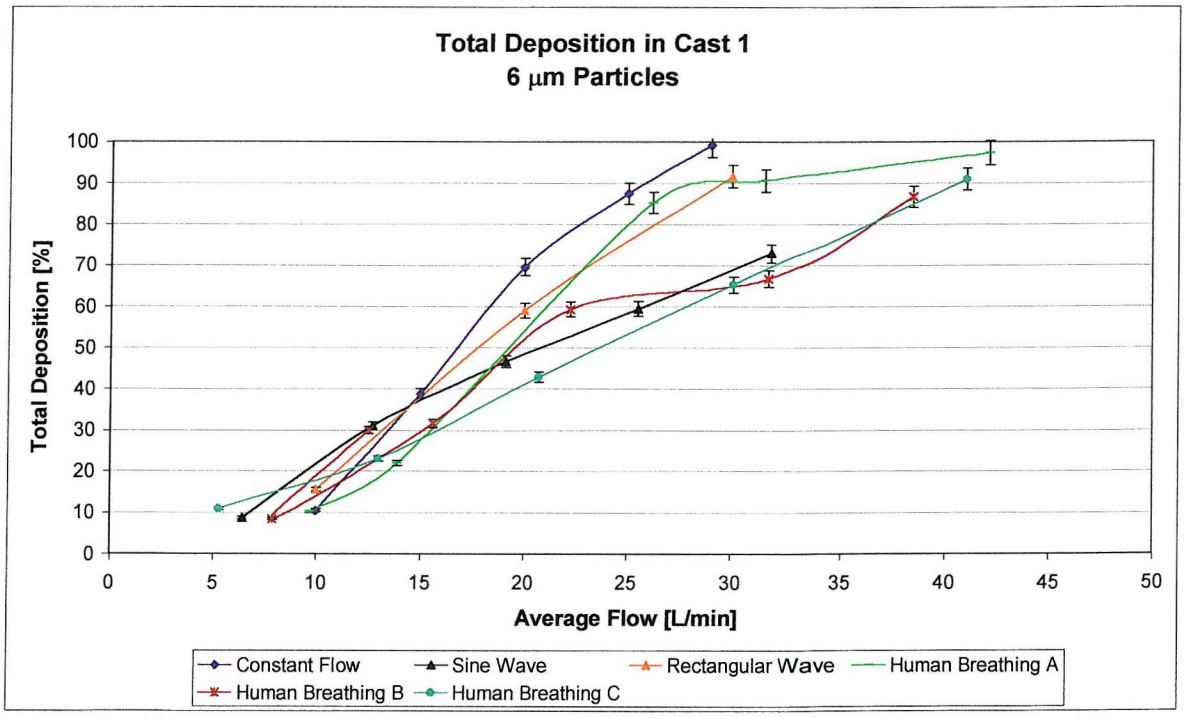

Figure 7.5: Total Deposition of 6 μm Particles Versus Flow Rate, Measured in Cast 1 at Different Breathing Patterns

The constant flow rate shows a slightly higher deposition then the other flow rates. It reaches 100 % earlier than the others. Human breathing A has a more pronounced S-shape and does not reach 100 % deposition as soon as constant flow. The difference to constant flow is more pronounced for the sine wave and human breathing B and C, which appear to have similar deposition to a sine wave.

Figure 7.6 shows the total deposition of 1.7 μm particles for constant flow and human breathing A. The difference in deposition for the two patterns is greatest with this particle size. Also the curve for human breathing A appears to slope down again towards the highest flow rate. While deposition for constant flow reaches about 100% deposition at a flow rate of 30 L/min, deposition for human breathing A never reaches more than 40 %.

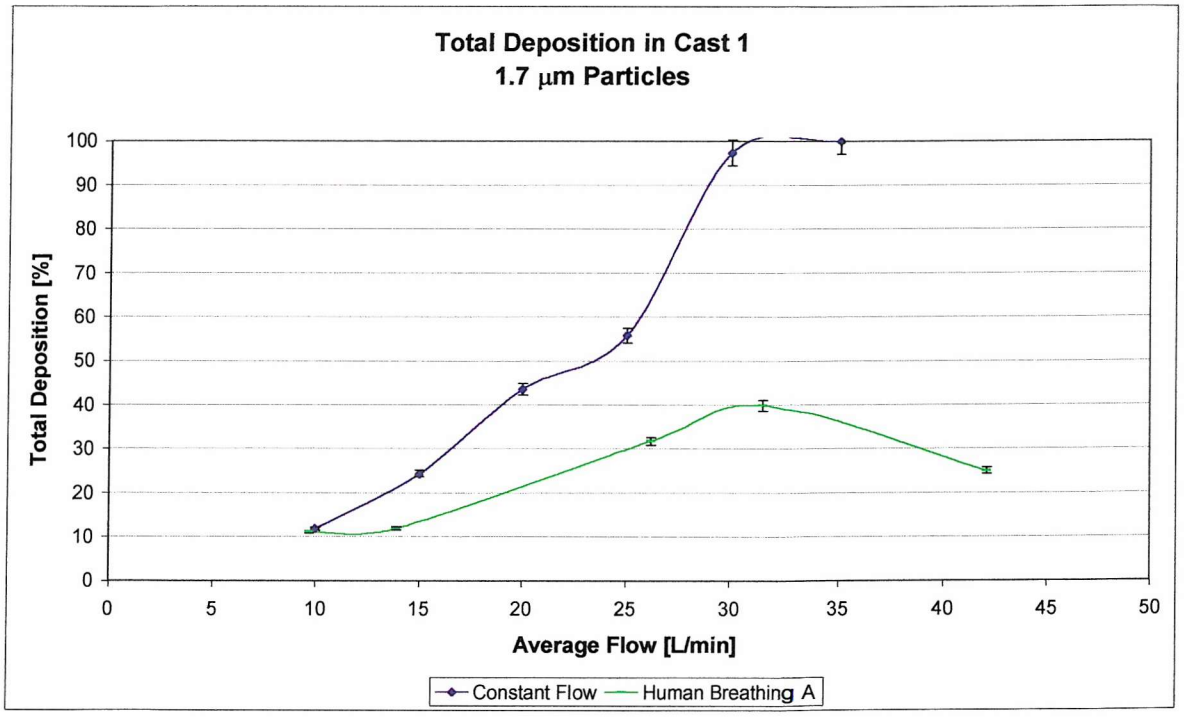

Figure 7.6: Total Deposition of 1.7 μm Particles Versus Flow Rate, Measured in Cast 1 at Constant flow and Human Breathing A

Figure 7.7 shows the deposition of 3 μm particles for constant flow and human breathing A. The difference is more dramatic then for 6 μm particles. At the lowest flow rate they start out to cause the same deposition rate, but immediately at the next higher flow rate

constant flow causes a higher deposition than human breathing A. Constant flow reaches nearly 100 % total deposition at a flow rate of 30 L/min, whereas human breathing A shows only 43 % deposition in the cast at this flow rate. At a average flow rate of 43 L/min human breathing A has still only 41 % deposition.

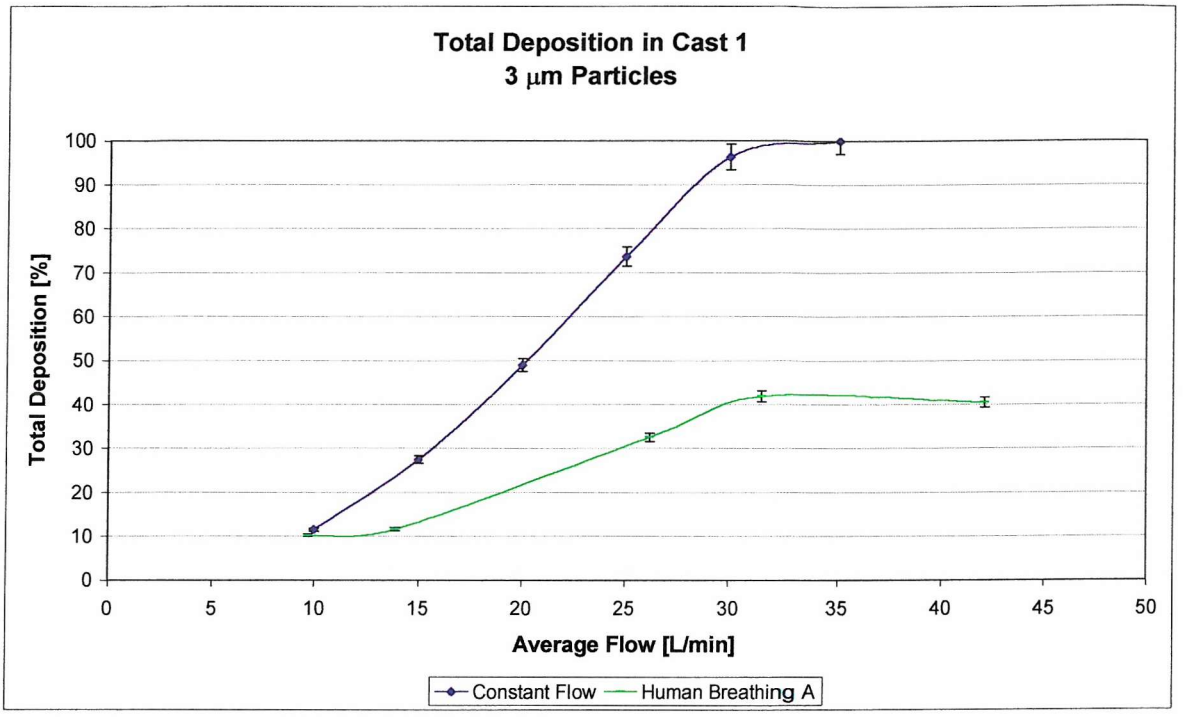

Figure 7.7: Total Deposition of 3 μm Particles Versus Flow Rate, Measured in Cast 1 at Constant flow and Human Breathing A

Figure 7.8 shows the deposition of 10 μm particles in cast 1 for constant flow and human breathing A. Even with a flow rate of 10 L/min the deposition was already 60 %. Towards higher flow rates human breathing A appeared to have slightly lower deposition than constant flow. But the difference becomes much smaller for larger particles.

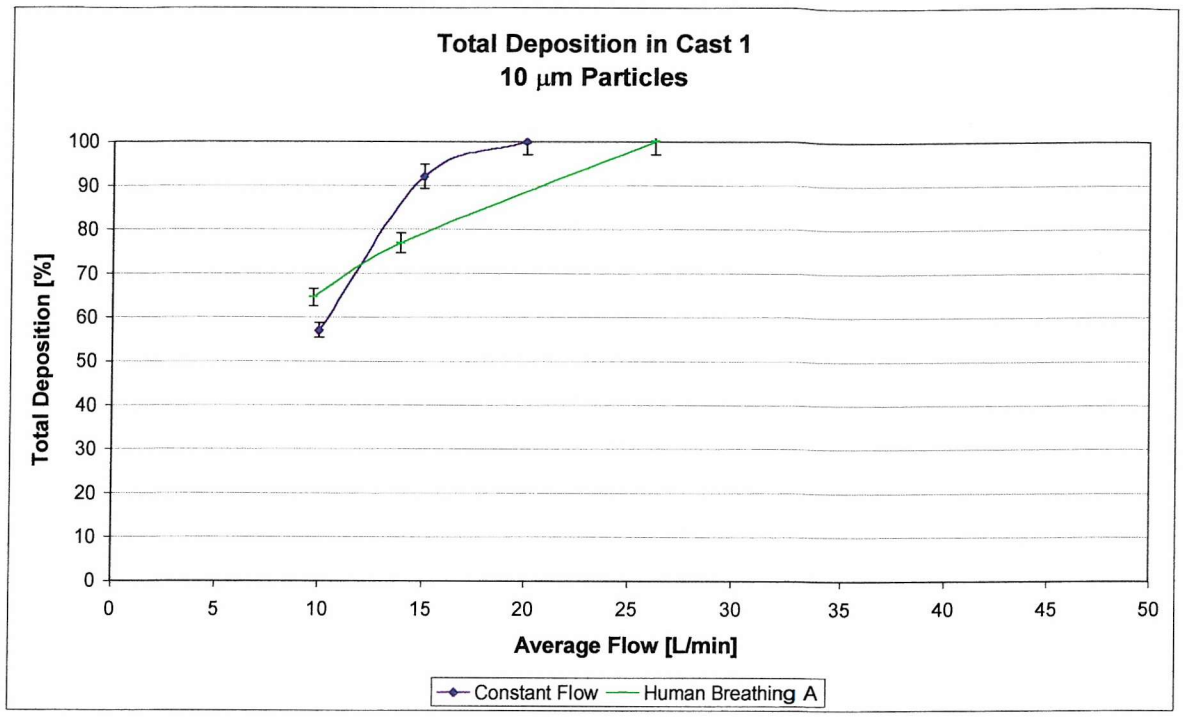

Figure 7.8: Total Deposition of 10 μm Particles Versus Flow Rate, Measured in Cast 1 at Constant flow and Human Breathing A

In each of the cases deposition measured with constant flow reaches a 100% deposition faster that the cyclic patterns. The reason why the different flow patterns show different deposition curves may be that it is not possible to compare simply their average values. A pattern can only be represented by its mean if deposition is directly proportional to flow rate over the entire range of instantaneous flow rates. To investigate this the breathing patterns were partitioned into small elements of approximately constant flow (6ms). The data points of constant flow were used to approximate a polynomial of order 2. This was used to calculate the deposition each element should cause. Adding the elements up gave the total deposition caused by one particular breathing pattern.

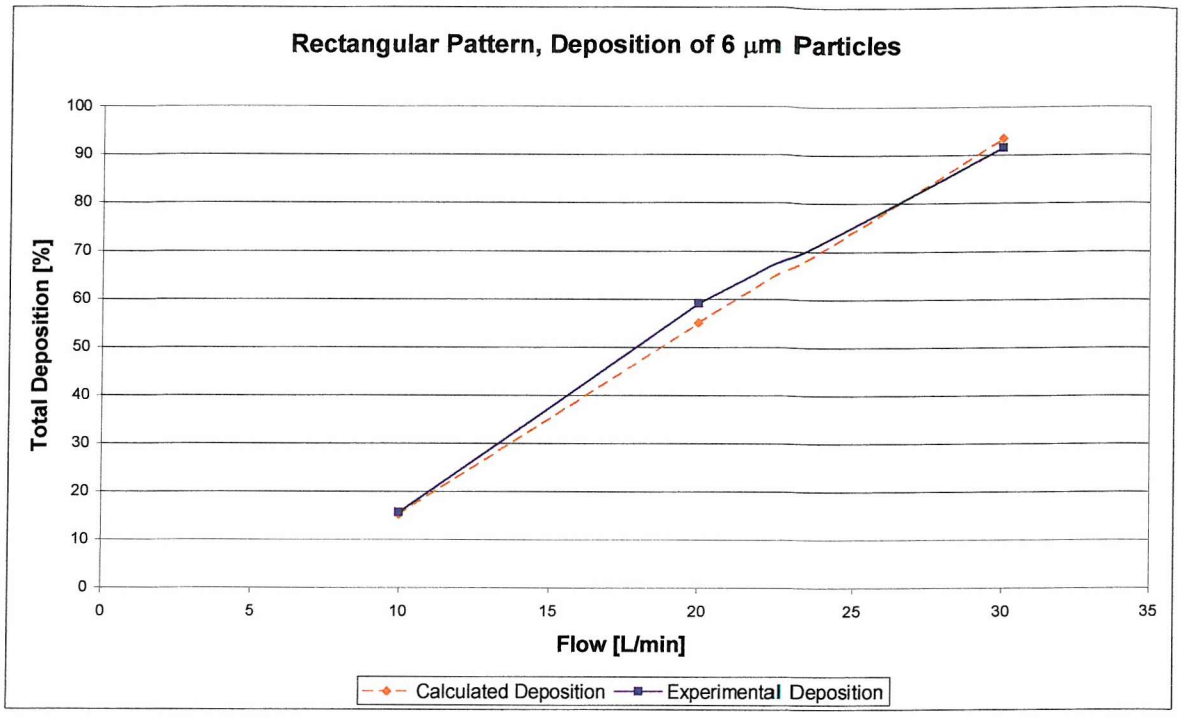

Figure 7.9: Comparison of Calculated and Experimental Deposition for 6 μm Particles and Rectangular Breathing Pattern

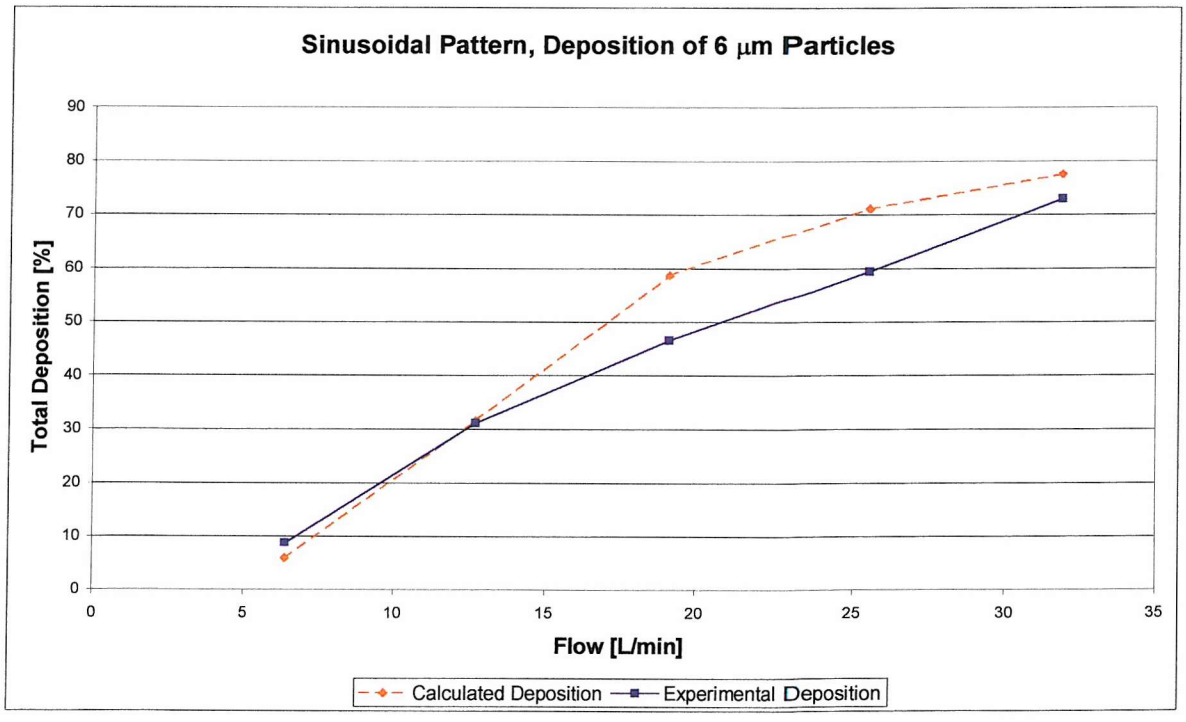

Figure 7.10: Comparison of Calculated and Experimental Deposition for 6 μm Particles and Sinusoidal Breathing Pattern

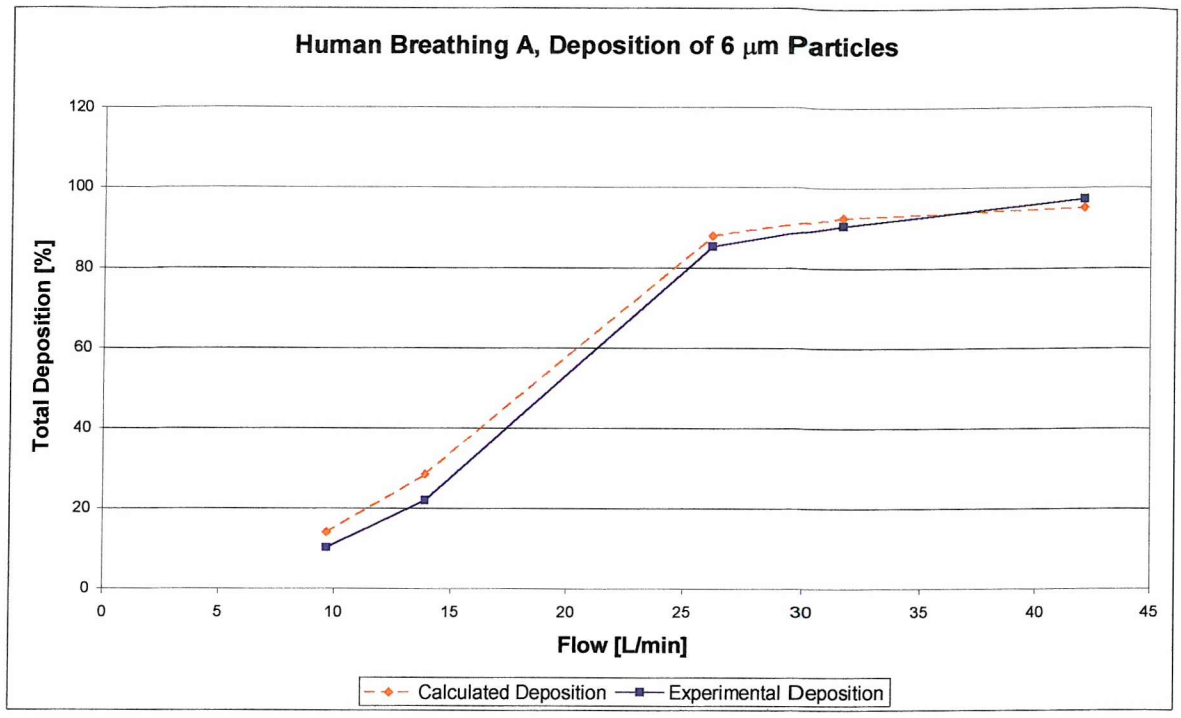

Figure 7.11: Comparison of Calculated and Experimental Deposition for 6 μm Particles and Human Breathing A

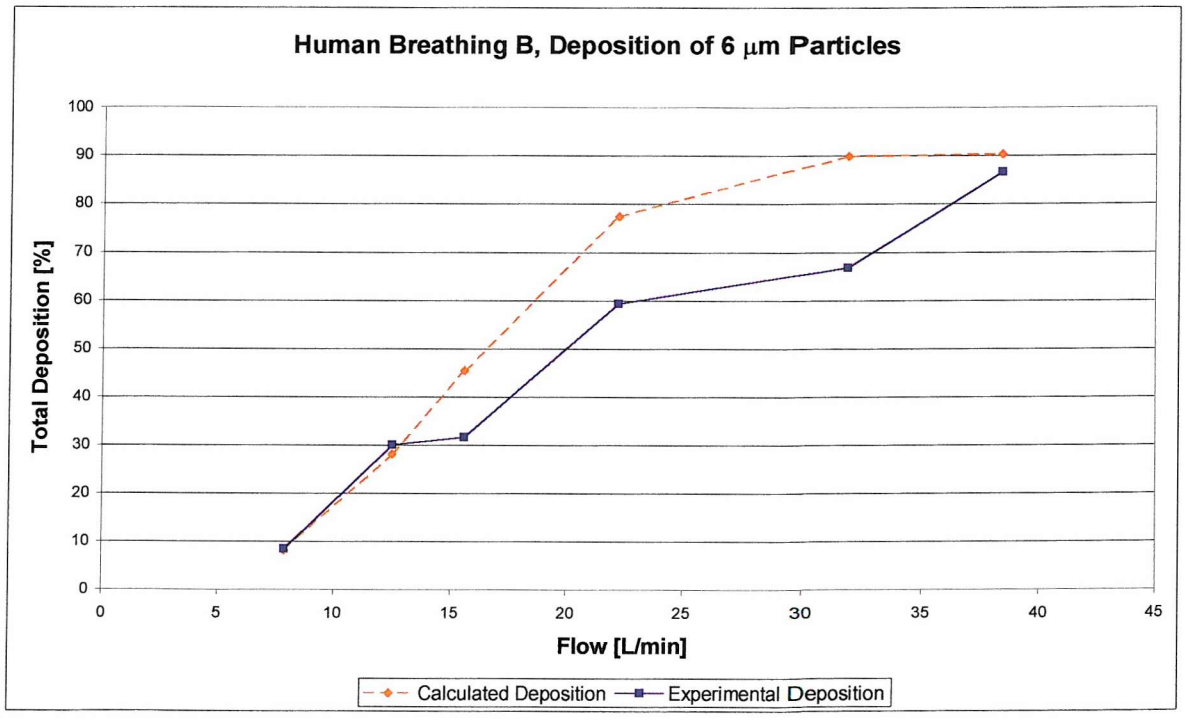

Figure 7.12: Comparison of Calculated and Experimental Deposition for 6 μm Particles and Human Breathing B

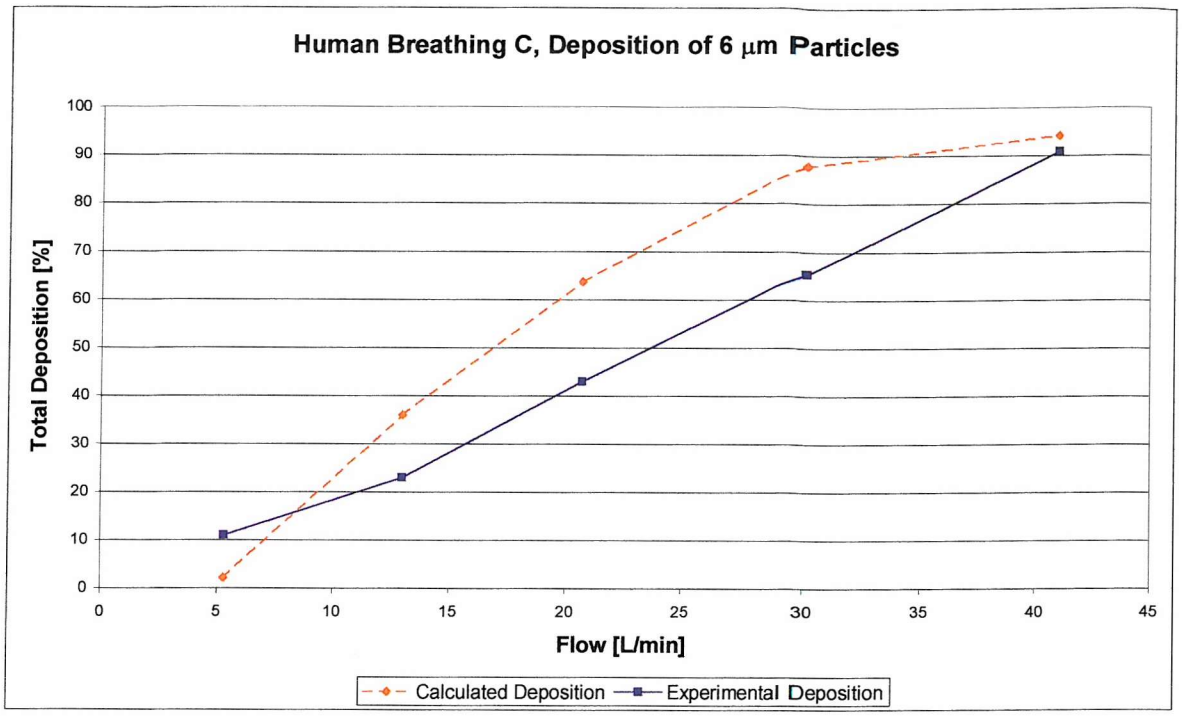

Figure 7.13: Comparison of Calculated and Experimental Deposition for 6 μm Particles and Human Breathing C

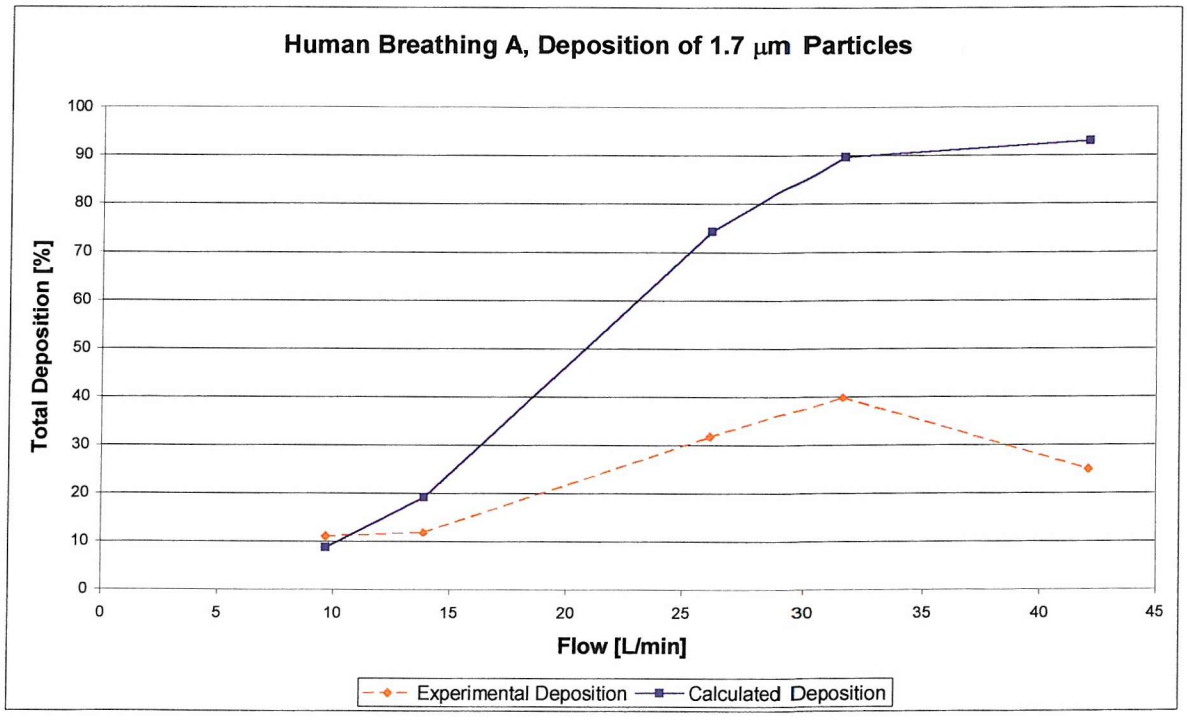

Figure 7.14: Comparison of Calculated and Experimental Deposition for 1.7 μm Particles and Human Breathing A

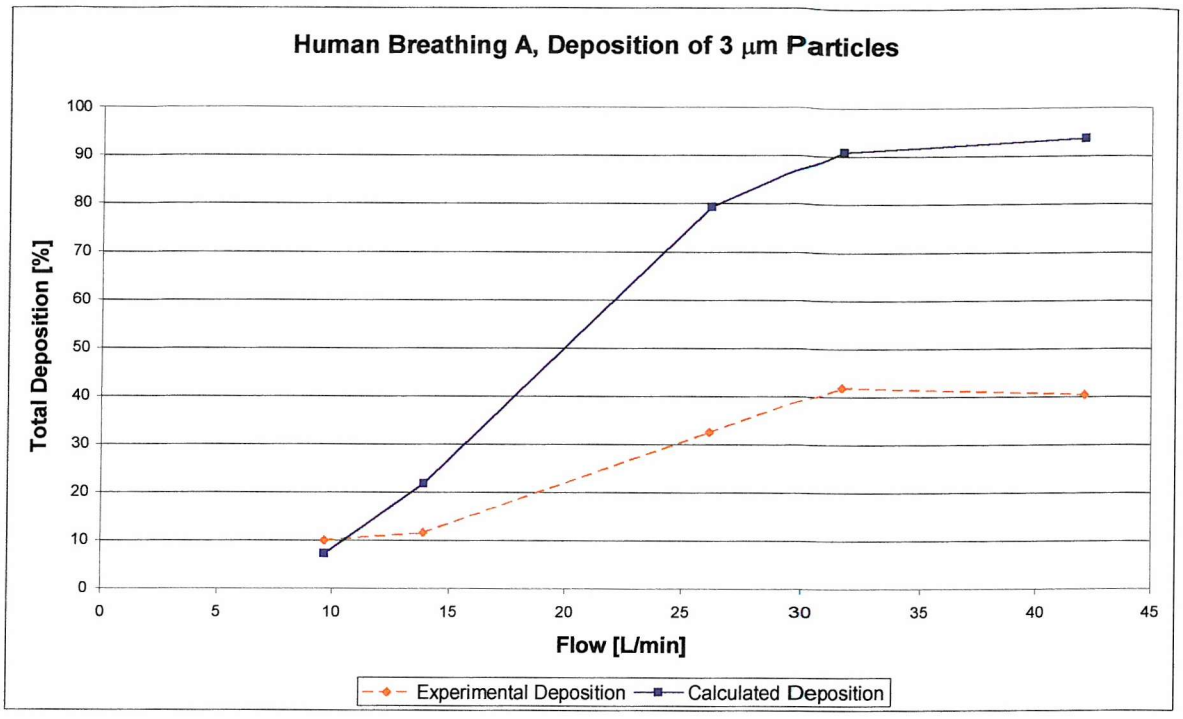

Figure 7.15: Comparison of Calculated and Experimental Deposition for 3 μm Particles and Human Breathing A

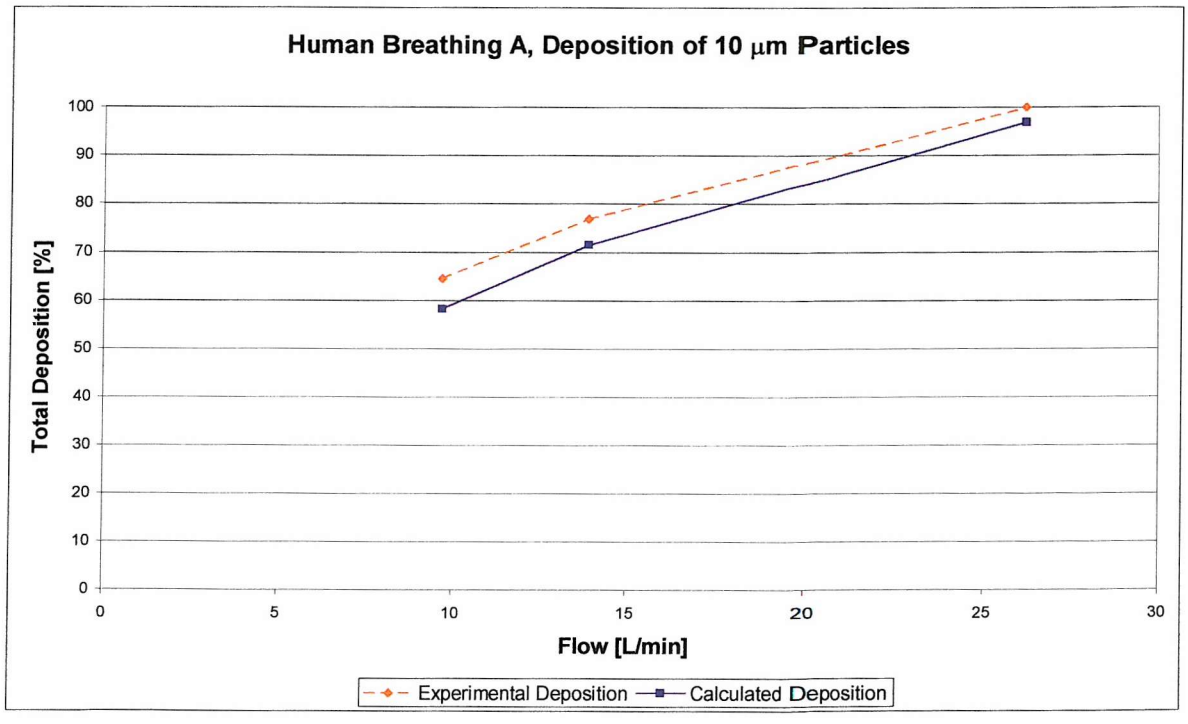

Figure 7.16: Comparison of Calculated and Experimental Deposition for 10 μm Particles and Human Breathing A

It appears that the method of simulating cyclic breathing patterns using constant flow is only valid for the larger particle sizes. The calculated patterns follow the experimental ones reasonably well for 6 μm and 10 μm droplets. For 1.7 μm and 3 μm particles the calculated deposition does not follow the experimental one at all.

7.3 Total Deposition Versus Impaction Factor

As stated before the impaction factor is widely used in the literature to describe deposition, which is mainly influenced by impaction. The impaction factor is $I = Q * d_{ae}^2$ where Q is the average volumetric flow rate in L/min and d_{ae} is the aerodynamic diameter. The total deposition versus impaction factor using constant flow shows the following results:

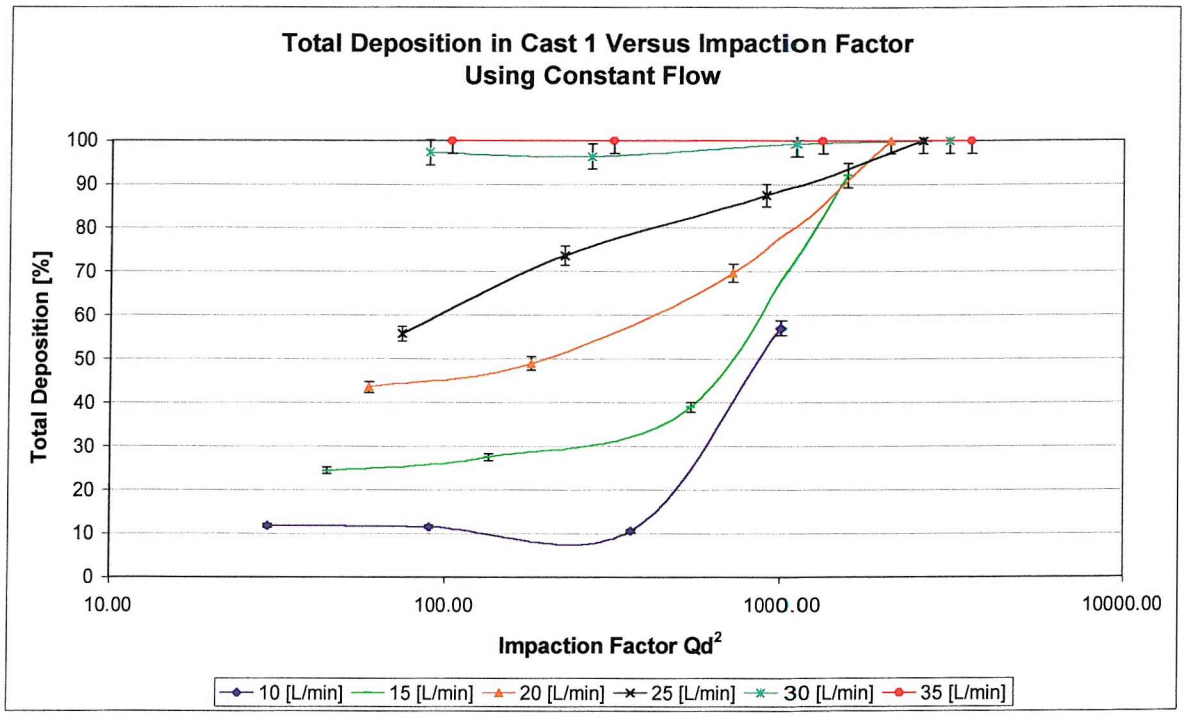

Figure 7.17: Total Deposition Versus Impaction Factor Measured in Cast 1 for Constant Flow

Especially for lower impaction factors the data points are still on the single curves. It appears that the points get closer together when the impaction factor becomes higher.

For human breathing A the scatter plot seems to be closer together and again the curves appear to converge with a higher impaction factor.

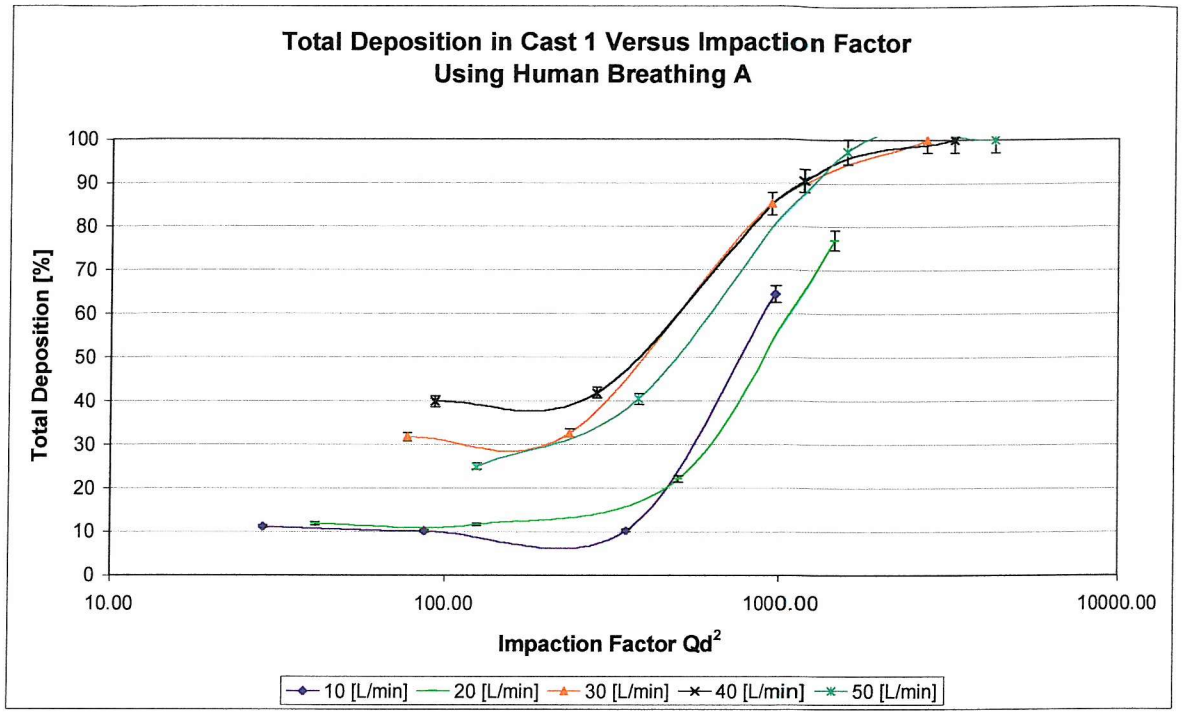

Figure 7.18: Total Deposition Versus Impaction Factor Measured in Cast 1 for Human Breathing A

7.4 TOTAL DEPOSITION VERSUS DIFFERENT ANATOMICAL FACTORS

The following graphs result from the investigation into the influence of anatomy on deposition. Human breathing A and constant flow were used together with 6 μm particles. The casts 1 and 2 were as mentioned before made from two Caucasian volunteers and nostril set 3 and 4 from an Afro-American and an Asian volunteer respectively.

Figure 7.19 and Figure 7.20 show the comparison of deposition in cast 1 plus nostril set 3 and cast 1 only for constant flow and human breathing respectively. Both diagrams show no apparent difference between the two curves.

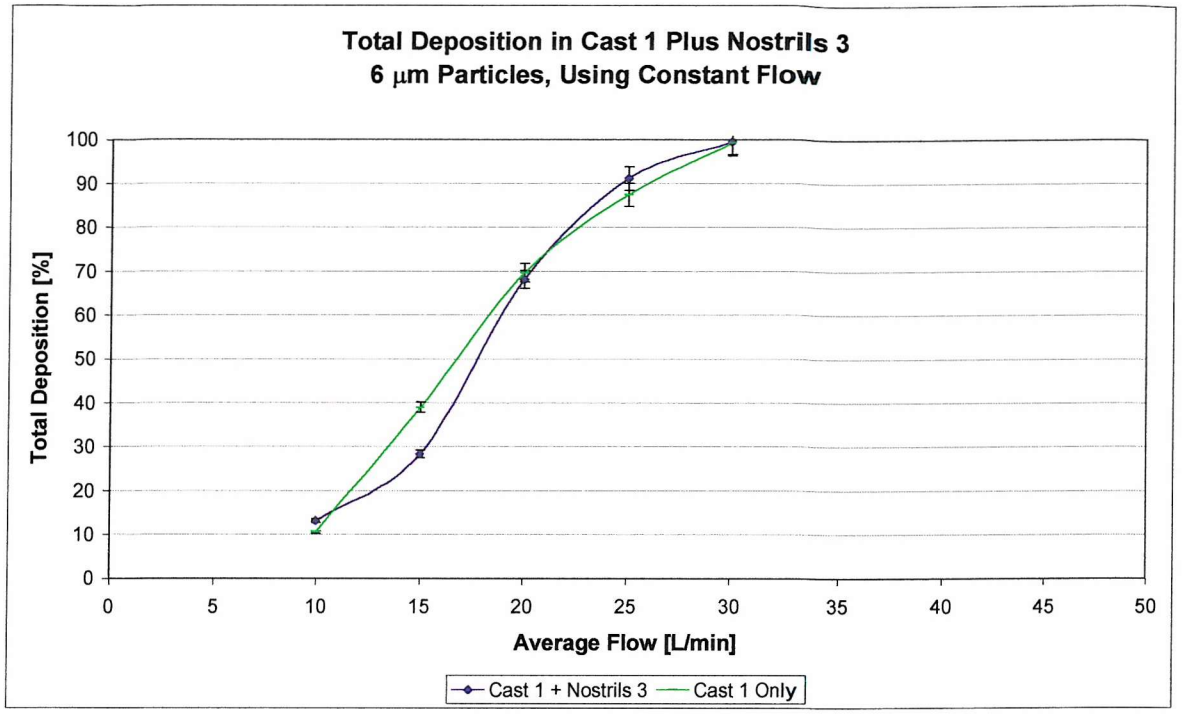

Figure 7.19: Comparison of Deposition in Cast 1 and Cast 1 with Nostril Set 3, for Constant Flow and 6 μm Particles

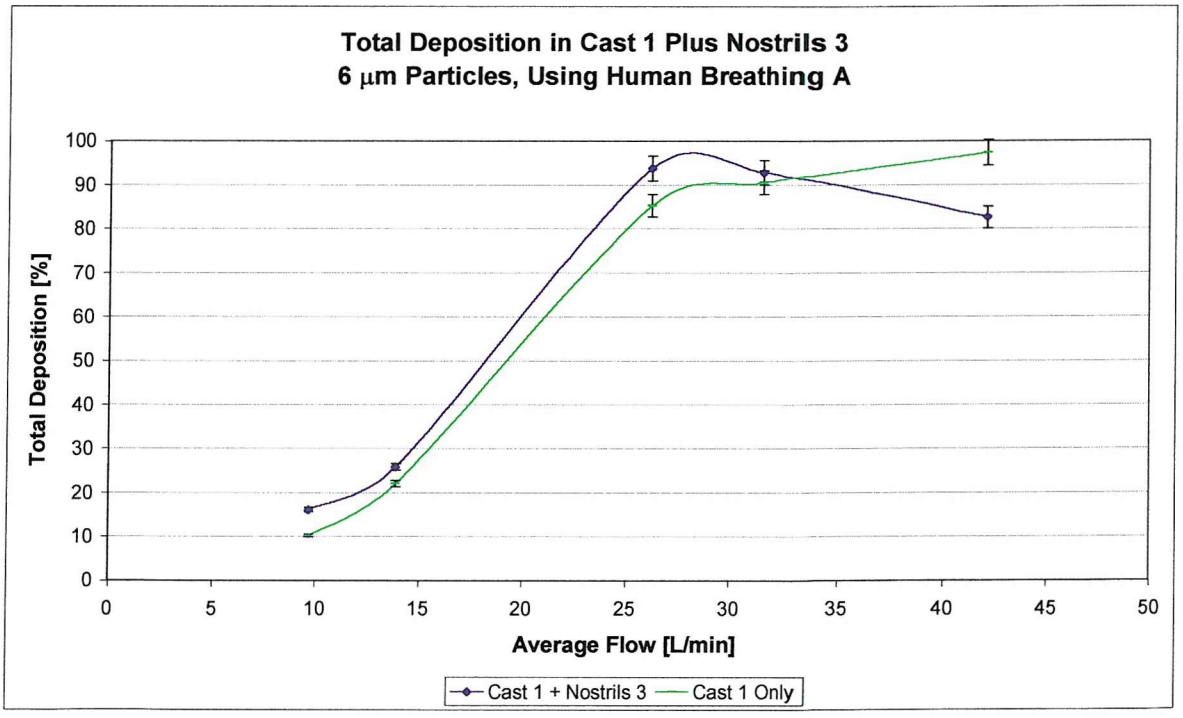

Figure 7.20: Comparison of Deposition in Cast 1 and Cast 1 with Nostril Set 3, for Human Breathing A and 6 μm Particles

Figure 7.21 and Figure 7.22 show the comparison of deposition in nostril set 4 attached to cast 1 and cast 1 only. Also here there is no apparent difference visible in either diagram.

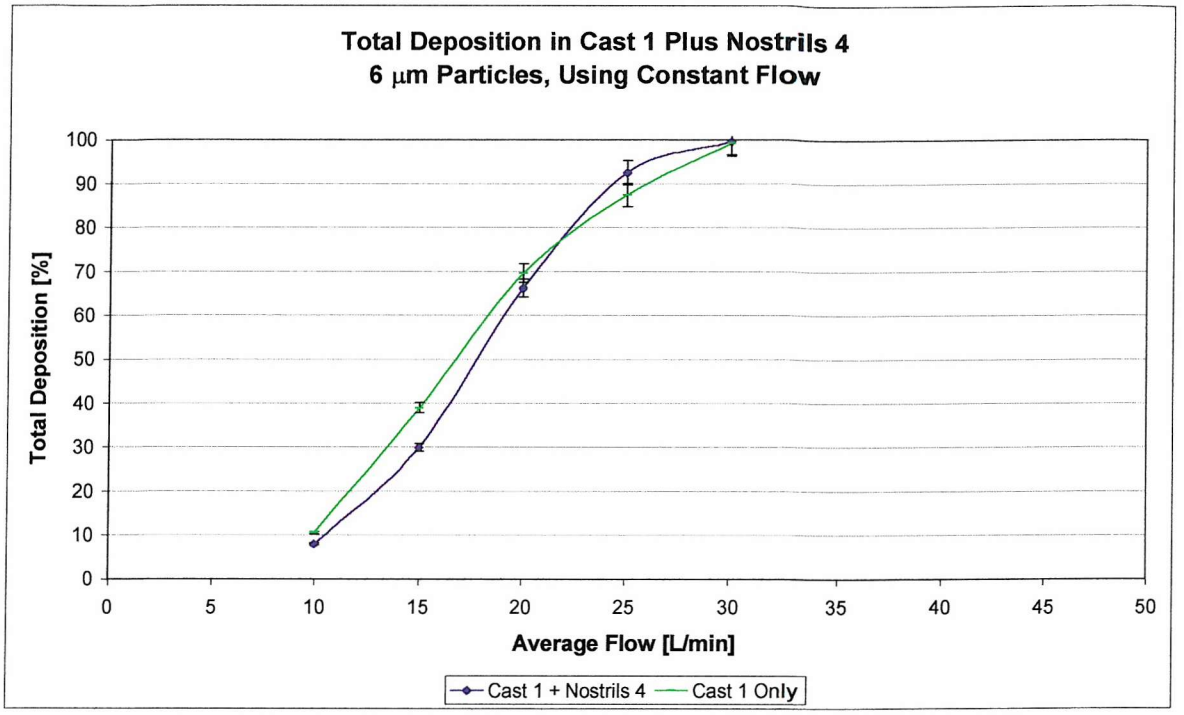

Figure 7.21: Comparison of Deposition in Cast 1 and Cast 1 with Nostril Set 4, for Constant Flow and 6 μm Particles

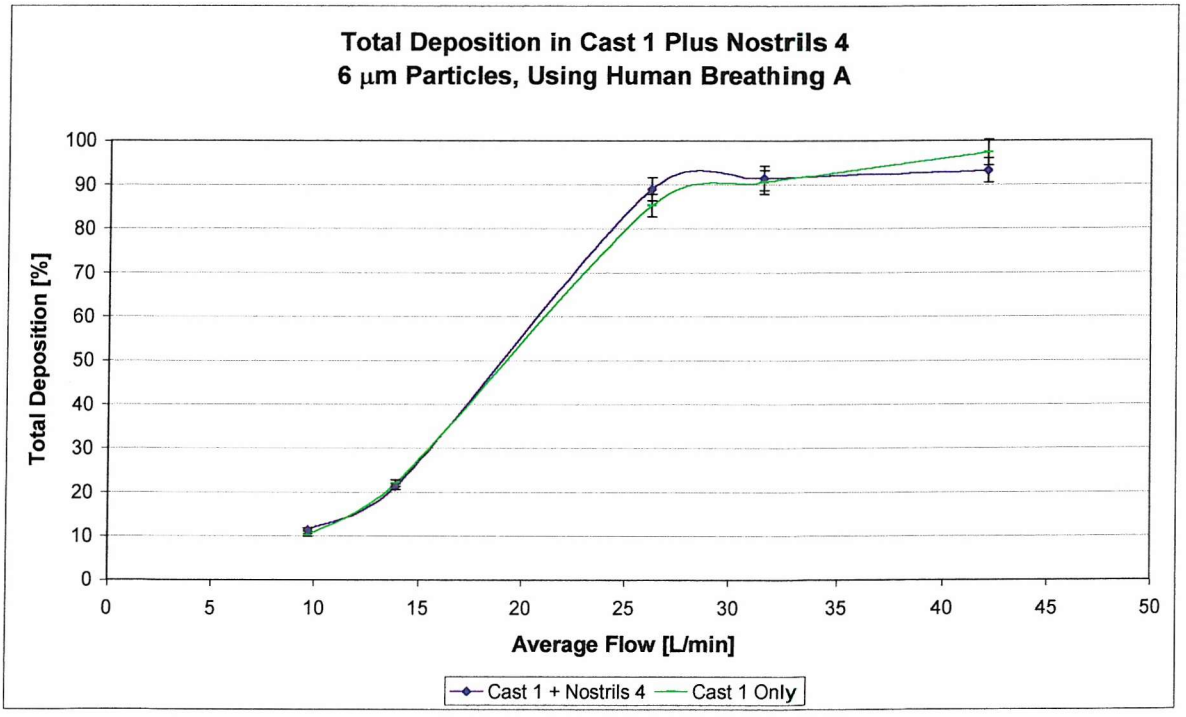

Figure 7.22: Comparison of Deposition in Cast 1 and Cast 1 with Nostril Set 4, for Human Breathing A and 6 μm Particles

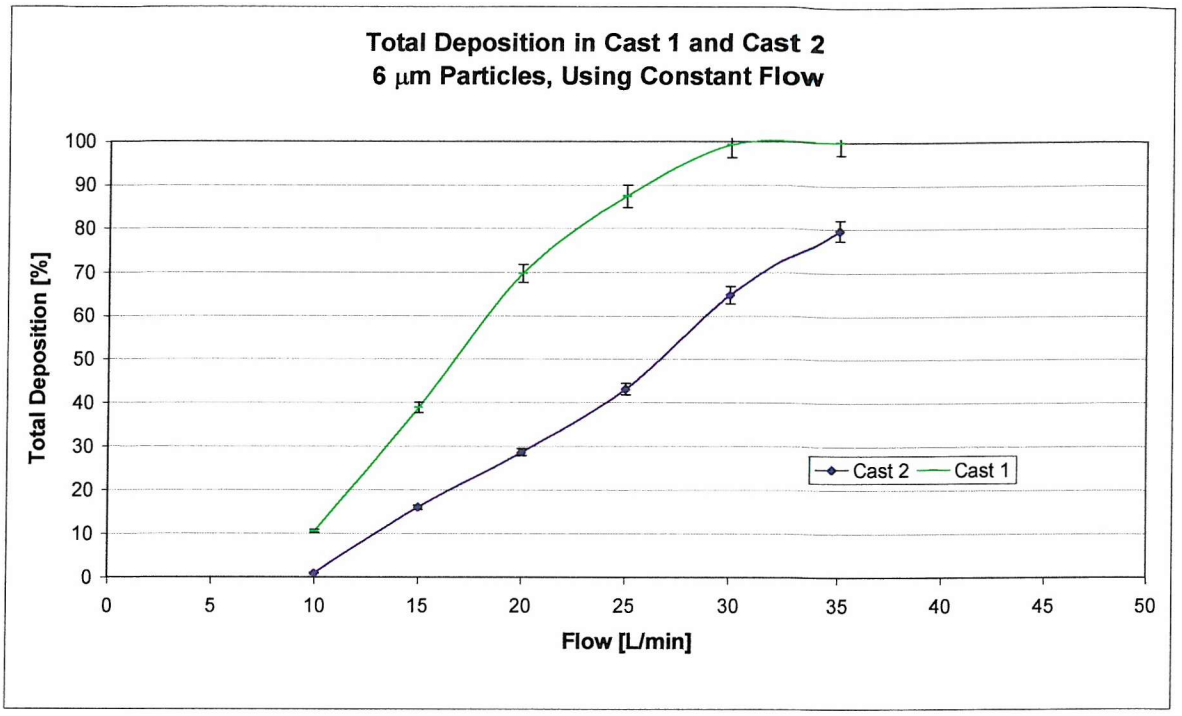

Figure 7.23: Comparison of Deposition in Cast 1 and Cast 2, for Constant Flow and 6 μm Particles

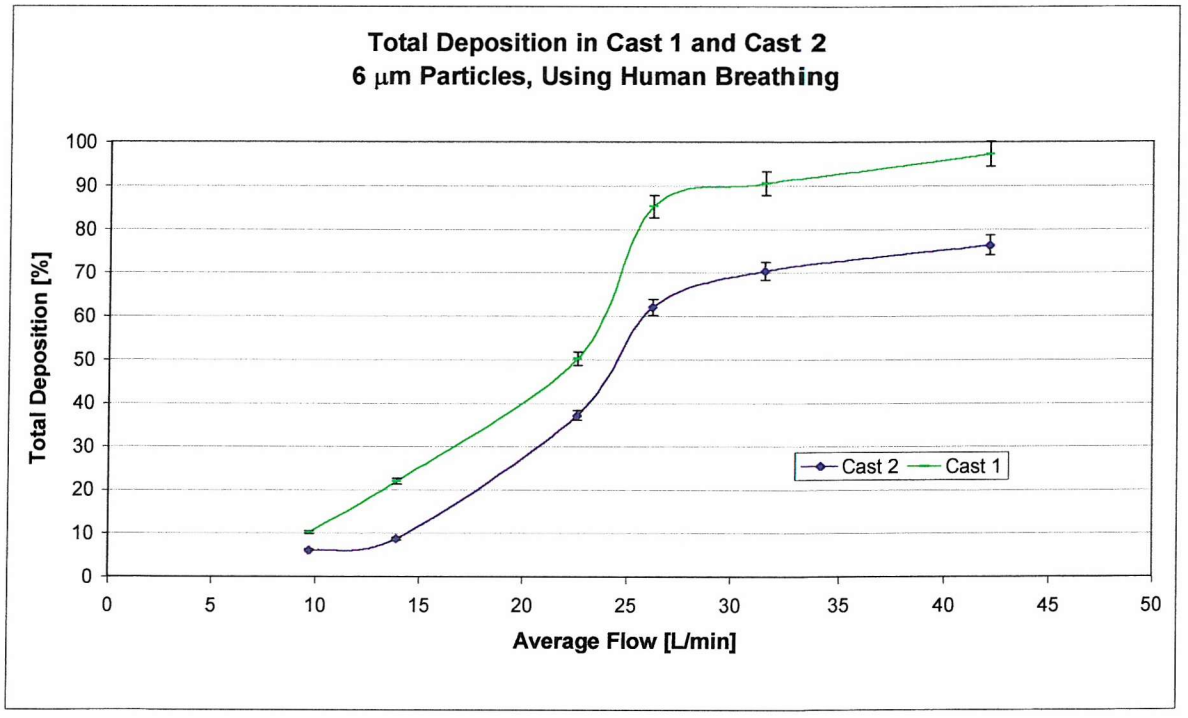

Figure 7.24: Comparison of Deposition in Cast 1 and Cast 2, for Human Breathing A and 6 μm Particles

The comparison of deposition between cast 1 and 2 shows significant difference. The deposition is lower in cast 2 and does not reach more than 80 % deposition for constant flow. The deposition measured using human breathing A shows a more pronounced S-shape in both casts. Also here cast 2 has a lower deposition than cast 1 and does not reach the 100 % deposition whereas cast 1 does.

7.5 DISCUSSION

Figure 7.1 and Figure 7.2 show the deposition as a function of particle size for distinct flow rates. Swift et al (Swift 1991) conducted comparable experiments, for the same particle range and at similar flow rates using constant flow. The results in this study show considerably lower deposition at 15 L/min than those of Swift. Swift's data show a deposition of 40 % at 15 L/min and 3 μm whereas the measurement here shows 28 %. At a particle size of 4 μm and the same flow rate Swift's is already up to 70 %, whereas here it is as low as 40 % for 6 μm. For the higher flow rates it is the other way around. The data of Swift show considerably lower deposition than the data here, for example 30 L/min flow rate shows 30 % deposition in Swift's data and 90 % deposition here. The greatest difference is that Swift's data show zero deposition for even high flow rates when the particles are small. The data here have a considerable amount of deposition for high flow rates even when the particle size is small. The difference between the cast used by Swift and the cast used here is first of all that they are made from different volunteers (same MRI scans as cast 2 was made from). But also Swift's cast is hand-carved with a larger cutting tool then the one used here. The tool used here had a diameter of 0.25 mm, whereas Swift's tool was larger than this (Kesavanathan 1998). The small tool used in this study together with a computer controlled milling machine enabled the precise cutting of even very fine passages as they occur in the turbinate region.

Itoh's data show considerably lower deposition for a flow rate of 26 L/min than the data presented here. Their deposition is around 1 % for 1.5 μm, whereas here it is already 40 % for this size and flow rate. It does not reach much more than 50 % in Itoh's study for about 6 μm whereas here it is around 70 % (Itoh et al 1985). Again here the most obvious difference is that Itoh's total deposition starts from a very low value at high flow rates,

which is not reached in this study. The same difference applies here, the cast used by Itoh was moulded from a corpse which has larger airways than a living human.

The results show that deposition caused by constant flow is generally higher than deposition caused by cyclic human breathing. The difference diminishes when the particle size becomes larger, but is still visible. The influence of breathing patterns on the deposition efficiency could have two explanations. First of all the cyclic flow patterns cause different flow conditions in the cast than the constant flow. Flow changes direction and is not stable at any point. This will cause different turbulence and vortices than constant flow.

Secondly the cyclic flow patterns have a high share of very low flow and comparing constant flow to the average flow value of the cyclic patterns might not be valid. A deposition pattern can only be represented by its mean values if deposition is directly proportional to the flow rate over the entire range of instantaneous flow rates. To investigate this, the breathing patterns were partitioned into small elements of approximately constant flow (6 ms). The deposition of each element was calculated on the basis of measured deposition at constant flow and hence deposition was calculated. But as shown in the results this does not fit for smaller particles, whereas it appears to fit well for the larger particle sizes. Therefore there must be another reason for the difference of cyclic breathing pattern and constant flow.

Gurman et al (Gurman et al 1984b) (Gurman et al 1984a) studied the deposition in a tracheo-bronchial cast using constant and cyclic flow. Their experimental work showed that cyclic flow enhances deposition compared to constant flow. They put it down to increased turbulence caused by the cyclic pattern, which increases the deposition by impaction. Gurman et al also observed a greater difference between deposition caused by cyclic breathing and constant flow for the smaller particles. They argued that the boundary layer thickness affects particle behaviour close to the wall. Turbulence decreases the boundary layer, which increases impaction. This affects small particles more than larger ones since the larger ones would deposit even with a thicker boundary layer.

For the nasal model the opposite is the case, the deposition is much lower for cyclic flow than for constant flow. The reason for this could be that due to the unique anatomy of the nose, turbulence is always present. Therefore turbulence will be there for constant flow as

well as cyclic flow patterns. But maybe the anatomy of the nose is optimised for cyclic flow and fewer vortexes are caused by it than by constant flow. The fact that the difference between deposition at constant flow and deposition at human breathing increases with decreasing particle size confirms this assumption. The smaller the particles are the more likely they are influenced by local eddies. As particle size increases the relaxation time of the particles increases (they do not adjust to new situations that quickly) and therefore local eddies do not influence them to that extend.

The deposition measured with human breathing patterns for 1.7 and 3 μm droplets decreases at the highest flow rate. Apparently the same does not occur for larger particles. Possibly higher flow rates cause different vortices to slower ones and the larger particles are less influenced by the vortices due to their high inertia.

Total deposition versus impaction factor does not show one curve for constant flow, but comes close to one curve for human breathing. Contrary to that Swift's (Swift 1991) data show a single curve when deposition efficiency is printed versus the impaction factor for constant flow. The reason for this is believed to be the same as mentioned above, the airways in Swift's cast are wider. The fact that the human breathing pattern comes closer to one curve than constant flow also indicates that there are more vortices at constant flow, since the impaction factor does not account for secondary flow (Scott et al 1978).

There is no significant difference in deposition with different nostril shapes for the measured particle size. This suggests that the shape of the nostrils does not influence the deposition in the nose contrary to the theory of Kesavanathan. It appears to be more likely that the effective difference lies further back in the nose maybe the valve and/or the turbinates determine the deposition. If deposition in the nose is mainly caused by impaction as suggested by several authors (see section 2.5 for reference) then it would be much more likely that the nasal valve influences the deposition. In the nasal valve is the first 90° bend and the particles which have to follow this, will be also accelerated because of its narrowness.

For different casts the difference in deposition is consequently much more pronounced. But as cross-sectional area comparison in Figure 6.5 shows the difference at the valve region is

not that pronounced between the two casts. It is a much larger difference in cross-sectional area towards the throat. Comparing the two casts it seems to be more likely that the airway close to the throat has more influence than the nasal valve, since the difference at the throat region is greater between the two casts. It is highly unlikely that there is only one site in the nose that determines the deposition behaviour, but each individual nose has its own characteristics and therefore it is unwise to draw general conclusions from the limited measurements reported here.

Figure 7.23 and Figure 7.24 show that the deposition curves are rather straight for constant flow and S-shaped for human breathing A, regardless which cast is used. That suggests that breathing pattern rather than anatomy influences the shape of the deposition curve.

8 PARTICLE DISTRIBUTION MEASUREMENT WITHIN THE CAST

To determine the distribution of particle deposition pattern in the cast, the aerosol was radioactively labelled and then drawn through the cast. The breathing patterns used to do this were human breathing A at rest and at light exercise. The particle sizes were 1.7, 3 and 6 μm. In the in-vivo study radioactively labelled particles were administered to volunteers at rest and light exercise. These settings were used to match the in-vivo study (Etherington & Smith 1996; Smith et al 1996, Etherington et al 1998) and be able to compare the results as described in chapter 9.

The total deposition on each plate was measured using NaI detectors and then the plates which had more activity than 1 kBq were put on an X-ray film to produce autoradiographs. For each experiment the total amount of activity is shown in a diagram versus the plate numbers. After this the individual geometries with the deposition as indicated on the X-ray film are sketched. The geometries as shown are in Figure 8.2, Figure 8.4, Figure 8.6, Figure 8.8 and Figure 8.10 are 3 mm apart.

8.1 DEPOSITION PATTERN OF 1.7 μm PARTICLES FOR HUMAN BREATHING AT REST

The total deposition in cast 1 was 17 % for 1.7 μm particles drawn through the cast using Human Breathing A at rest. The distribution within the cast is shown in Figure 8.1.

The figure shows the amount of radioactivity on the plates of the cast, beginning at the left-hand side with the nostril part and ending at the right-hand side with the throat.

The two maxima in the cast were in the middle of the turbinate region and at the throat. Other major points of deposition: Second half of nostrils, lower nasal valve, appearance of first and second turbinate, generally the turbinate region.

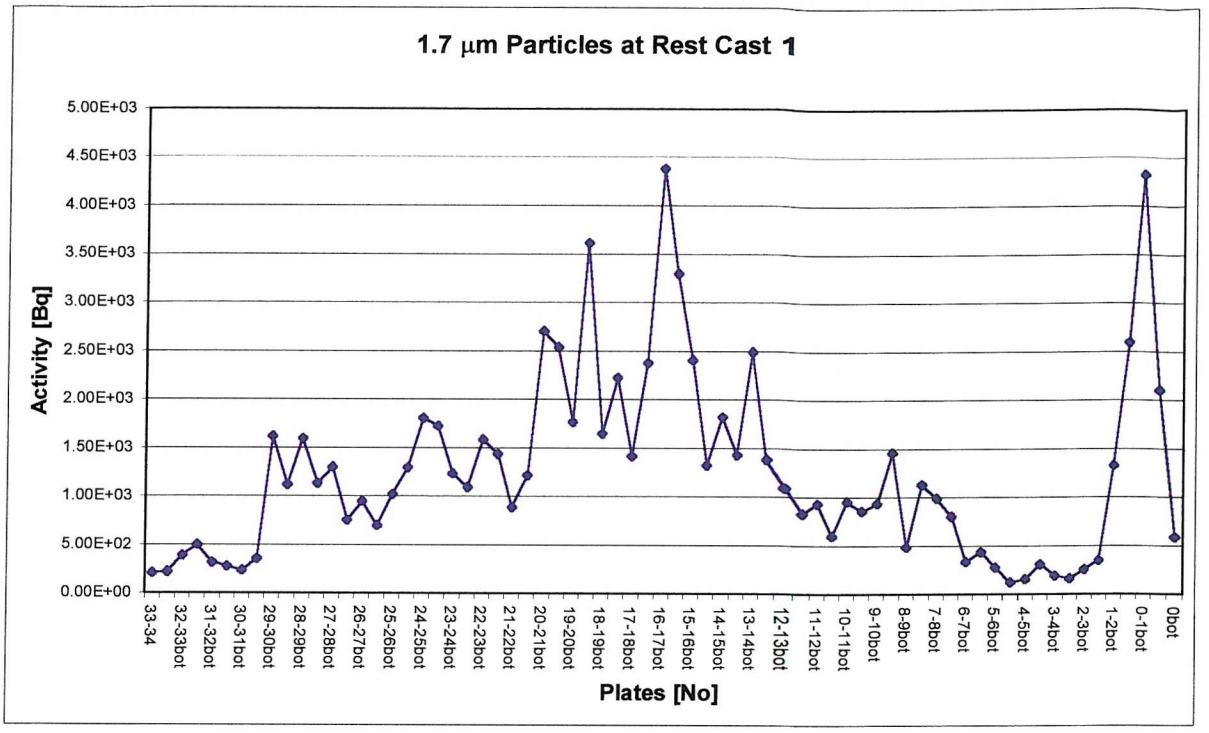

Figure 8.1: Deposition of 1.7 μm Particles on Each Plate in Cast 1 for Human Breathing A at Rest

The first region of higher deposition is from plate 30 – 27. This corresponds to the second half of the nostrils and the deposition is around the side of the alae. The second plateau is from plate 24 to 23, which is the nasal valve. The deposition here is in the lower region of the valve. Also, further on when the first turbinate starts to form at plates 22 and 21, the deposition is in the lower part for both airways. In geometry 20 and 19 the middle turbinates start and here the deposition is also in the middle part as well as to the lower part. Around these plates is a relative maximum, probably because of the starting middle turbinate. The absolute maximum is around plate 16. This geometry has two hot spots: On the right-hand side there is one around the lower turbinate towards the septum and on the left-hand side around the middle turbinate. Some deposition is also visible in the olfactory bulb on the left-hand side. Geometry 15 shows deposition almost all over the right-hand side without visible hot spots whereas the left-hand side has one pronounced hot spot between the middle and the superior turbinate. Geometries 14 and 13 have both the main deposition on the right-hand side.

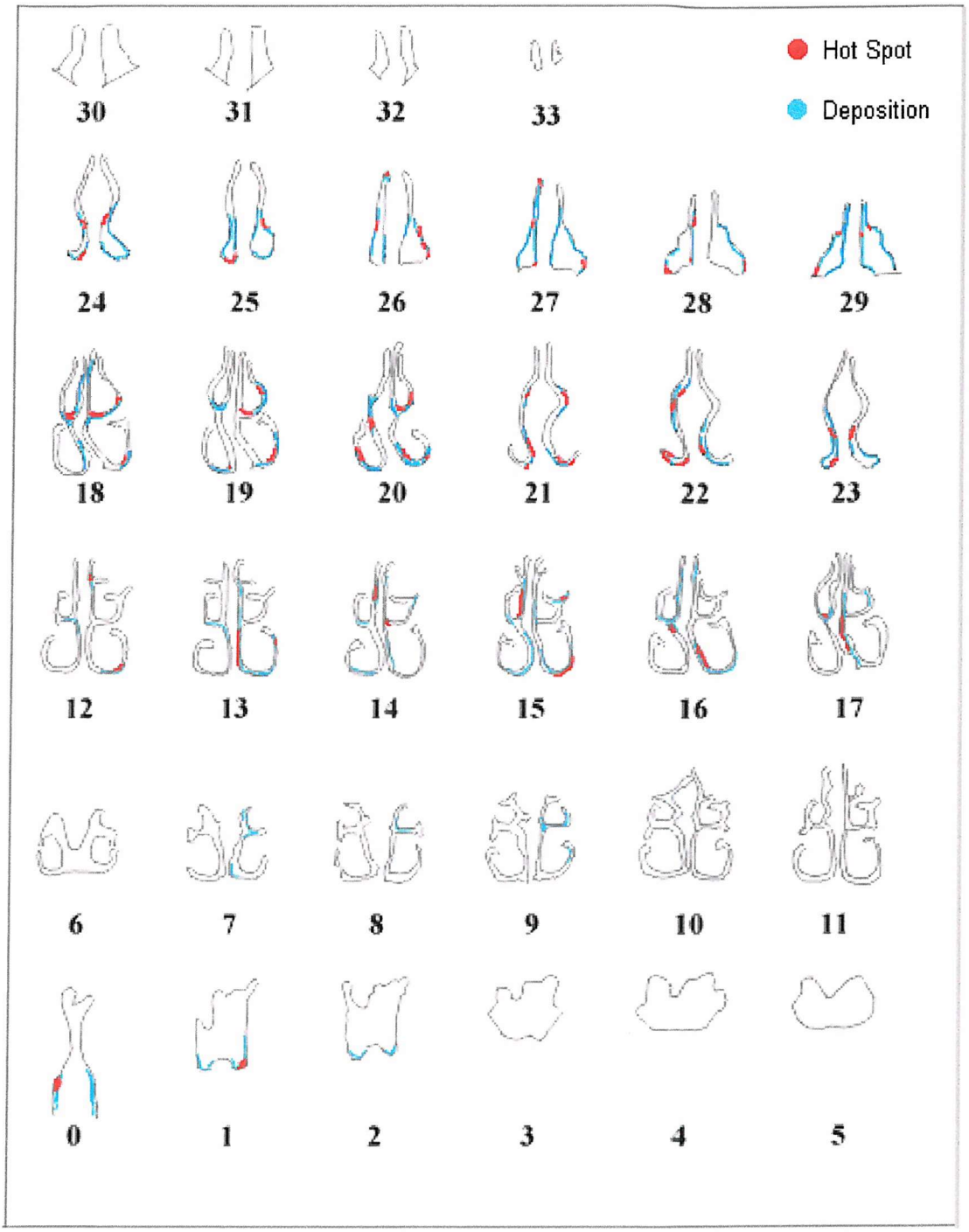

Figure 8.2: Deposition Pattern of 1.7 μm Particles on Geometries of Cast 1 for Human Breathing at Rest

The plates in between down to 9 were too low to trace by the X-ray film. Plates 9 to 7 show the main deposition still on the right-hand side, but now in the upper section of the airway (which is due to the changes in geometry about the same height as the middle section was a few plates before). Activity on the plates was too low for the X-ray film from

plate 6 to 3. But from plate 2 onwards it increases again. Geometries 2 and 1 have hot spots on the bottom of the airway sideways. Geometry 0 has the hotspot at about the same height as 3 and 2 on the side. Note that the cast ends at geometry 0 and the hot spots on this geometry are at the side of the airway, not in the middle as one might have expected them to impact.

8.2 Deposition Pattern of 3 μm Particles for Human Breathing at Rest

The total deposition for 3 μm particles drawn through the cast for human breathing A at rest is 24 %.

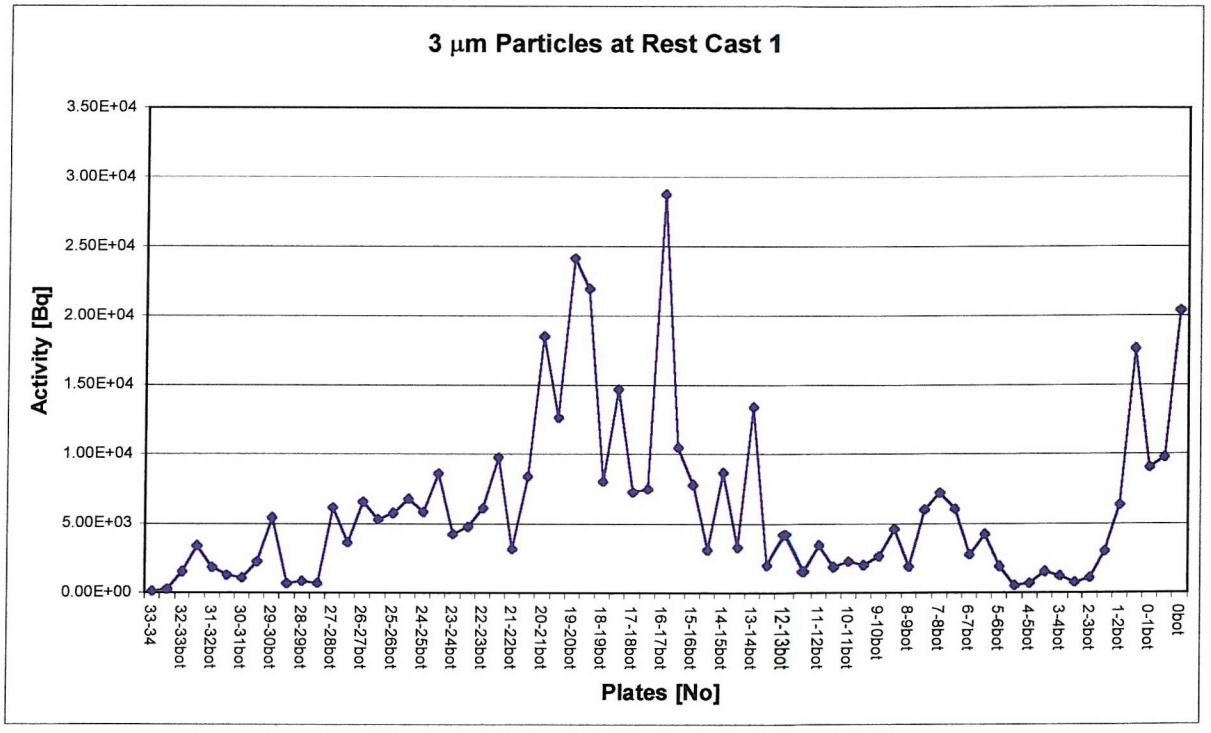

Figure 8.3: Deposition of 3 μm Particles on Each Plate in Cast 1, for Human Breathing A at Rest

The deposition of 3 μm particles in cast 1 is mainly in the first half of the turbinate region and the second site of deposition is at the throat. Deposition is rather low in the nostrils. Deposition in the nostrils is in the upper part or on the roof of the nostrils. The first higher plateau is from plate 26 on, which is the region of the nasal valve. The deposition in the

nasal valve is in the lower half of both airways on the sides. After the nasal valve, when the inferior turbinate starts (geometry 23-24) deposition is also found in the upper half of the airways. The first relative maximum is found at geometry 20, where the middle turbinate starts to develop. The hot spots on both sides of the airways are at the bottom of the middle turbinate. The next higher peak is around geometry 18 and here again the hot spots are around the bottom of the middle turbinate. Some deposition is also found in the right airway on the right-hand side of the inferior turbinate. From geometry 18 to 16 the deposition is distributed over the airways, even though it looks like the right-hand side has higher deposition than the left-hand side. And the left inferior turbinate has next to nothing. Also remarkable is that from geometry 17 downwards there is deposition found in the olfactory region. The highest peak is at geometry 16. The deposition here is apparently higher on the right-hand side and the hot spots are found where the superior turbinate starts, at the bottom of the middle turbinate and at the right-hand side of the inferior turbinate. Geometries 15 and 14 still have more deposition on the right-hand side, but the deposition site around the inferior turbinate seems to move from the right side towards the middle. The next peak is at geometry 13. Here the deposition is alongside the inferior turbinate but now only in the middle and at the bottom. From this geometry on down to geometry 8 there is not much deposition and most of it in the right-hand side airway. Around 8 to 7 is the next relative maximum in deposition, the location of it is still at the right-hand side and rather distributed over the whole airway. From 7 to 2 is the deposition very low, and most of it is in the upper parts of the airway, which is already merged here. From geometry 2 onwards the deposition is on the bottom of the airway. Also for geometry 1, the hot spots are on the bottom of the airway. Geometry 0 shows also the deposition on the bottom, note that the deposition is at the side of the airway.

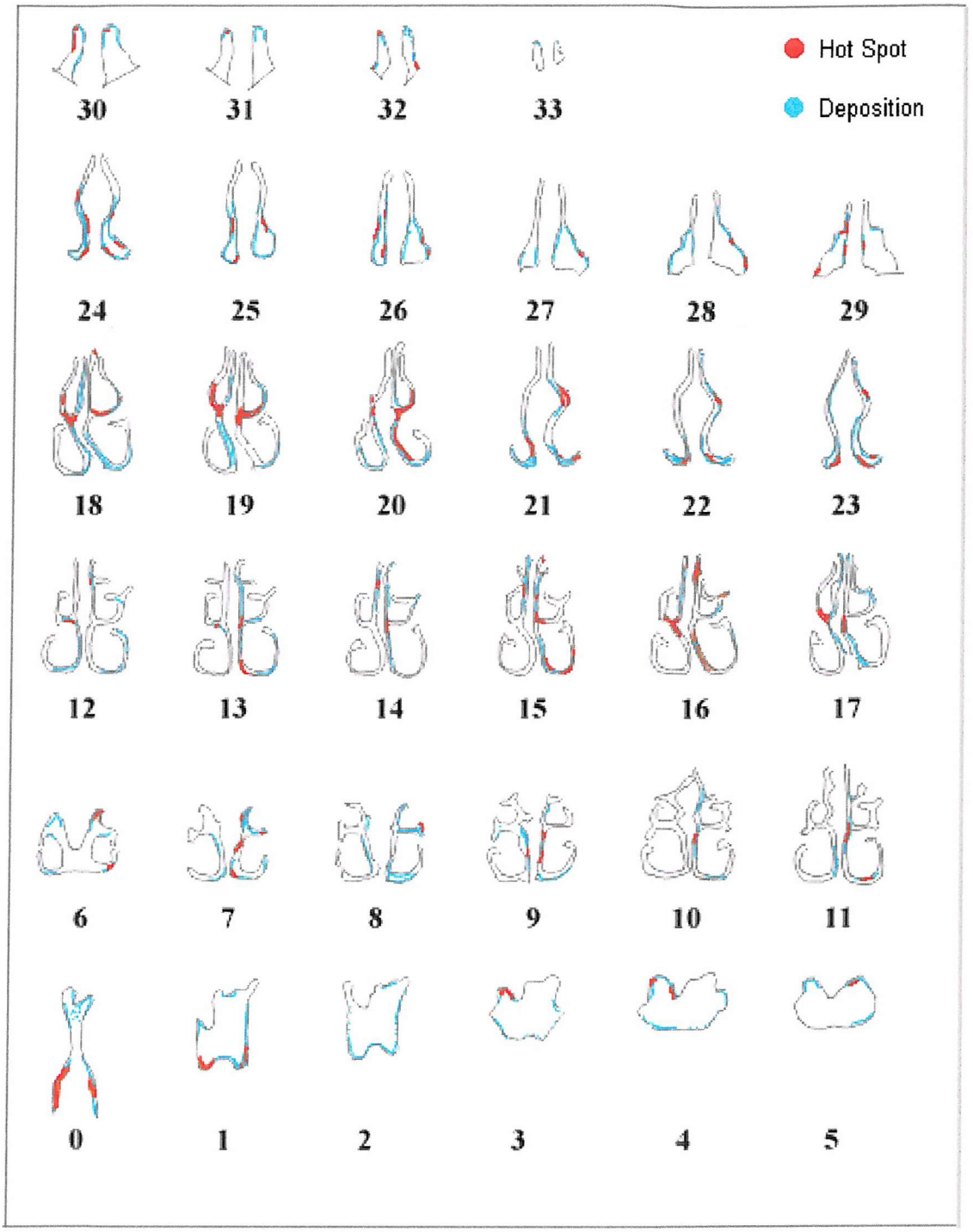

Figure 8.4: Deposition Pattern of 3 μm Particles on Geometries of Cast 1 for Human Breathing at Rest

8.3 Deposition Pattern of 3 μm Particles for Human Breathing at Light Exercise

Particle deposition for 3 μm particles drawn through the cast using human breathing A at light exercise is 51 %.

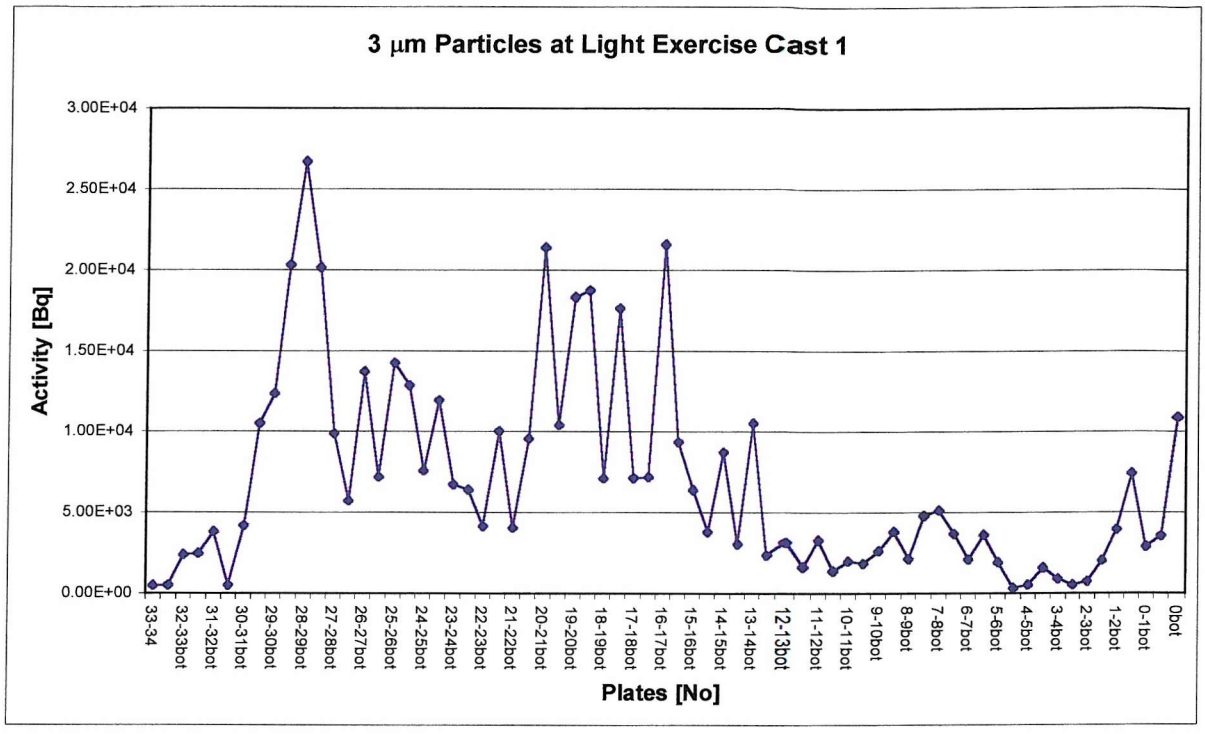

Figure 8.5: Deposition of 3 μm Particles on Each Plate in Cast 1 for Human Breathing A at Light Exercise

Deposition is at its maximum at the second half of the nostrils. The second major site of deposition is in the first half of the turbinate region and the third highest deposition site is in the nasal valve.

At the maximum around geometry 28 The deposition shows mainly at the side of the nostrils. From plates 26 down to 21 the total deposition is high, but no extreme peaks are found. The deposition site is mainly in the middle and lower part of the airways. It is definitely higher up in the airway than it was in the two previous experiments with breathing pattern at rest. The second highest peak of deposition is at the beginning of the middle turbinate at plate 20. Here the hot spots are around the middle turbinate and at the right-hand side of the inferior turbinate. At plate 19 the depositions are at the same sites.

From 18 onwards the hot spots distribute more around the airway, they are in the upper and middle part of the airways.

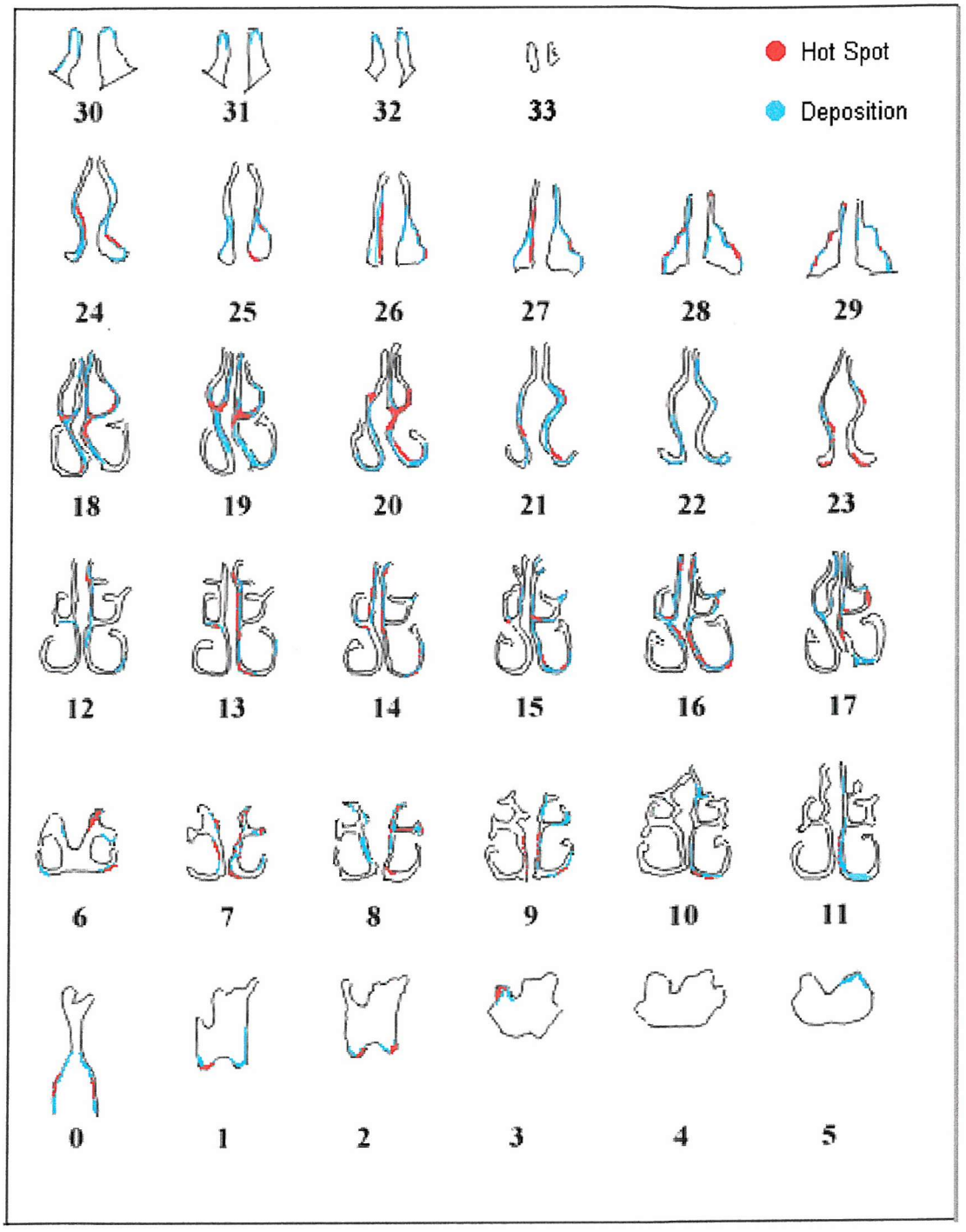

Figure 8.6: Deposition Pattern of 3 μm Particles on Geometries of Cast 1 for Human Breathing at Light Exercise

In geometries 17 and 16 the deposition is all over the right-hand side and in the upper part of the left-hand side. And in 17 there is deposition in the olfactory region on both sides. From geometry 15 downwards the peaks are lower and the deposition is mainly in the upper part of both sides, much of it in the olfactory region. The last peak before the throat is at geometry 14, apparently the deposition is mainly in the right-hand side here. The deposition from geometry 13 onwards is rather low, but appears to be mainly in the right-hand side airway. Only at geometries 1 and 0 where the airway bends down to the throat the deposition is higher. It is at the bottom mainly of geometry 1 and 0 and notable at the side of the airway on geometry 0.

8.4 Deposition Pattern of 6 μm Particles for Human Breathing at Rest

The total deposition in cast 1 is 49 % for 6 μm particles draw through it by human breathing A at rest.

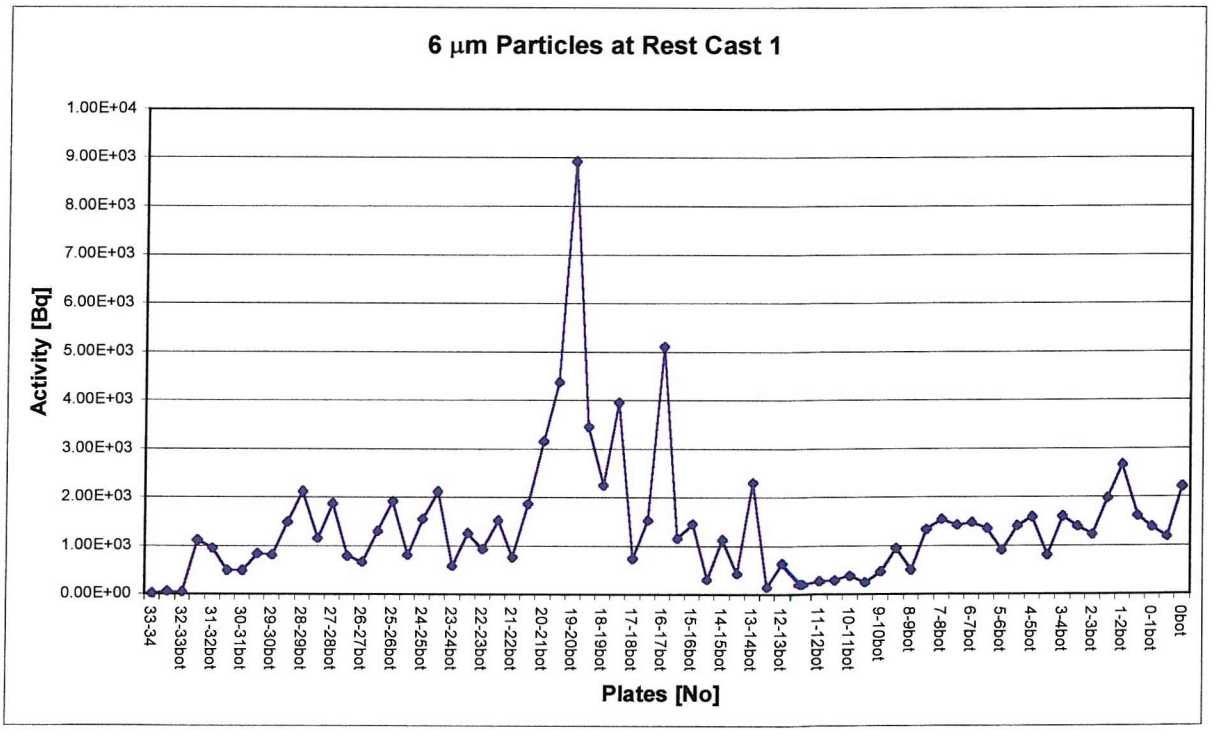

Figure 8.7: Deposition of 6 μm Particles on Each Plate in Cast 1 for Human Breathing A at Rest

The deposition is mainly in the front part of the turbinates. It has its peak at the beginning of the middle turbinate. Generally deposition is rather distributed over the whole cast.

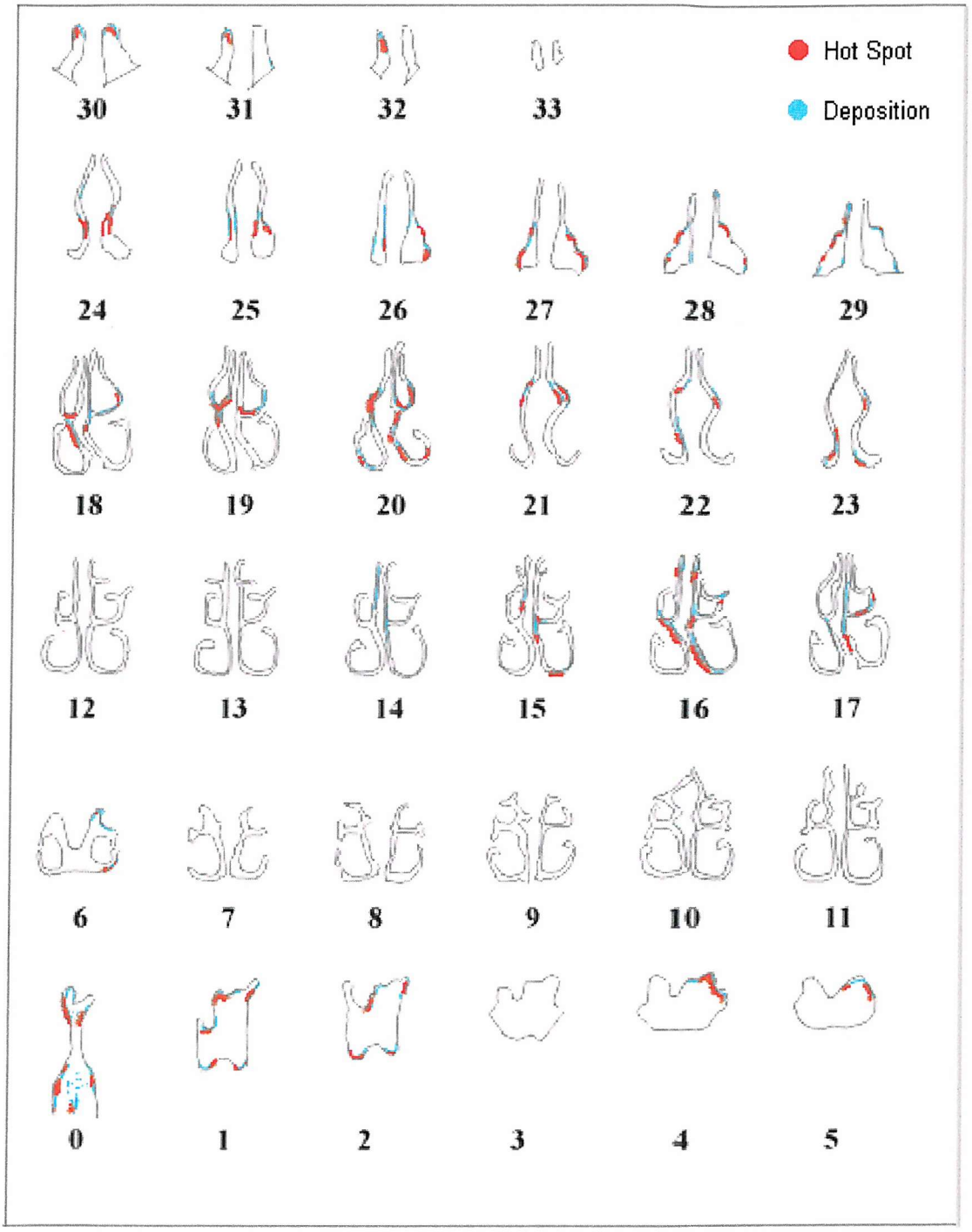

Figure 8.8: Deposition Pattern of 6 μm Particles on Geometries of Cast 1 for Human Breathing at Rest

Deposition in the nostrils starts out at their roof and then goes sideways mainly at the alae. Towards the nasal valve deposition is in the middle part of the airways, and some spots in the lower part as well. The first and main peak is at geometries 20 and 19. These are the geometries where the middle turbinate starts out. Deposition is very pronounced around the middle turbinate of both sides. Two smaller peaks are at 18 and 16. Deposition seems to be more on the right airway. It is distributed along the septum. From plate 15 down to plate 9 deposition is very low, but from 8 to 2 it is about as high as in the nostrils. Deposition around the throat is not as high as in the experiments before. The location of the hot spots is at the bottom sideways of the airway as it was before, but some visible deposition also at the roof of the airway.

8.5 Deposition Pattern of 6 μm Particles for Human Breathing at Light Exercise

The total deposition in cast 1 of 6 μm particles is 96 % for human breathing A at light exercise.

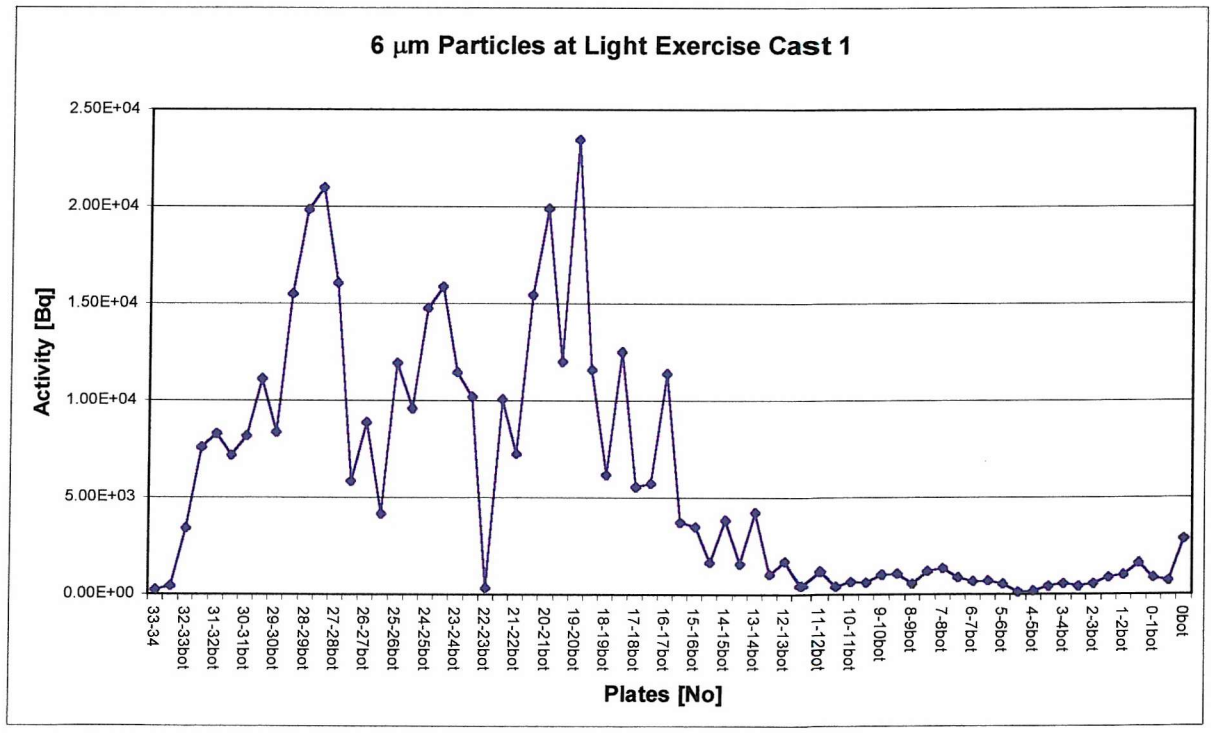

Figure 8.9: Deposition of 6 μm Particles on Each Plate in Cast 1 for Human Breathing A at Light Exercise

90 % of all particles deposit in the first half of the cast, down to plate 17. The main sites are the second half of the nostrils, the nasal valve and the beginning of the turbinates.

At the beginning of the nostril openings the hot spots are as before at the roof of the nostrils, but now as well towards the sides. At the second half of the nasal vestibule, the deposition comes to its first peak, the location of the deposition is at the side first at the alae and later towards the septum. The deposition decreases around the nasal valve (plate 25) and increases again at the appearance of the inferior turbinate (plate 24). But deposition is around the middle of both sides of the airways, not around the first turbinate. Note there is a pronounced minimum at plate 23, which could be an measurement-error, because it is not visible in Figure 8.10. The next peak is at plate 20 and as in all the experiments before the deposition is around the beginning of the middle turbinate. The difference here is that the absolute maximum is at plate 19, again deposition is around the middle turbinate. From plate 18 to 15 deposition is still high, and seems to be more in the right airway. Deposition visible in the olfactory region. From plate 14 downwards the deposition is very low. Only towards the throat at plate 0 it becomes a bit higher again, but not as much as at the smaller particle sizes. Note here for the first time deposition is in the middle of the back throat not only at the sides of it.

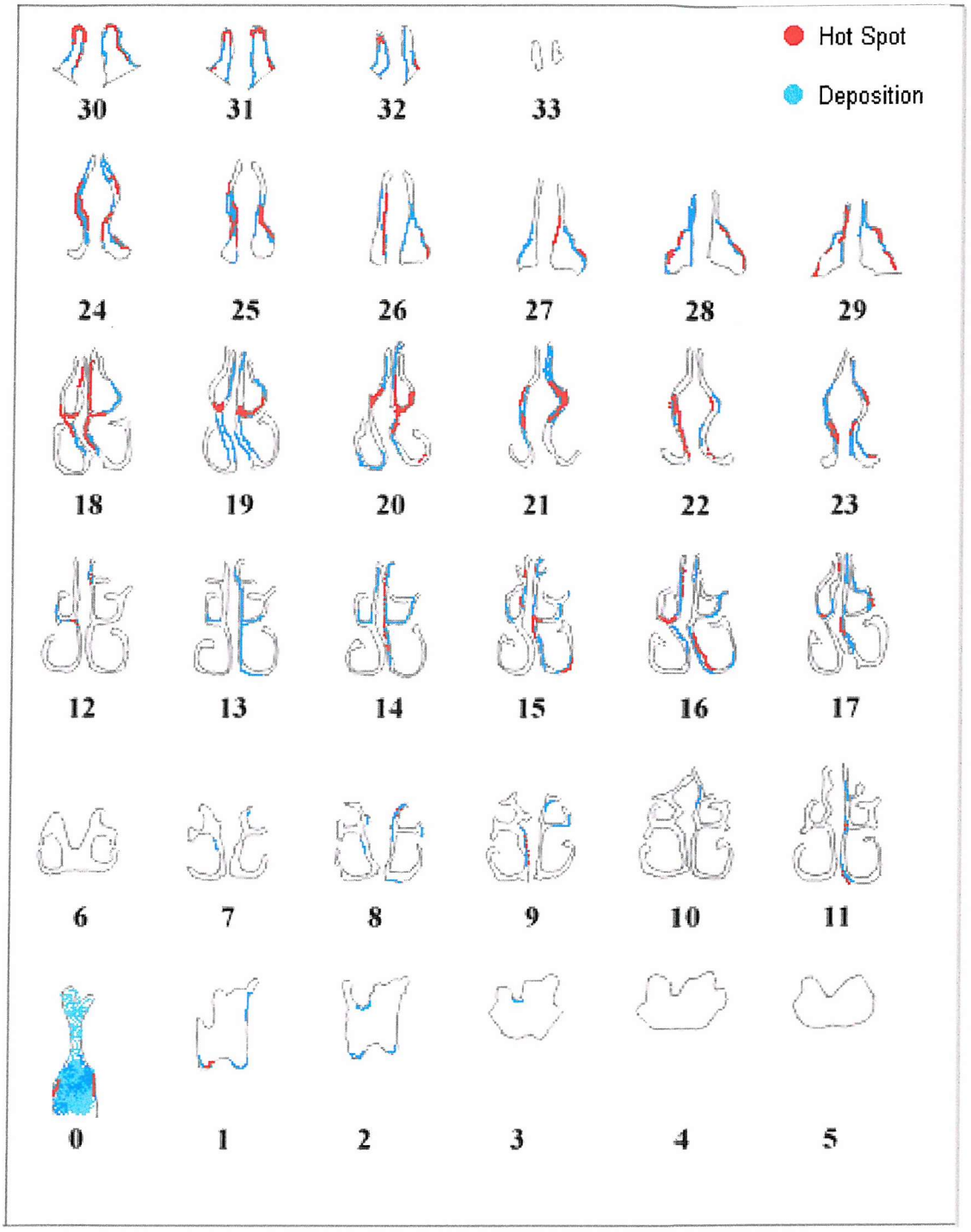

Figure 8.10: Deposition Pattern of 6 μm Particles on Geometries of Cast 1 for Human Breathing at Light Exercise

8.6 DISCUSSION

Particles of 1.7 μm, 3 μm and 6 μm in diameter were deposited in cast 1 using human breathing A either at rest or at light exercise. It is important to know the flow pattern of air in the nose to consider the deposition patterns of particles. As mentioned in section 2.3 the air enters the nostrils vertically and has to follow a 90° bend towards the nasal valve. The nasal valve is very narrow and therefore the air gets accelerated here. Towards the anterior part of the turbinates the bend is complete and the airflow is horizontal. At this point the airways widen again, which causes local eddies. The flow throughout the nose is considered to be unstable and especially turbulent in the turbinates region. After the turbinates cease the airways merge into one and finally bend again 90° towards the throat.

Figure 8.1 shows the deposition distribution of 1.7 μm particles within the cast. Deposition is mainly at the front and middle of the turbinate region and at the back of the throat, but there is also some deposition in the anterior part of the nose and the posterior part of the turbinates. The deposition for 3 μm particles at rest is less distributed and more concentrated at the beginning and middle of the turbinate region and the back of the throat as shown in Figure 8.3. Figure 8.5 shows the deposition of 3 μm particles at light exercise and here the deposition is more distributed over the whole cast again, but still the major deposition sites are the beginning and the middle of the turbinates and the back of the throat. Even though the maximum deposition is in the nostrils. Figure 8.7 shows the distribution of deposition for 6 μm particles at rest which is rather concentrated at the beginning and middle of the turbinate region. Figure 8.9 shows the deposition of 6 μm particles at light exercise and it is more distributed as at rest. It has the maxima at the nostrils and the beginning of the turbinate region.

Apparently breathing at rest does not create as much turbulence, therefore the 3 and 6 μm particles deposit mainly by impaction at the beginning of the turbinates. For light exercise or very small particles the deposition is more distributed throughout the cast. All particle sizes except 6 μm deposited at the side of the throat rather than at the middle of it as one would expect. It is not know what causes this effect.

The major deposition site in these experiments is the anterior end of the middle turbinate, which matches with the results of Itoh et al (Itoh et al 1985). The match becomes closer for

larger particles. The larger the particles are the longer is their relaxation time, which means they need longer to adapt to a new flow direction in this case. Consequently smaller particles do not deposit as much on the anterior end of the middle turbinate. Itoh et al put this fact down to local eddies after the nasal valve and say the smaller particles follow the vortices more and therefore deposit more before the appearance of the middle turbinate, whereas the larger particles are not as much influenced by the eddies and they therefore impact on the middle turbinate. Those conclusions can be only confirmed with regard to the larger particles. The small particles do not have significantly higher deposition in the nasal valve region or afterwards. They deposit more further back in the turbinates and at the back of the throat. The reason for this could be, that Itoh et al used first of all another cast and secondly constant flow to draw particles through the cast and constant flow causes different flow patterns and therefore different deposition patterns.

Zwartz and Guilmette (Zwartz & Guilmette 1999) used a duplicate of cast 2. The total deposition in the cast of 5.5 μm particles at 20 L/min constant flow rate was 36 %. Measurement of the individual plates showed that the deposition was almost entirely before the nasal valve. This difference from the deposition pattern here is probably due to the anatomy (here only cast 1 was used), but more so because a cyclic breathing pattern was used here, in contrast to the constant flow they used.

These two studies imply that the vortices caused by constant flow as mentioned in the section 7.5 occur in the anterior part of the nose, the nostrils and the nasal valve.

Taking the clearance zones into account that are described in section 2.1.2 it would imply that the particles are cleared from the nose as follows: For a breathing pattern at rest, particles seem to deposit mainly in the turbinate region. This implies that they are cleared by mucociliary action towards the throat and then swallowed if they are insoluble or taken into the bloodstream takes place if they are soluble. The smaller particle sizes arrive to the back of the nose and therefore a percentage of this deposit at the back of the throat, where they are immediately swallowed.

Only particles deposited with breathing pattern light exercise have a high deposition before the nasal valve, where no mucociliary clearance takes place. But also a high percentage deposits in the ciliated region and is cleared by mucociliary action. Virtually no particles get through to the throat for 6μm light exercise.

9 IN-VIVO IN-VITRO COMPARISON

Artificial nasal cavities are used more and more to simulate deposition in the nose. This chapter is concerned with the validation of the nasal cast, and therefore experiments done on the human volunteer are compared to the experiments done on the cast, which is made according to the anatomy of this volunteer. Not only total deposition is compared, but also the deposition distribution in the human nose, which was evaluated by the time the particles needed to clear, and the deposition distribution in the nasal cast.

The human volunteer study was carried out by the National Radiological Protection Board (Etherington & Smith 1996; Smith et al 1996, Etherington et al 1998). Particles of sizes 1.7, 3 and 6 μm were administered to volunteers at rest and light exercise, and then deposition and clearance measured. The in-vitro experiments are the same as in chapter 8, particles of different sizes were drawn through cast 1 with human breathing A at rest and at light exercise.

In the first section of this chapter the total depositions in the cast and in the human volunteer are compared, followed in the next section by deposition sites in the cast and in the human volunteer. The deposition sites in-vivo were evaluated according to the clearance of the nose. The activity which cleared very fast (2-3 minutes) was considered to be deposited at the back of the throat. Activity which is cleared within 16 minutes was considered to be deposited in the ciliated region of the nasal cavity. Activity that stayed longer than this or was cleared by nose-blow was considered to be deposited in the anterior part of the nose (Smith 1999).

The regions referred to above were identified in-vitro as well. It was assumed that the non-ciliated region is from plate 33 to 23. The nasal valve is difficult to establish since it is not in the same plane as the coronal MRI scans, but the ciliated region is said to start when the first turbinate appears. From plate 22 to plate 3 is the region of the nose that is cleared by mucociliary action. Plates 2 to 0 are considered to represent the bend of the throat.

To be able to compare these regions in-vivo and in-vitro the total deposition was normalised to 100 %.

9.1 COMPARISON OF TOTAL DEPOSITION

The total deposition was measured in-vivo in the head during the inhalation of radio-labelled particles using NaI detectors. In-vitro the total deposition was measured as described in section 6.5.

Figure 9.1 shows the difference in deposition characteristics between the human volunteer and the cast. In general the deposition in the cast is higher than in the human volunteer: less so for smaller particles and low breathing rates, more so for high breathing rates and larger particles. The extreme difference is at 6μm light exercise were the deposition in the volunteer is only 42 % and the deposition the cast is 98 %.

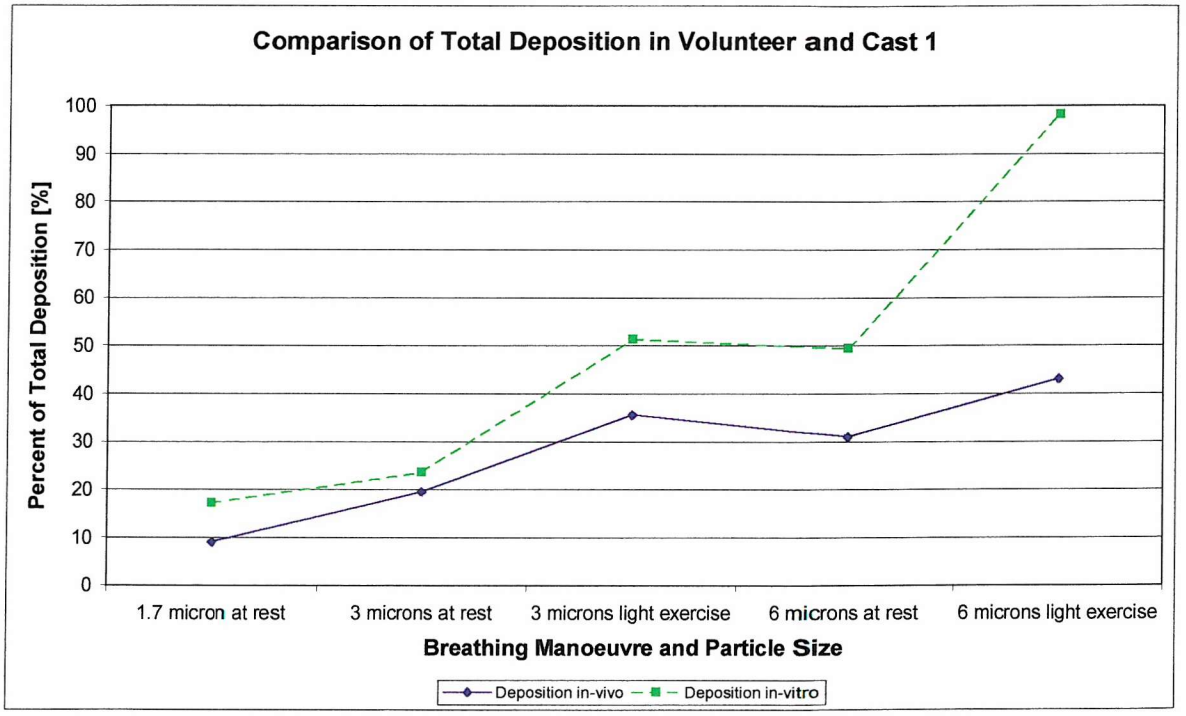

Figure 9.1: Total Deposition in Human Volunteer and Cast 1

9.2 Comparison of Data Calculated from Clearance In-Vivo with Data Measured In-Vitro

For the experiment, shown in Figure 9.2, 1.7 μm particles were administered to the sitting volunteer. For the cast experiment the same particle size and volunteers breathing at rest were used.

The fast clearance section is higher in-vivo than the deposition in the comparable sites in the cast. The same applies for the deposition in the throat. The section cleared by mucociliary action is three times lower than the deposition in this part of the cast.

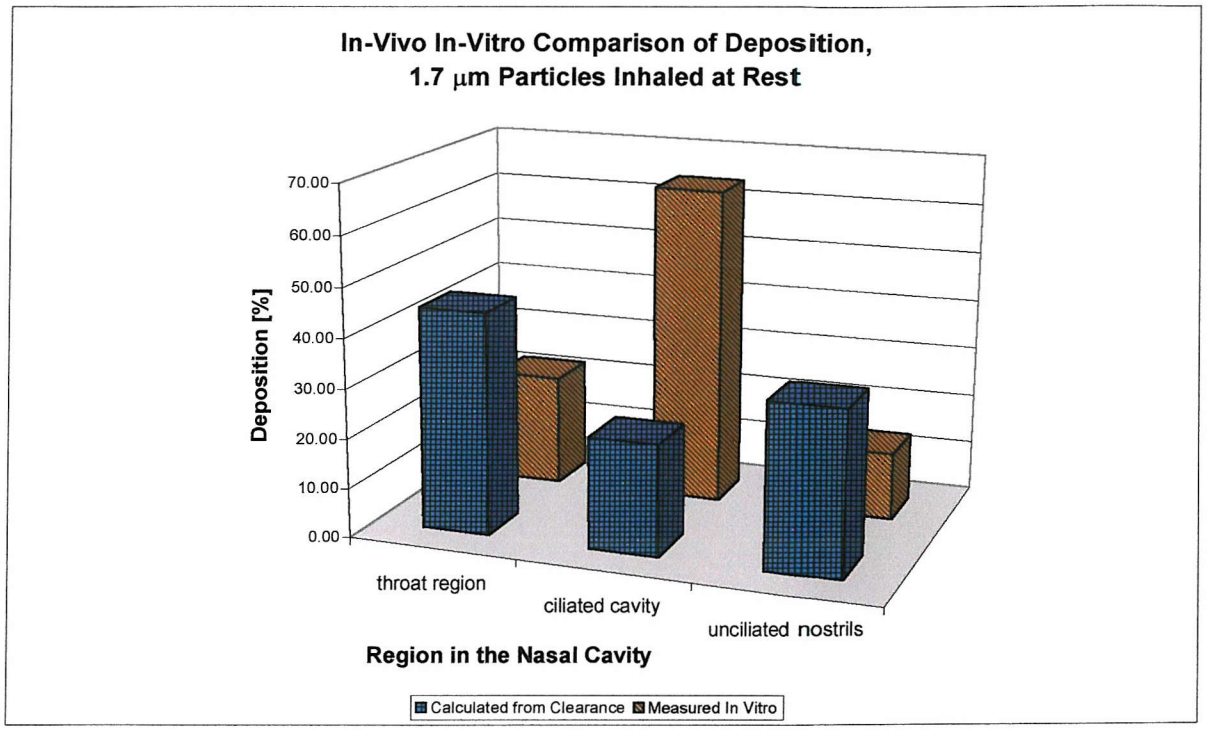

Figure 9.2: Three Clearance Sections in the Human Volunteer and in the Cast for 1.7 μm Particles Administered at Rest

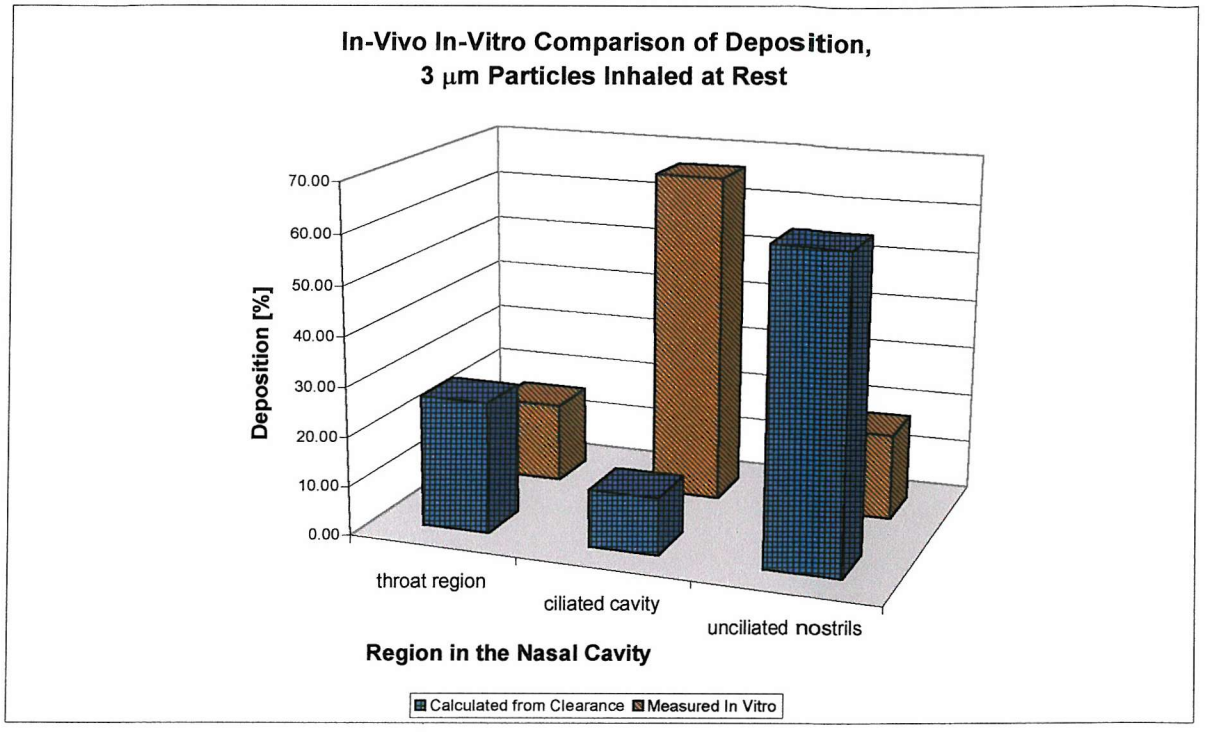

Figure 9.3: Three Clearance Sections in the Human Volunteer and in the Cast for 3 μm Particles Administered at Rest

For the experiment shown in Figure 9.3, 3 μm particles were administered to the human volunteer and to the cast inhaled at rest.

The part considered to be deposited in the throat is not significantly higher in-vivo than in-vitro. But the deposition in the ciliated part of the nasal cavity appears to be more than six times higher in the cast than in the human volunteer. Deposition in the anterior part of the nose is consequently more than three times higher in-vivo than in the cast.

Figure 9.4 shows the results of 3 μm particles administered to the human volunteer at light exercise and also to the cast using the breathing pattern for light exercise.

The deposition at the back of the throat is about three times higher in-vivo than in-vitro. Deposition in the ciliated part of the nose appears to be zero in-vivo whereas in-vitro it is as high as 50 %. The anterior part of the nose has a higher deposition in-vivo than in-vitro.

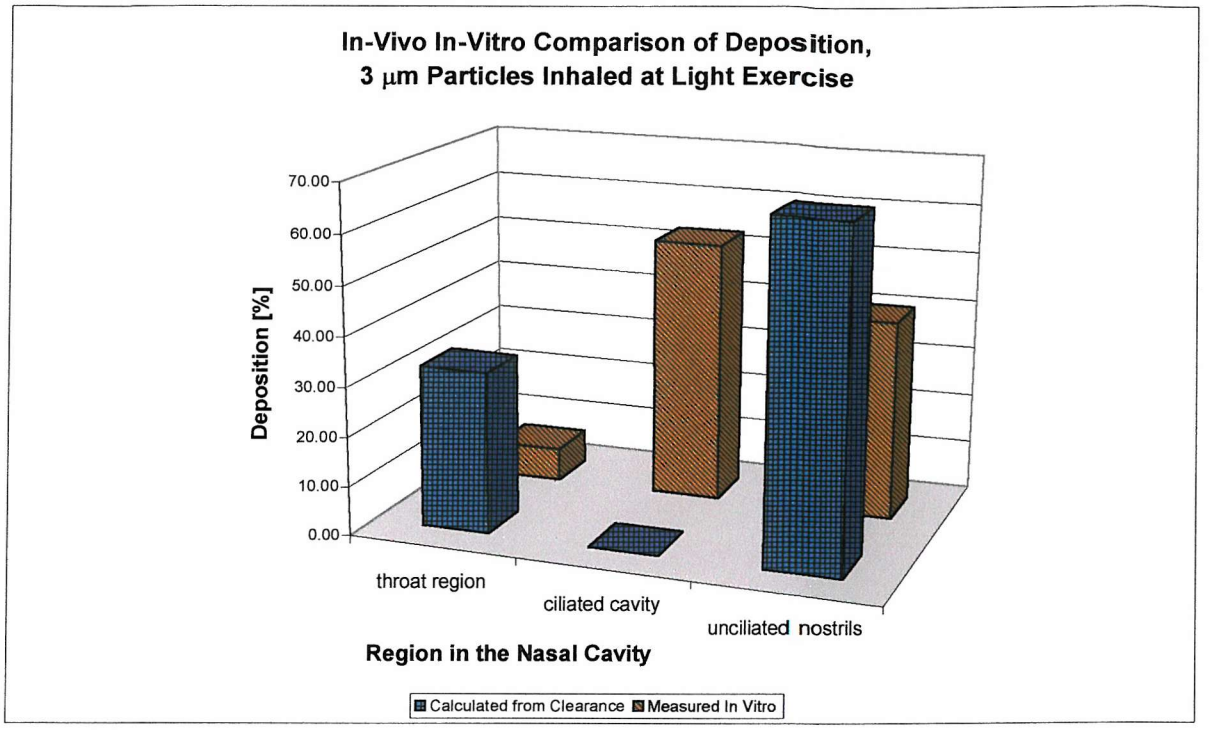

Figure 9.4: Three Clearance Sections in the Human Volunteer and in the Cast for 3 μm Particles Administered at Light Exercise

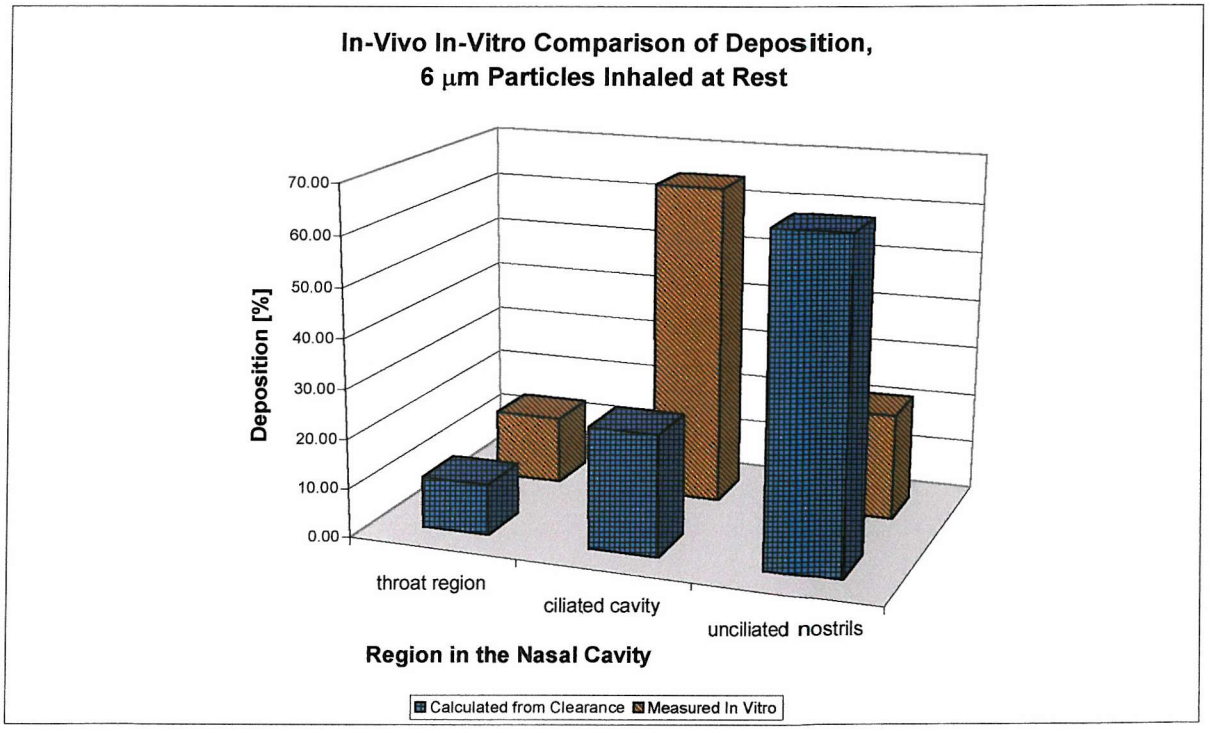

Figure 9.5: Three Clearance Sections in the Human Volunteer and in the Cast for 6 μm Particles Administered at Rest

Figure 9.5 shows the results of the experiment for 6 μm particles administered at rest to the volunteer and the cast. As before the deposition in the throat is very similar for the human volunteer and the cast, but the deposition in the ciliated region is three times higher in the cast than in the human volunteer. The anterior part shows exactly the opposite, the amount of particles in the human nose is three times higher than in the cast.

The experiment for 6 μm particles administered at light exercise is shown in Figure 9.6. Here the different compartments seem to agree much better than in the experiments before, the difference is not significant.

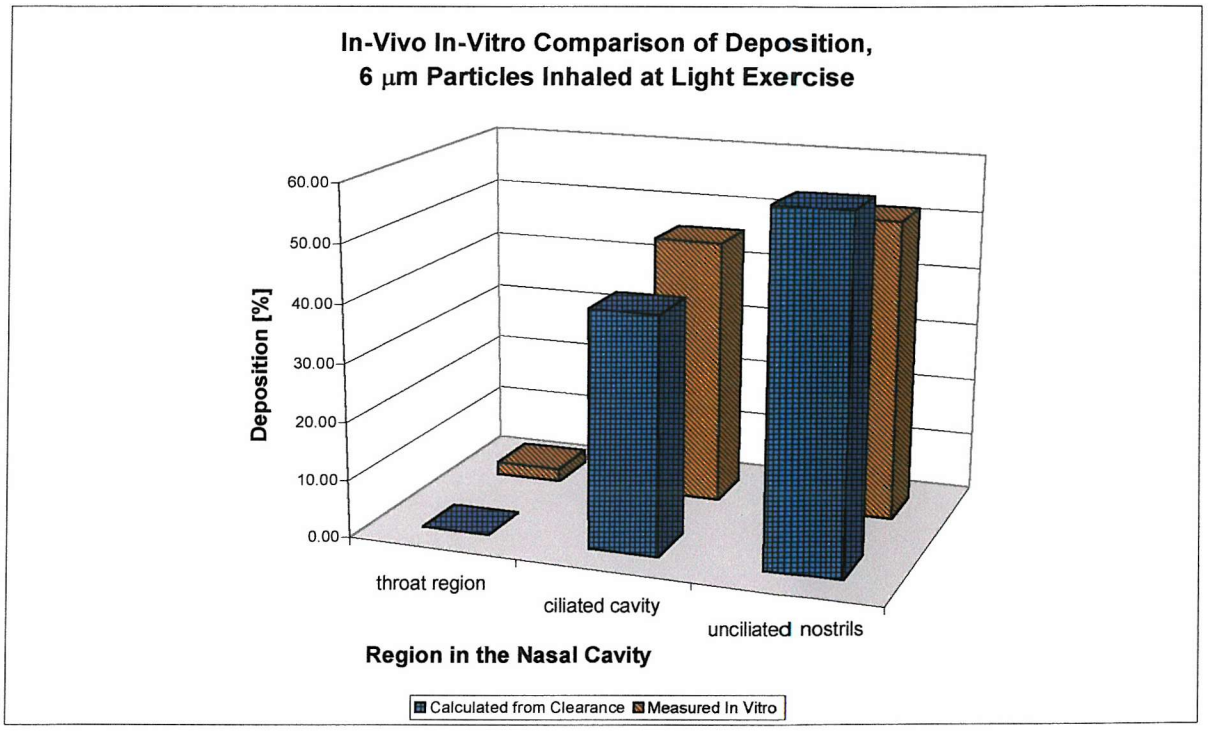

Figure 9.6: Three Clearance Sections in the Human Volunteer and in the Cast for 6 μm Particles Administered at Light Exercise

9.3 DISCUSSION

The total deposition is generally lower in the human subject than in the artificial nasal cavity. But both total deposition curves appear to have a similar trend. The reason for the difference could be that the cast is made from MRI scans of a recumbent volunteer,

whereas the administrations were done on a sitting volunteer or a volunteer at light exercise. As pointed out in section 2.3 the resistance of the nose can depend on posture and state of the volunteer. The rhinometry measurements done after the nine administrations of the aerosol to the human volunteer show in three cases a de-congested turbinate region at the right-hand side. Two of the administrations were done at light exercise and both of them are amongst the three de-congested (Smith 1999). This leads to the assumption that the volunteer's airways change with light exercise and the deposition in-vivo is therefore lower for this breathing pattern.

Regarding the throat deposition usually agrees well in-vivo and in-vitro, only for 3 μm light exercise the throat deposition in-vitro is considerably lower than in-vivo. This affirms the conclusion drawn before, more particles came through in-vivo because of the diluted airways. For 6 μm particles the impaction at the front of the nose is so dominant that most of the particles deposit before the turbinates. Therefore the narrowness of the airways around the turbinates does not have such a great influence and the deposition at the throat is the same for in-vivo and in-vitro at 6 μm light exercise.

The deposition which is assumed to be in the ciliated region is generally significant higher in the cast than in the human volunteer. Also the deposition in the nostrils is considerably lower in the cast than in-vivo. Since the regions of deposition in-vivo were calculated from clearance data and all activity which stayed longer than 16 min was assumed to be in the nostrils it appears that this fraction did not actually deposit in the nostrils, but in the front of the turbinate region. This means that there is a fraction of particles which is cleared slowly from the turbinates, and therefore stays long enough for uptake if soluble.

10 CONCLUSIONS

It is common knowledge that particle deposition in the nose increases with increasing airflow rate and diameter of particles. This work shows that also breathing pattern influences the total amount of deposition and most probably the deposition site as well. The difference is especially high between constant flow and cyclic breathing pattern (e.g. human breathing), but is also visible between various cyclic breathing patterns. The total deposition for constant flow is significantly higher than that of human breathing. This is surprising because it could be assumed that constant flow is more stable than cyclic flow and further similar experiments with lung casts showed the opposite results (Gurman et al 1984a; Gurman et al 1984b). The most plausible explanation why constant flow causes higher deposition than cyclic flow is that the nose is "optimised" for the cyclic flow and therefore causes less eddies. Therefore the difference in deposition ceases with increasing particle size, since the larger particles are not that much influenced by vortices.

The impaction factor is an indicator of deposition by impaction. In an ideal impactor the deposition efficiency versus impaction factor would follow one single curve (Swift 1991). The results in this work show that the impaction factor is definitely not applicable for constant flow in cast 1, but is better for the human breathing pattern. Since the impaction factor does not account for secondary flows (Scott et al 1978), the assumption is confirmed that more vortices are caused in the nose by constant flow than by the human breathing pattern. Moreover the deposition efficiencies appear to be less different for higher impaction factors, where secondary flows lose influence on particle behaviour.

The experiments conducted to determine the influence of nostril the shape on particle deposition in this study do not show any significant difference for the investigated particle size. The nostrils were only different up to the nasal valve and therefore the influence of the valve was excluded.

The comparison of total deposition in the two casts though showed significant differences. Many authors as for example Haight or Schwab (Haight & Cole 1983; Schwab & Zenkel 1998) have suggested that the nasal valve determines the deposition in the nose. By comparing the cross-sectional area of the two casts it seemed to be more likely that the

airway close to the throat has more influence than the nasal valve, since the difference at the throat region is greater between the two casts. It is highly unlikely that there is only one site in the nose which determines the deposition behaviour, but each individual nose has its own characteristics and therefore it is unwise to draw general conclusions from the limited measurements reported here.

The major deposition site in the nose appears to be the anterior end of the middle turbinate. All the particle sizes have a high deposition there. The smaller particles also have high deposition at the back of the throat. Only for high flow rates particle deposition in the nostrils has a maximum.

Not only the total deposition, but also the distribution over the cast is likely to differ for different breathing patterns. As shown by Zwartz et al (Zwartz & Guilmette 1999) using constant flow causes mainly deposition before the nasal valve, whereas using human breathing pattern (comparable flow rate and particle size) causes some deposition before the nasal valve, but much more in the turbinate region.

Another study was concerned with particle distribution in a cast (Itoh et al 1985). Large particle deposition sites of this study match the results of Itoh et al, but differ for the smaller sizes. For small particles, the results of Itoh et al show high deposition at and after the nasal valve, but nothing at the throat, whereas the results here show little deposition around the nasal valve but pronounced maximas at the throat. The difference is thought to be caused again by different flow patterns, Itoh et al used constant flow, in contrast to this study.

It is difficult to compare those two experiments with the work conducted in this study, because both of them used different casts, but their result is so considerably different that it implies a different deposition site for different breathing patterns. It also implies that the vortices caused by constant flow occur in the anterior part of the nose.

The comparison between the human volunteer and the corresponding cast matched for small particles and breathing pattern at rest, but differed for 6 μm particles and light exercise. The reason for this is thought to be that the subject is likely to have different airway dimensions at rest and at light exercise. It is very likely that the airways become

larger for light exercise, and therefore the deposition in-vivo much smaller than in-vitro. Rhinometry measurements which are currently made on volunteers at NRPB confirm this assumption (Smith 2000).

The comparison between clearance zones in the nose always shows higher deposition in the volunteer's nostrils compared to the cast and lower deposition in the volunteer's ciliated region than in the cast. These facts lead to the assumption that the clearance zones in-vivo can not be defined as they were. The clearance zones were defined as follows: particles which are swallowed immediately were deposited in the throat, particles which stay for 16 minutes are deposited in the ciliated region and particles which stay longer or are cleaned by nose blow are deposited in the nostrils. The reason for the difference is probably due to the amount of particles which is deposited in the ciliated region, but is not cleared within 16 minutes.

The fact that deposition at the throat is usually much higher in-vivo than in-vitro could have two explanations. The airways of the human volunteer widen with light exercise, allowing more particles to reach the throat, or more particles are cleared rapidly than only the ones which directly deposit at the throat. There is not enough deposition between the turbinates and the throat to account for this difference. Therefore it is more likely that more particles reach the throat.

11 FUTURE WORK

The work described in this thesis laid the foundations for many more experiments than possibly achievable in the limited amount of time. The breathing simulator and the casts could be used to investigate influences such as:

- The influence of charge on total deposition and distribution of deposited particles in the cast
- The deposition of larger particles up to the point when all particles deposit in the nostrils, even for breathing patterns at rest. Also the comparison between the human volunteer and the cast with regard to the clearance zones for larger particles, because the differences in the human volunteers might be more pronounced
- Determine the particle distribution in cast 1 caused by constant flow. This would enable a comparison to the one with cyclic flow.
- Deposition distribution in cast 2 using constant flow and human breathing patterns and determine if different anatomies differ much in deposition pattern
- Measurement of deposition during exhalation only
- Deposition of smaller particles using different nostrils, because they are more influence by local eddies and might show different total deposition

The measurements described above could be done without building new equipment, but it would be also desirable to research in other directions like:

- writing software to get the cross-sectional area of the nasal airways perpendicular, and therefore comparable with the rhinometry measurements
- Manufacturing casts of different volunteers to determine the influence of anatomy on deposition further and also different casts of volunteers in different states to converge the results in-vivo and in-vitro
- Develop a numerical model of deposition in the nose using the results of experiments above

12 REFERENCES

APS Inc. (1987) Aerosizer User Manual

Bailey, A. G. (1988) Electrostatic Spraying of Liquids. Research Studies Press, Taunton, England

Bailey, A. G. (1997) The Inhalation and Deposition of Charged Particles Within the Human Lung. Journal of Electrostatics 42: 25-32

Bailey, A. G., Hashish, A. H., Williams, T. J. (1998) Drug Delivery by Inhalation of Charged Particles. Journal of Electrostatics 44: 3-10

Bang, B. G., Mukherjee, A. L., Bang, F. B. (1967) Human Nasal Mucus Flow Rates. Johns Hopkins Medical Journal 121: 38-48

Baron, P. A., Willeke, K. (1993a) Aerosol Fundamentals. In: Willeke, K., Baron, P. A. (eds) Aerosol Measurement: principles, techniques and applications. Van Nostrand Reinhold, New York, pp 8-22

Baron, P. A., Willeke, K. (1993b) Gas and Particle Motion. In: Willeke, K., Baron, P. A. (eds) Aerosol Measurement: principles, techniques and applications. Van Nostrand Reinhold, New York, pp 23-40

Becquemin, M. H., Swift, D. L., Bouchikhi, A., Roy, M., Teillac, A. (1991) Particle Deposition and Resistance in the Noses of Adults and Children. European Respiratory Journal 4: 694-702

Beitz, W., Kuettner, K.-H. (1995) Dubble, Taschenbuch fuer den Maschinenbau. 18 edn. Springer, Berlin

Breysse, P. N., Swift, D. L. (1990) Inhalability of Large Particles into the Human Nasal Passage: In-vivo Studies in Still Air. Aerosol Science and Technology 13: 459-464

Bridger, G. P. (1970) Physiology of the Nasal Valve. Archive of Otolaryngology 92: 543-553

Brindley, A., Sumby, B. S., Smith, I. J. (1994) The Characterisation of Inhalation Devices By an Inhalation Simulator - the Electronic Lung. Journal of Aerosol Medicine-Deposition Clearance and Effects in the Lung 7: 197-200

Burnell, P. K. P., Malton, A., Reavill, K., Ball, M. H. E. (1998) Design, validation and initial testing of the Electronic Lung(TM) Device. Journal of Aerosol Science 29: 1011-1025

Cheng, K. H., Swift, D. L. (1995) Calculation of Total Deposition Fraction of Ultrafine Aerosols in Human Extrathoracic and Intrathoracic Regions. Aerosol Science and Technology 22: 194-201

Cheng, K.-H., Cheng, Y.-S., Yeh, H.-C., Swift, D. L. (1995) Deposition of Ultrafine Aerosols in the Head Airways During Natural Breathing and During Simulated Breath Holding Using Replicate Human Upper Airway Casts. Aerosol Science and Technology 23: 465-474

Cheng, Y. S., Yeh, H. C., Smith, S. M., Cheng, K. H., Swift, D. L. (1998) Deposition of Ultrafine Particles in the Nasal and Trachobronchial Airways. Journal of Aerosol Science 29: S941-S942

Cheng, Y.-S., Su, Y.-F., Yeh, H.-C., Swift, D. L. (1993) Deposition of Thoron Progeny in Human Head Airways. Aerosol Science and Technology 18: 359-375

Cheng, Y.-S., Yamada, Y., Yeh, H.-C., Swift, D. L. (1988) Diffusional Deposition of Ultrafine Aerosols in A Human Nasal Cast. Journal of Aerosol Science 19: 741-751

Cheng, Y.-S., Yeh, H.-C., Guilmette, R. A., Simpson, S. Q., Cheng, K.-H., Swift, D. L. (1996) Nasal Deposition of Ultrafine Particles in Human Volunteers and Its Relationship to Airway Geometry. Aerosol Science and Technology 25: 274-291

Cole, P. (1988) Nasal Airflow Resistance. In: Mathew, O. P., Sant'Ambrogio, G. (eds) Respiratory Function of the Upper Airway. Marcel Dekker, Inc, New York, Basel, pp 391-445

Cole, P., Haight, J. S. J. (1986) Posture and the Nasal Cycle. Annals of Otology Rhinology and Laryngology 95: 233-238

Cole, P., Haight, J. S. J., Love, L., Oprysk, D. (1985) Dynamic Components of Nasal Resistance. American Review of Respiratory Diseases 132: 1229-1232

Crane, R., Evans, R. (1977) Inertial Impaction of Particles in a Bent Pipe. Journal of Aerosol Science 8: 161-170

Eccles, R. (1978) The Central Rhythm of the Nasal Cycle. Acta Otolaryngol 86: 464-468

Etherington, G., Smith, J. (1996) NRPB Volunteer Study: Deposition and Clearance of Inhaled Particles. Radiological Protection Bulletin 175: 16-21

Etherington, G., Smith, J. R. H., Bailey, M. R., Dorrian, M. D., Shutt, A. L., Youngman, M. J. (1998) Deposition and Clearance of Inhaled Particles in the Human Nasal Passage: Implications for Dose Assessment. Radiation Protection Dosimetry 79: 249-252

Ferris, B. G., Jr, Mead, J., Opie, L. H. (1964) Partitioning of Respiratory Flow Resistance in Man. Journal of Applied Physiology 19: 653-658

Ferron, G. A. (1977) The Size of Soluble Aerosol Particles as a Function of the Humidity of the Air. Application to the Human Respiratory Tract. Journal of Aerosol Science 8: 251-267

Flanagan, P., Eccles, R. (1997) Spontaneous Changes of Unilateral Nasal Airflow in Man. A Re-Examination of the 'Nasal Cycle'. Acta Oto-Laryngologica 117: 590-595

Fry, F. (1970) Charge Distribution on Polystyrene Aerosols and Deposition in the Human Nose. Journal of Aerosol Science 1: 135-146

Fry, F. A., Black, A. (1973) Regional Deposition and Clearance of Particles in the Human Nose. Journal of Aerosol Science 4: 113-124

Girardin, M., Bilgen, E., Arbour, P. (1983) Experimental-Study of Velocity-Fields in a Human Nasal Fossa By Laser Anemometry. Annals of Otology Rhinology and Laryngology 92: 231-236

Gradon, L., Yu, C. P. (1989) Diffusional Particle Deposition in the Human Nose and Mouth. Aerosol Science and Technology 11: 213-220

Guilmette, R. A., Gagliano, T. (1995) Development of a Physical Replica of Human Nasal Airways Based on in-vivo Measurement Data. Abstract

Guilmette, R. A., Wicks, J. D., Wolff, R. K. (1989) Morphometry of Human Nasal Airways In Vivo Using Magnetic Resonance Imaging. Journal of Aerosol Medicine 2: 365-377

Gurman, J. L., Lioy, P. J., Lippmann, M., Schlesinger, R. B. (1984a) Particle Deposition in Replicate Casts of the Human Upper Tracheobronchial Tree Under Constant and Cyclic Inspiratory Flow .2. Empirical-Model. Aerosol Science and Technology 3: 253-257

Gurman, J. L., Lippmann, M., Schlesinger, R. B. (1984b) Particle Deposition in Replicate Casts of the Human Upper Tracheobronchial Tree Under Constant and Cyclic Inspiratory Flow .1. Experimental. Aerosol Science and Technology 3: 245-252

Hady, M. R. A., Shehata, O., Hassan, R. (1983) Nasal Mucociliary Function in Different Diseases of the Nose. The Journal of Laryngoloy and Otology 97: 497-502

Hahn, I., Scherer, P. W., Mozell, M. M. (1993) Velocity Profiles Measured for Airflow Through a Large-Scale Model of the Human Nasal Cavity. Journal of Applied Physiology 75: 2273-2287

Haight, J. S. J., Cole, P. (1983) The Site and Function of the Nasal Valve. Laryngoscope 93: 49-55

Hashish, A. H., Bailey, A. G. (1991) Electrostatic Enhancement of Particle Deposition in the Lung When Using Jet and Ultrasonic Nebulisers. Electrostatics. Oxford. Institute of Physics

Hilberg, O., Jensen, F. T., Pedersen, O. F. (1993) Nasal Airway Geometry: Comparison between Acoustic Reflections and Magnetic Resonance Scanning. Journal of Applied Physiology 75: 2811-2819

Hilberg, O., Pedersen, O. F. (1996) Acoustic Rhinometry: Influence of Paranasal Sinuses. Journal of Applied Physiology 80: 1589-1594

Hildesheim, A., Levine, P. H. (1993) Etiology of Nasopharyngeal Carcinoma: A Review. Epidemiologic Reviews 15: 466-485

Hinds, W. C. (1982) Aerosol Technology. John Wiley&Sons, Los Angeles

Hinds, W. C., Liu, W. C., Froines, J. R. (1985) Particle Bounce in a Personal Cascade Impactor - a Field-Evaluation. American Industrial Hygiene Association Journal 46: 517-523

Hornung, D. E., Leopold, D. A., Youngentob, S. L., Sheehe, P. R., Gagne, G. M., Thomas, F. D. (1987) Airflow Patterns in a Human Nasal Model. Archives of Otolaryngology-Head & Neck Surgery 113: 169-172

Hounam, R. F., Black, A., Walsh, M. (1969) Deposition of Aerosol Particles in the Nasopharyngeal Region of the Human Respiratory Tract. Nature 221: 1254-1255

Hounam, R. F., Black, A., Walsh, M. (1971) The Deposition of Aerosol Particles in the Nasopharyngeal Region of the Human Respiratory Tract. Journal of Aerosol Science 2: 47-61

Hsu, D. J., Swift, D. L. (1999) The Measurements of Human Inhalability of Ultralarge Aerosols in Calm Air Using Mannikins. Journal of Aerosol Science 30: 1331-1343

ICRP. (1994) Human Respiratory Tract, Model for Radiological Protection. ICRP Publication

Itoh, H., Smaldone, G. C., Swift, D. L., Wagner, H. N. J. (1985) Mechanisms of Aerosol Deposition in a Nasal Model. Journal of Aerosol Science 16: 529-534

John, W. (1995) Particle-Surface Interactions - Charge-Transfer, Energy-Loss, Resuspension, and Deagglomeration. Aerosol Science and Technology 23: 2-24

John, W., Sethi, V. (1993) Threshold For Resuspension By Particle Impaction. Aerosol Science and Technology 19: 69-79

Kesavanathan. (1998) Personal Communication

Kesavanathan, J., Bascom, R., Swift, D. L. (1998) The Effect of Nasal Passage Characteristics on Particle Deposition. Journal of Aerosol Medicine-Deposition Clearance and Effects in the Lung 11: 27-39

Kesavanathan, J., Swift, D. L. (1998) Human Nasal Passage Particle Deposition: The Effect of Particle Size, Flow Rate, and Anatomical Factors. Aerosol Science and Technology 28: 457-463

Kim, C. S., Eldrige, M. A., Sackner, M. A., Swift, D. L. (1985) Deposition of Aerosol Particles in the Human Nose. American Review of Respiratory Diseases 131: A370

Kreit, J. W., Sciurba, F. C. (1996) The Accuracy of Pneumotachograph Measurements During Mechanical Ventilation. American Journal of Respiratory and Critical Care Medicine 154: 913-917

Kreyling, W. (1999) Personal Communication

Leopold, D. A. (1994) Nasal Toxicity - End-Points of Concern in Humans. Inhalation Toxicology 6: 23-39

Lippman, M. (1970) Deposition and Clearance of Inhaled Particles in the Human Nose. Annals of Otology, Rhinology and Laryngology 79: 519-528

Lippman, M. (1977) Regional Deposition of Particles in the Human Respiratory Tract Handbook of Physiology. American Physiology Society, Maryland, pp 213-232

Liu, B. Y. H., Pui, D. Y. H. (1974) Electrical Neutralization of Aerosols. Aerosol Science 5: 465-472

MacArthur, D. S., Fleck, S. G. (1997) The Electro Lung; Bridging the Gap between In-vitro and In-vivo Testing.

Malarbet, J. L., Bertholon, J. F., Becquemin, M. H., Taieb, G., Bouchikhi, A., Roy, M. (1994) Oral and Nasal Flow-Rate Partitioning in Healthy-Subjects Performing Graded-Exercise. Radiation Protection Dosimetry 53: 179-182

Martini, L. J. (1984) Practical Seal Design. Marcel Dekker, New York, Basel

Martonen, T. B., Zhang, Z. (1992) Comments on Recent Data for Particle Deposition in Human Nasal Passages. Journal of Aerosol Science 23: 667-674

McFarland, A. R., Gong, H., Muyshondt, A., Wente, W. B., Anand, N. K. (1997) Aerosol deposition in bends with turbulent flow. Environmental Science and Technology 31: 3371-3377

Mercer, T. T. (1975) The Deposition Model of the Task Group on Lung Dynamics: A Comparsion with recent experimental Data. Health Physics 29: 673-680

Miller, D. S. (1971) Internal Flow - A Guide to Losses in Pipe and Duct Systems. The British Hydromechanics Research Association, Cranfield-England

Miller, D. S. (1978) Internal Flow Systems. The British Hydromechanics Research Association, Cranfield

Miller, M. R., Pincock, A. C. (1986) Linearity and Temperature Control of the Fleisch Pneumotachograph. Journal of Applied Physiology 60: 710-715

Mirza, N., Kroger, H., Doty, R. L. (1997) Influence of Age on the 'Nasal Cycle'. Laryngoscope 107: 62-66

Naito, K., Iwata, S. (1997) Current Advances in Rhinomanometry. European Archives of Oto-Rhino-Laryngology 254: 309-312

Niinimaa, V., Cole, P., Minitz, S., Shepard, R. J. (1980) The Switching Point from Nasal to Oronasal Breathing. Respiration Physiology 42: 61-71

Paw U, K. T. (1983) The Rebound of Particles from Natural Surfaces. Journal of Colloid and Interface Science 93: 442-452

Proctor, D. F. (1977) Nasal Physiology and Defence of the Lung. American Review of Respiratory Disease 115: 97-129

Proctor, D. F., Andersen, I. (1976) Nasal Mucociliary Function in Normal Man. Rhinology 14: 11-17

Proctor, D. F., Swift, D. L. (1971) The Nose - A Defence Against the Atmospheric Environment. Inhaled Particles III 1: 59-70

Rasmussen, T. R., Swift, D. L., Hilberg, O., Pedersen, O. F. (1990) Influence of Nasal Passage Geometry on Aerosol Particle Deposition in the Nose. Journal of Aerosol Medicine 3: 15-24

Schlesinger, R. B. (1985) Comparative Deposition of Inhaled Aerosols in Experimental Animals and Humans: A Review. Journal of Toxicology and Environmental Health 15: 197-214

Schreck, S., Sullivan, K. J., Ho, C. M., Chang, H. K. (1993) Correlations Between Flow Resistance and Geometry in a Model of the Human Nose. Journal of Applied Physiology 75: 1767-1775

Schwab, J. A., Zenkel, M. (1998) Filtration of Particulates in the Human Nose. Laryngoscope 108: 120-124

Scott, W. R., Taulbee, D. B., Yu, C. P. (1978) Theoretical Study of Nasal Deposition. Bull Math Biol 40: 581-603

Smith, J. (2000) Personal Communication.

Smith, J. R. (1999) Personal Communication

Smith, J. R. H., Dorrian, M. D., Youngman, M. J., Bailey, M. R., Etherington, G., Shutt, A. L. (1996) Design of Volunteer Study to Determine the Clearance of Inhaled Particles from the Human Nasal Passage. Annals of Occupational Hygiene 41: 116-122

Stahlhofen, W., Rudolf, G., James, A. C. (1989) Intercomparison of Experimental Regional Aerosol Deposition Data. Journal of Aerosol Medicine 2: 285-308

Strong, J. C., Swift, D. L. (1987) Deposition of Ultrafine Particles in a Human Nasal Cast. Aerosols: Their Generation, Behaviour and Applications. Loughborough, UK. Aerosol Society

Swift, D. L. (1981) Aerosol Deposition and Clearance in the Human Upper Airways. Annals of Biomedical Engineering 9: 593-604

Swift, D. L. (1991) Inspiratory Inertial Deposition of Aerosols in Human Nasal Airway Casts: Implication for the Proposed NCRP Lung Model. Radiation Protection Dosimetry 38: 29-34

Swift, D. L., Kesavanathan, J. (1996) The Anterior Human Nasal Passage as a Fibrous Filter for Particles. Chem. Eng. Comm. 151: 65-78

Swift, D. L., Montassier, N., Hopke, P. K., Karpen-Hayes, K., Cheng, Y.-S., Fong Su, Y., Yeh, H.-C., Strong, J. C. (1992) Inspiratory Deposition of Ultrafine Particles in Human Nasal Replicate Casts. Journal of Aerosol Science 23: 65-72

Wang, H. C., John, W. (1987) Comparative Bounce Properties of Particle Materials. Aerosol Science and Technology 7: 285-299

Wang, H. C., Stukel, J. J., Leong, K. H. (1986) Particle Deposition On Spheres By Inertial and Electrostatic Forces. Aerosol Science and Technology 5: 391-408

Xu, M., Willeke, K., Biswas, P., Pratsinis, S. E. (1993) Impaction and Rebound of Particles At Acute Incident Angles. Aerosol Science and Technology 18: 143-155

Yamada, Y., Cheng, Y.-S., Yeh, H.-C., Swift, D. L. (1988) Inspiratory and Expiratory Deposition of Ultrafine Particles in a Human Nasal Cast. Inhalation Toxicology : 1-22

Yu, C. P., Diu, C. K., Soong, T. T. (1982) Statistical Analysis of Aerosol Deposition in Nose and Mouth. American Industrial Hygiene Association Journal 42: 726-733

Zwartz, G. J., Guilmette, R. A. (1999) A charge coupled device system to image local particle deposition patterns in a model of a human nasal airway. Aerosol Science and Technology 30: 489-504

13 GLOSSARY

Actual signal	The response signal of a controlled system, eg the breathing simulator, indicates at which point the piston really is
Aerodynamic diameter	Diameter of a unit density sphere having the same gravitational settling velocity as the particle in question
Aerosol	An assembly of liquid or solid particles suspended in gaseous medium long enough to be observed and measured. Generally about 0.001-100 μm in size
Alae	Ala is the medical term for a wing-like organ, used in the context of the nose for the sides of the outer nose
Anterior	Medical term for the front of an organ
APS Aerodynamic Particle Sizer	A particle spectrometer that uses and acceleration system to differentiate particles by aerodynamic diameter and a laser velocimeter to detect particles
Boltzman charge distribution	Residual or minimum charge distribution on particles after exposure to a bipolar field
Brownian motion	Random motion of small particles due to collisions with gas molecules
Ciliae	Very fine hair, which cover the cells of certain tissues, such as the epithelium lining of the nose, and help those cells sweep away fluids or particles
Clearance	Physiologic term which is the rate at which a substance is removed from the respiratory tract
Closed loop control	A closed-loop control system uses a measurement of the output and feedback of this signal to compare it with the desired output.
Compliance	expression to measure the elasticity of an air of fluid filled organ, e.g., the lung (lung compliance), in terms of unit of volume change per unit of pressure change

Constant flow	Flow of a steady rate which does not vary over time
Corona	Region of intense ionisation, often surrounding an electrode at high voltage
D/A converter	Digital to analogue converter, coverts a digital signal in an analogue one
DAQ Card	Data Acquisition Card, card built in a computer for digital and analogue input and output
Desired Signal	Set signal
Drag force	Resistance experienced by a particle when moving in a fluid
Electrical mobility	Ration of particle velocity to the electrical force procuring that velocity
FEV1	Forced Expired Volume within 1 second
Half-life	Time interval required to reduce the rate of emission of a radioactive isotope by a factor of two
Inhalation efficiency	Fraction of ambient aerosol that can enter the human
Inhalable fraction	respiratory system
Laminar flow	Gas flow with a smooth non-turbulent pattern of streamlines with no streamline looping back on itself usually occurs at very slow Reynolds numbers
Monodisperse	Composed of particles with a single size or a small range of sizes
Nasal valve	Minimal cross-sectional area in the nose
Olfactory region	Region in the nasal cavity, superior of the turbinates, which is for smelling
Open loop	An open-loop control system utilises an actuating device to control the process directly without using feedback.
Particle	A small discrete object, often having a density approaching the intrinsic density of the bulk material; it may be homogeneous or contain a variety of chemical species; it may consist of solid or liquid materials or both
Particle bounce	Rebound of particles that fail to adhere after impaction on a collecting surface

P-controller	The relationship between input and output is proportional and proportionality depends on the relationship between voltage and speed.
Pneumotachograph	A device which measures the pressure loss across a resistance to airflow and so determines the airflow
Posterior	Medical term for the back of an organ
Relaxation time	An indicator of a particles ability to adjust to changes in flow velocity
Reynolds Number	Flow similitude parameter expressed as the ratio of the inertial force of the gas to the friction force of the gas moving over the surface of an object; flow Reynolds number the gas flow in a tube and particle Reynolds number describes the gas flow around a particle
Secondary flow	Vortices which develop for example at bends or openings, even if the flow is otherwise laminar
Set signal	The signal in closed loop system which sets the desired signal, eg the breathing simulator: the signal where the piston should travel to
Sonic pen	A device which sends a sound signal which is received from two microphones, so its position can be determined; was used for digitising geometries of the nasal airways from the MRI images
Stereo lithography	A method to cure photo-sensitive liquid plastic three dimensional using a laser beam
Stoke's number	Ratio of particles stopping distance to the characteristic dimension generally used as an indicator of similitude in particle behaviour in a given aerosol flow configuration
Stopping distance	Product of relaxation time and the initial particle velocity; an indicator of a particles ability to adjust to directional changes in aerosol flow
Tidal volume	Volume of gases inhaled or exhaled during each breath
Total deposition	Total percentage of particles deposited in the respiratory tract

Turbinates	The scroll-like bony plates with curved margins on the lateral wall of the nasal cavity, lined with mucosal tissue
Turbulent flow	Chaotic flow with streamlines looping back on themselves

A ANNEX BREATHING SIMULATOR

A.1SOFTWARE CODE FOR CONTROLLING THE BREATHING SIMULATOR

```
#include <analysis.h>
#include <dataacq.h>
#include <easyio.h>
#include <formatio.h>
#include <ansi_c.h>
#include <utility.h>
#include <cvirte.h>     /* Needed if linking in external compiler; harmless otherwise */
#include <userint.h>
#include "BP_v13.h"

/*Defines*/
#define RUNS    1
#define DOESNT_RUN  0
#define SINE    0
#define TRIANGLE    1
#define HUMAN   2
#define INFINITE    1
#define FINITE  0
#define OFFSET -0.5
#define POSITION 8.0
#define O_POSITION 0.0
#define VOLT_LITER -3.58
#define RAMP 0.1
#define CHART_RATE -0.33
#define CHART_POSITION -3.5
#define POLY 1.025

/* Function Prototypes*/
int Breathe (void);             // defines DB Output to motor using AO channel 0

static short ChannelVector [1]={0};         //Vector defenition
static int sabine;
static int Experiment = DOESNT_RUN;
static double BreathingPatternHandle;
char data[500];
static int BreathingPattern = HUMAN;
double volume;
int n=1;
static int LoopCount=0;
double Aquisition_Rate = 0.006;
double Daq_Rate =0.006;
double y;

int main (int argc, char *argv[])
{
```

```
    if (InitCVIRTE (0, argv, 0) == 0)
        return -1;  /* out of memory */
    if ((sabine = LoadPanel (0, "BP_v13.uir", SABINE)) < 0)
        return -1;
    DisplayPanel (sabine);
    RunUserInterface ();
    AO_Configure (1, 0, 1, 0, 10.0, 0);
    AOUpdateChannel (1, "0", O_POSITION);
 return 0;
 }

 int CVICALLBACK Set_Position (int panel, int control, int event,
        void *callbackData, int eventData1, int eventData2)
 {
    switch (event) {
        case EVENT_COMMIT:
 AO_Configure (1, 1, 1, 0, 10.0, 0);
 AOUpdateChannel (1, "0", POSITION);
            Delay (0.5);
            break;
    }
    return 0;
 }

 int CVICALLBACK Reset_Position (int panel, int control, int event,
        void *callbackData, int eventData1, int eventData2)
 {
    switch (event) {
        case EVENT_COMMIT:
         AO_Configure (1, 1, 1, 0, 10.0, 0);  //Takes Piston in 0-Position
         AOUpdateChannel (1, "0", O_POSITION);
         MessagePopup ("", "Please reset the counters");
          SetCtrlAttribute (SABINE, SABINE_SETPOSITION, ATTR_DIMMED, 0);
          SetCtrlAttribute (SABINE, SABINE_OPENFILE, ATTR_DIMMED, 0);
          break;
    }
    return 0;
 }

 int CVICALLBACK Open_File (int panel, int control, int event,
        void *callbackData, int eventData1, int eventData2)
 {
    switch (event) {
        case EVENT_COMMIT:
            FileSelectPopup ("", "*.txt", "*.dat", "Open File",
                             VAL_SELECT_BUTTON, 0, 0, 1, 1, data);
            InsertTextBoxLine (SABINE, SABINE_CURRENT_FILE, 0, data);
            SetCtrlAttribute (SABINE, SABINE_START, ATTR_DIMMED, 0);
            break;
    }
    return 0;
 }
```

```
int CVICALLBACK StartStop (int panel, int control, int event,
      void *callbackData, int eventData1, int eventData2)
{
   switch (event)
   {
    case EVENT_COMMIT:
    if(Experiment == DOESNT_RUN)
        {
          SetCtrlAttribute (SABINE, SABINE_START, ATTR_CMD_BUTTON_COLOR,
                  VAL_RED);
          SetCtrlAttribute (SABINE, SABINE_START, ATTR_LABEL_TEXT, "Stop");
          ProcessDrawEvents ();
          ClearStripChart (SABINE, SABINE_FLOW);
          SetCtrlVal (SABINE, SABINE_CURRENTLOOP, LoopCount=0) ;
          GetCtrlVal (SABINE, SABINE_AQUISITIONRATE, &Aquisition_Rate);
          GetCtrlVal (SABINE, SABINE_AQUISITIONRATE, &Daq_Rate);
          ProcessSystemEvents ();
          Experiment = RUNS;
          WriteToDigitalLine (1, "0", 0, 8, 0, 1);
          Breathe ();
        }
        else
        {
          WFM_Group_Control (1, 1, 0);      //Clears waveform
          AOUpdateChannel (1, "0", POSITION);
          SetCtrlAttribute (SABINE, SABINE_START, ATTR_CMD_BUTTON_COLOR,
VAL_GREEN);
          SetCtrlAttribute (SABINE, SABINE_START, ATTR_LABEL_TEXT, "Start");
          Experiment = DOESNT_RUN;
          Delay (1);
          WriteToDigitalLine (1, "0", 0, 8, 0, 0);
        }
        break;
     case EVENT_RIGHT_CLICK:
        break;
   }
   return 0;
}

int CVICALLBACK Quit (int panel, int control, int event,
      void *callbackData, int eventData1, int eventData2)
{
   switch (event)
   {
     case EVENT_COMMIT:
        QuitUserInterface (0);
        break;
     case EVENT_RIGHT_CLICK:
        break;
   }
   return 0;
}
int Breathe (void)              //Function to time and buffer the output
```

```
{
  unsigned long DaqPoints;
  short DaqStatus;
  short DaqStopped;
  short GainVector[2]={1,4};
  short ChannelVector[2]= {0,1};
  short Daq_Buffer[1000];
  short ScaleStatus;
  short DaqRateStatus;
  double Daq_Screen[1000];
  unsigned short DaqUpdateInterval;
  short DaqTimeBase;
  static short Timebase;
  static unsigned long UpdateInterval;
  static double time;
  static double CurrentFlowRate;
  static short Buffer[1000], HalfBuffer [500];
  static double Low [500], High [500];
  static int tmp;
  static int HighLow;
  static double VoltageOutput [1000];
  static double FlowRateBuffer [1000];
  static int LoopNumbers;
  static double Frequency;
  static double Phase = 360;
  static double FlowChartBuffer[1000] ;
  static double Coeff [2]={1,1.025};
      BreathingPatternHandle = OpenFile (data, VAL_READ_ONLY,
                              VAL_OPEN_AS_IS, VAL_ASCII);
      for (tmp=0; tmp<1000; tmp++)
      {
        ScanFile (BreathingPatternHandle, "%f\n", &FlowRateBuffer[tmp]);
        FlowRateBuffer[tmp] *=VOLT_LITER;
        FlowRateBuffer[tmp] +=POSITION;
        FlowChartBuffer[tmp] = FlowRateBuffer[tmp] ;
        FlowChartBuffer[tmp] *= CHART_RATE;
        FlowChartBuffer[tmp] -=CHART_POSITION;
      }
      WFM_DB_Config (1, 1, ChannelVector, 1, 1, 0);
      WFM_Group_Setup (1, 1, ChannelVector, 1);
      WFM_Scale (1, 0, 1000, 1.0, FlowRateBuffer, Buffer);
      WFM_Load (1, 1, ChannelVector, Buffer, 1000, 0, 0);
      WFM_Rate (Aquisition_Rate, 1, &Timebase, &UpdateInterval);
      WFM_ClockRate (1, 1, 0, Timebase, UpdateInterval, 0);
      WFM_Group_Control (1, 1, 1);
      PlotStripChart (SABINE, SABINE_FLOW, FlowChartBuffer, 1000, 0, 0,
                      VAL_DOUBLE);
      GetCtrlVal (SABINE, SABINE_LOOPNUMBERUSER, &LoopNumbers);
      while (Experiment == RUNS)
      {
        short DaqStopped;
        short DaqHalfReady;
        static short Status;
```

```
static short DaqStatus;
static short HalfReady;
static int EndOfData = 0;
static int ItemsFormatted;
Status = WFM_DB_HalfReady (1, 1, ChannelVector, &HalfReady);
if ((HalfReady ==1) && (Status == 0))
{
  for (tmp=0; (tmp<500 && !EndOfData); tmp++)
  {
      ItemsFormatted = ScanFile (BreathingPatternHandle, "%f\n",
            &FlowRateBuffer[tmp]);
      if ( ItemsFormatted < 1)
      {
        static int Loop;
        GetCtrlVal (SABINE, SABINE_LOOPSWITCH, &Loop);
        switch (Loop)
        {
          case INFINITE:
            SetFilePtr (BreathingPatternHandle, 0, 0);
            LoopCount++;
            ItemsFormatted = ScanFile (BreathingPatternHandle, "%f\n",
                  &FlowRateBuffer[tmp]);
            break;
          case FINITE:
            LoopCount++;
            if (LoopCount <LoopNumbers)
            {
              SetFilePtr (BreathingPatternHandle, 0, 0);
              ItemsFormatted = ScanFile (BreathingPatternHandle, "%f\n",
                    &FlowRateBuffer[tmp]);
            }
            else
            {
              while (tmp < 500)
              {
                FlowRateBuffer[tmp] = POSITION;
                tmp++;
              }
              Experiment=DOESNT_RUN;
              EndOfData = 1;
            }
            break;
        }
        SetCtrlVal (SABINE, SABINE_CURRENTLOOP, LoopCount);
      }
      FlowRateBuffer[tmp] *=VOLT_LITER;
      FlowRateBuffer[tmp] +=POSITION;
      FlowChartBuffer[tmp] = FlowRateBuffer[tmp];
      FlowChartBuffer[tmp] *= CHART_RATE;
      FlowChartBuffer[tmp] -=CHART_POSITION;
}
if (Experiment == RUNS)
{
```

```
                WFM_Scale (1, 0, tmp, 1.0, FlowRateBuffer, HalfBuffer);
                WFM_DB_Transfer (1, 1, ChannelVector, HalfBuffer, tmp;
                PlotStripChart (SABINE, SABINE_FLOW, FlowChartBuffer, tmp, 0, 0,
                        VAL_DOUBLE);
            }
            else
            {
                static unsigned long PointsGenerated;
                static unsigned long IterationsDone;
                static short WFMStopped;
                WFM_Scale (1, 0, 500, 1.0, FlowRateBuffer, HalfBuffer);
                WFM_DB_Transfer (1, 1, ChannelVector, HalfBuffer, 500);
                PlotStripChart (SABINE, SABINE_FLOW, FlowChartBuffer, 500, 0, 0,
                        VAL_DOUBLE);
                do
                {
                    static short WFMStatus;
                    WFMStatus = WFM_Check (1, 0, &WFMStopped, &IterationsDone,
&PointsGenerated);
                }
                while (WFMStopped != 1);
                WFM_Group_Control (1, 1, 0);
                AOUpdateChannel (1, "0", POSITION);
                SetCtrlAttribute (SABINE, SABINE_START,
ATTR_CMD_BUTTON_COLOR,VAL_GREEN);
                SetCtrlAttribute (SABINE, SABINE_START, ATTR_LABEL_TEXT, "Start");
                CloseFile (BreathingPatternHandle);
            }
        }
        ProcessSystemEvents();
    }
    return 0;
}
```

A.2 Specifications of Individual Parts

A.2.1 Motor and Control Unit

Motor and control Unit were supplied by :

Mattke Antriebstechnik

Leinenwebergasse 12

79108 Freiburg

Germany

Tel: 0049-(0)761-15234-0

Fax 0049-(0)761-15234-56

Product: 4 Quadrant Electronic Speed Control Unit

Brushless servo motor (including resolver): MBR0200/L4-30-0

4Q controller: type MRS 6V 300/12-30

Single-phase toroidal transformer

Potentiometer: type "L"

A.2.2 Linear Actuator

The linear actuator was supplied by:

SKF Engineering Products Limited

Linear Motion Division

Turnberry House

Caldecotte Buisness Park

Milton Kenynes MK7 8LE

Tel 01908-637000

Fax 01908637002

Product: Linear Actuator

Linear motion device: CATR33Hx300x4 G2

Micro switches: CAXC 33

A.2.3 VALVES

The ball valves were supplied by:

W. Adolph

Postfach 120142

65079 Wiesbaden

Germany£152

Tel. 0049-(0)611-188770

Fax. 0049-(0)611-1887722

Product: Ball Valves

2/2 Way Ball-Vavle (pneumatic acutator): type PKB Baureihe 70, D55

Ventiladapter, Artikel Nr 1174

5/2 Wege Ventile 1/8“ Artikel Nr 68-15974 Mod. 358-015-02

A73 Spulen 22x22 24VDC, Artikel Nr 68-27466

122-800 Geraetesteckdosen, Artikel Nr 68-21410

B ANNEX BREATHING PATTERNS

B.1 BREATHING PATTERNS

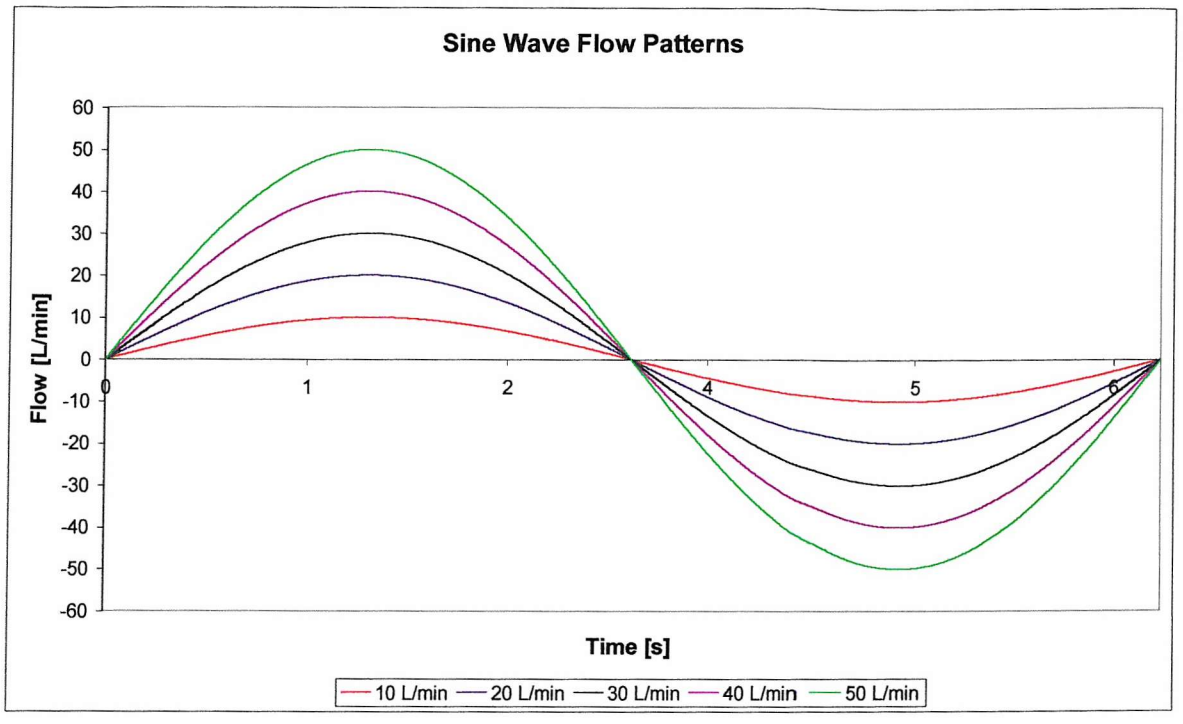

Figure B1: Sinusoidal breathing patterns

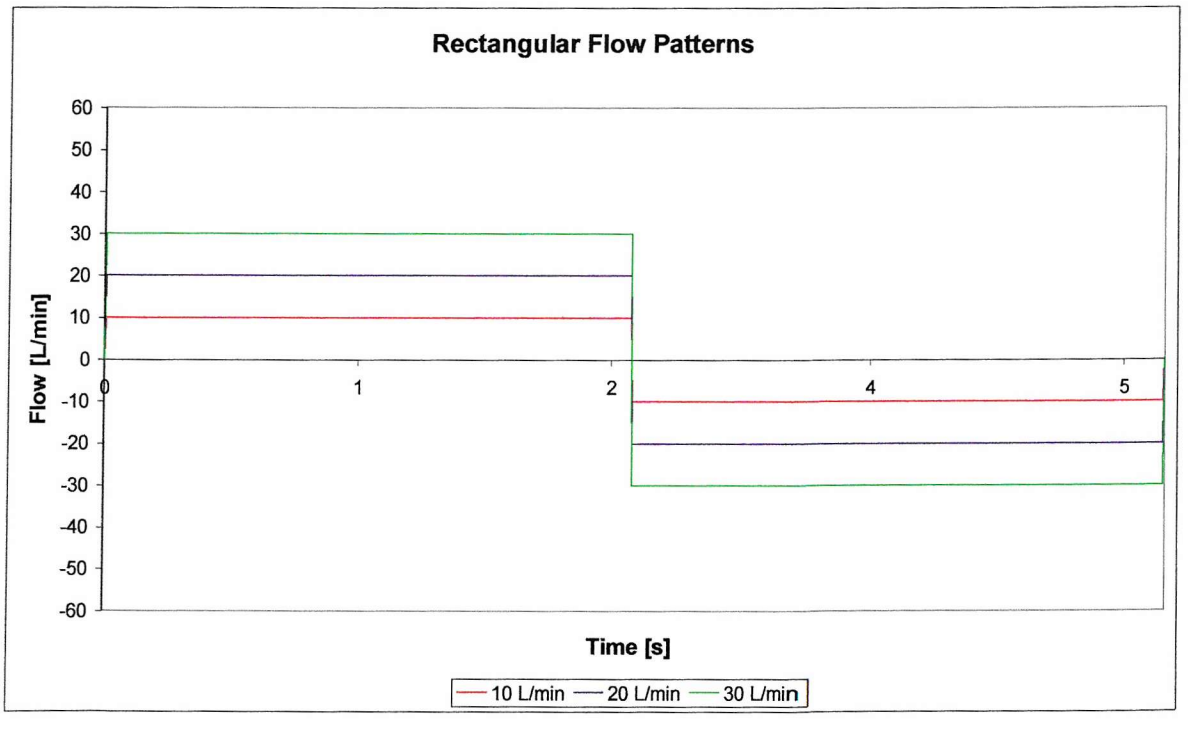

Figure B2: Rectangular breathing patterns

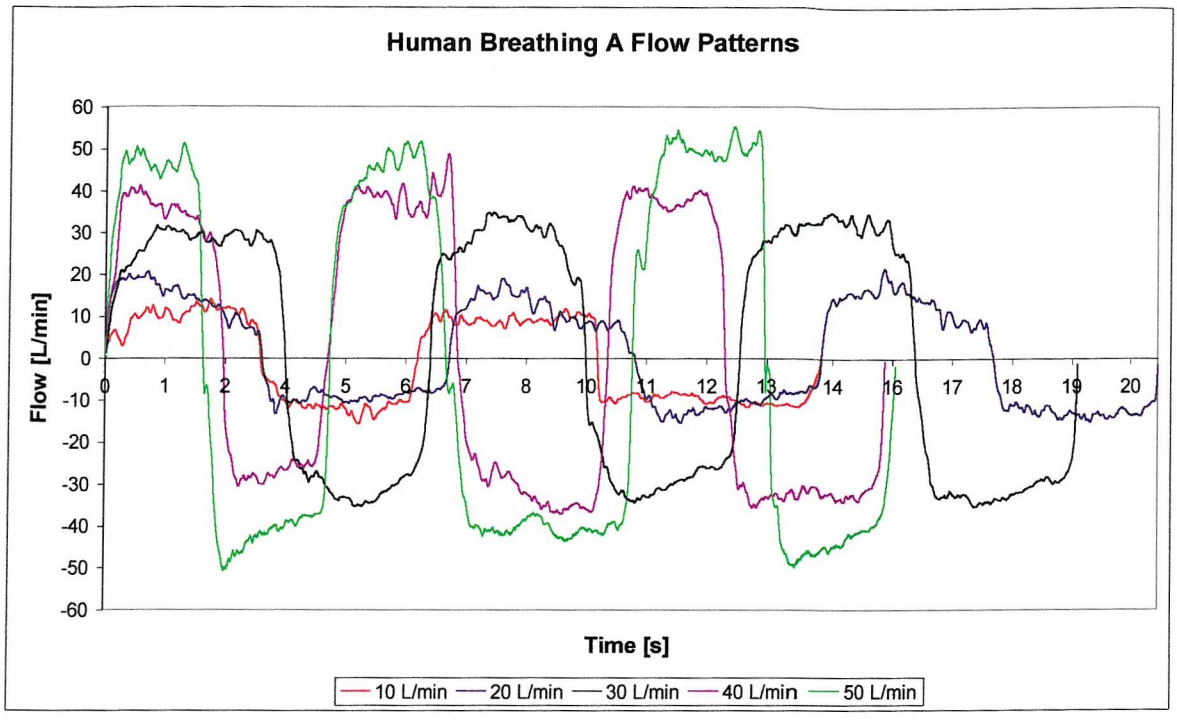

Figure B3: Human A breathing patterns

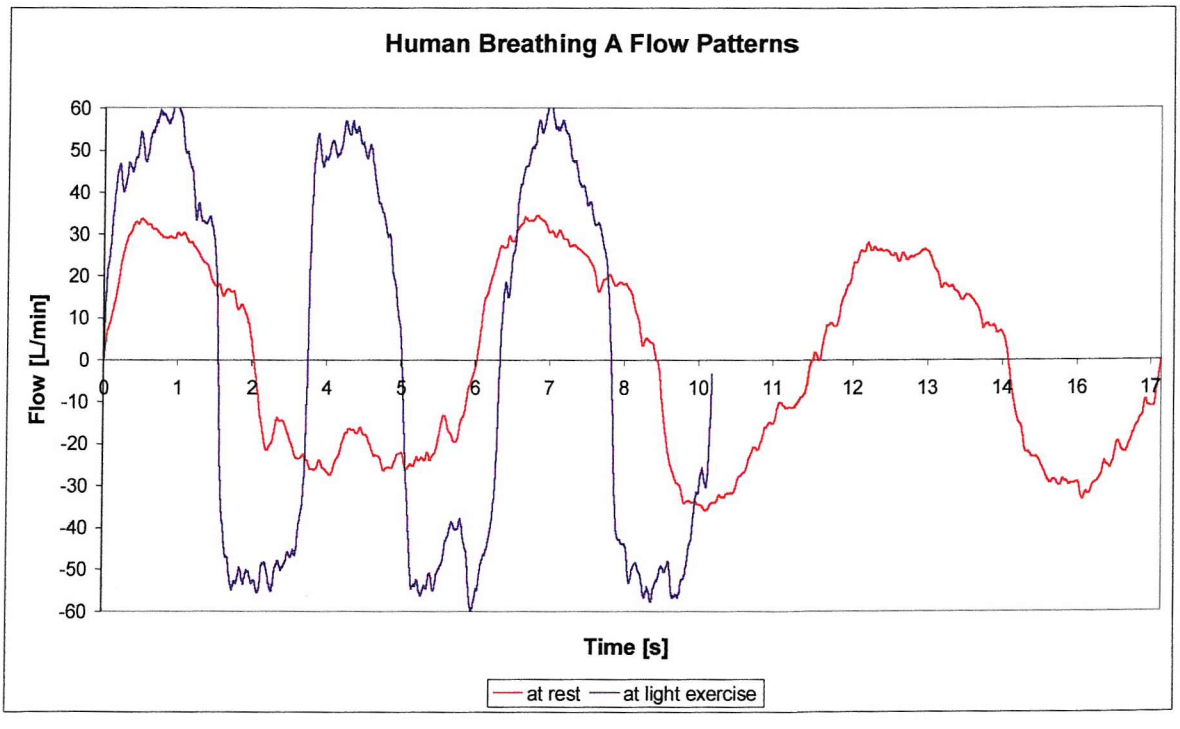

Figure B4: Human A breathing patterns, at rest and light exercise

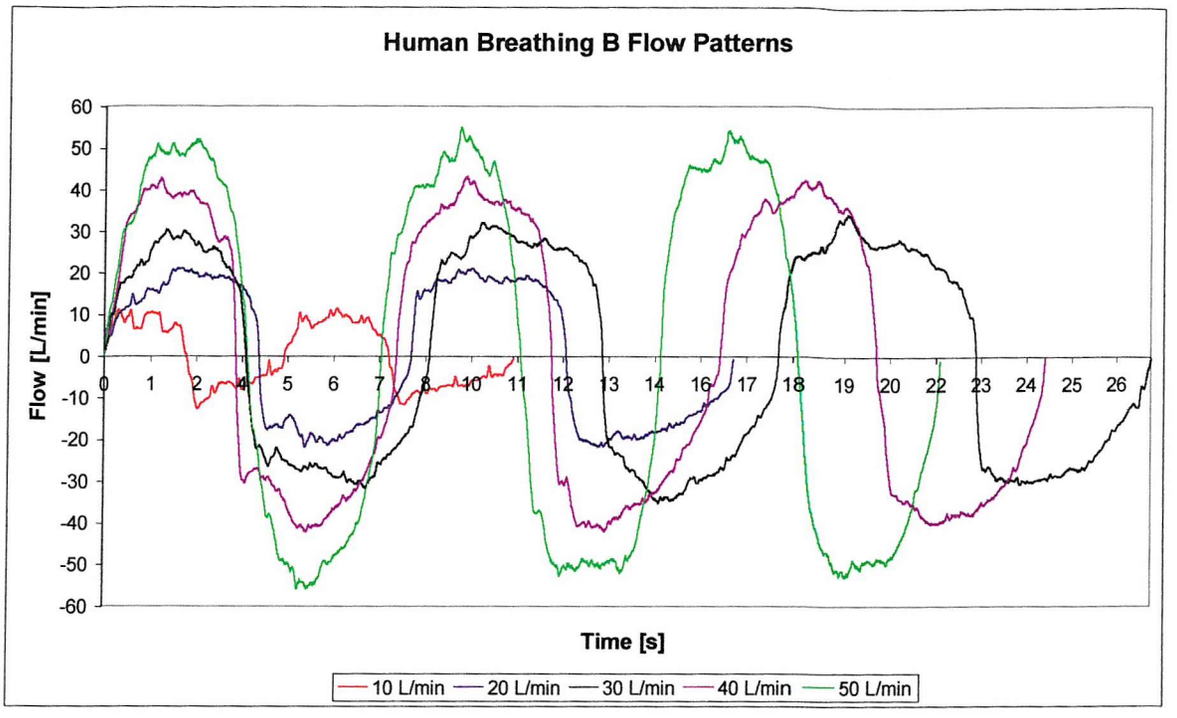

Figure B5: Human B breathing patterns

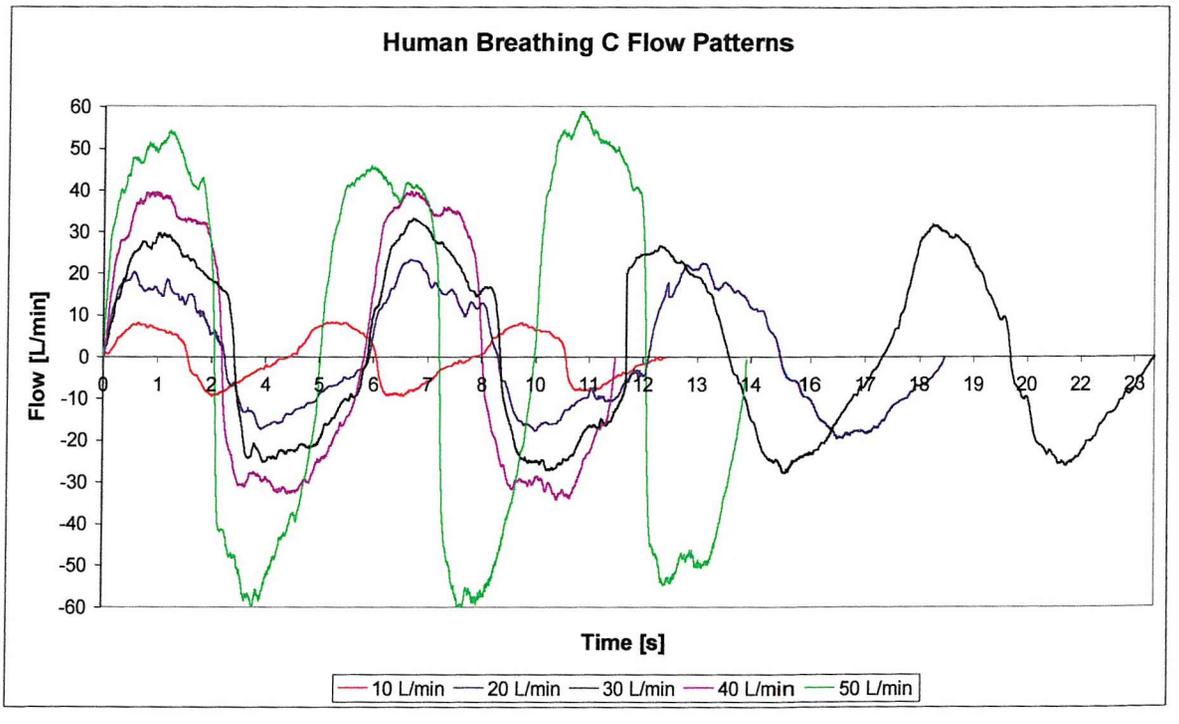

Figure B6: Human C breathing patterns